UNIVERSITY OF CALIFORNIA, SAN DIEGO

The Role of Gfi1 Family Oncogenes in Medulloblastoma

A dissertation submitted in partial satisfaction of the requirements for the degree Doctor of Philosophy

in

Biomedical Sciences

by

Catherine Lee

Committee in charge:

Professor Robert J. Wechsler-Reya, Chair
Professor Steven F. Dowdy, Co-Chair
Professor Frank B. Furnari
Professor Paul S. Mischel
Professor Jing Yang

2016

The Dissertation of Catherine Lee is approved, and it is acceptable in quality and form for publication on microfilm and electronically:

_____

_____

_____

_____

Co-Chair

_____

Chair

University of California, San Diego

2016

TABLE OF CONTENTS

LIST OF ABBREVIATIONS

3H-Td – [Methyl-3H]-Thymidine (tritiated Thymidine)

4OHT – 4-hydroxytamoxifen

γ-IRR – gamma irradiation

APC/C – anaphase-promoting complex

BBB – blood brain barrier

CED – convection enhanced delivery

ChIP-seq – chromatin immunoprecipitation sequencing

CIS – common insertion sites

CNS – central nervous system

co-IP – co-immunoprecipitation

CRISPR – clustered regularly interspaced short palindromic repeats

CSF – cerebral spinal fluid

DMSO – dimethyl sulfoxide

DNp53 – dominant negative p53 (p53 DD construct)

DSB – double-strand break

FFPE – formalin-fixed paraffin-embedded (tissue samples)

GEP – gene expression profile/profiling

Gfi1-N382S – Gfi1 zinc finger mutant (asparagine to serine substitution at amino acid position 382)

Gfi1-P2A – Gfi1 SNAG domain mutant (proline to alanine substitution at amino acid position 2)

GNP – granule neuron precursor/progenitor

GSK - GlaxoSmithKline

Gy – Gray

HAT – histone acetyltransferase

HDAC – histone deacetylase

HDM – histone demethylase

HMT – histone methyltransferase

IHC – immunohistochemistry

IP – immunoprecipitation

i.p. – intraperitoneal (injection)

MB – medulloblastoma

MBEN – medulloblastoma with extensive nodularity

MG – Myc + Gfi1 tumor model (mouse)

MGB – Myc + Gfi1b tumor model (mouse)

MP – Myc + dominant negative p53 tumor model

NGS – next generation sequencing

NP – nanoparticle

NSC – neural stem cell

NSG – NOD-scid IL2Rgamma^{null} immunocompromised mice

PCA – principal component analysis

PCR – polymerase chain reaction

PFA – paraformaldehyde

PDX – patient derived xenograft

PLGA – Poly(lactic-co-glycolic acid)

qPCR – quantitative PCR (Real-time PCR)

RNAi – RNA interference

SB – Sleeping Beauty (transposon)

SCN – severe congenital neutropenia

SCNA – somatic copy number aberration

shRNA – short hairpin RNA

SHH – Sonic hedgehog

SV – structural variant

WES – whole exome sequencing

WGS – whole genome sequencing

WGBS – whole genome bisulfite sequencing

WHO – World Health Organization

WNT – Wingless

WT – wildtype

LIST OF FIGURES

LIST OF TABLES

ACKNOWLEDGEMENTS

I would like to acknowledge my mentor and committee chair, Professor Robert J. Wechsler-Reya, for his continuous support and encouragement over the past five years. His mentorship, dedication, and unwavering faith in my abilities as a scientist have really shaped the past 5 years of my graduate career. Not only was Rob an extremely patient and brilliant teacher, but there were many times when he believed in me much more than I believed in myself. I could always count on him to lend me some optimism whenever I had doubts about grad school or when nothing I did seemed to work. He constantly pushed me to think outside the box, to design better (but not necessarily easier) experiments, and to be open and willing to share my findings with other scientists. I can't emphasize enough how thankful I am for your help throughout this entire process. I am truly very grateful and very proud to have been a student in your lab.

I would also like to give a huge thank you to my family and friends for always being as supportive and understanding as they are. Mom, dad, Adrienne (and Puppy!), you have always stood behind my decisions and been ready to help me whenever and however I needed it. Gary, thank you for putting up with me for the last two years, and for keeping things together (ie. making sure I had coffee, food, and hugs) whenever I was overwhelmed with work. And to all the friends I made here in the last six years, I can't imagine being in any better company than yours during this crazy grad school journey, and I'm glad that we can finally all be doctors together!

Finally, I want to acknowledge everyone who has collaborated with me over the years. Much of the work I accomplished in graduate school would not have been possible without the help of those indicated below:

Chapter 3 contains material that also appears in Nature 2014: Northcott, Paul A.*; Lee, Catherine*; Zichner, Thomas*; Stütz, Adrian M.; Erkek, Serap; Kawauchi, Daisuke; Shih, David J.H.; Hovestadt, Volker; Zapatka, Marc; Sturm, Dominik; Jones, David T.W.; Kool, Marcel; Remke, Marc; Cavalli, Florence M.G.; Zuyderduyn, Scott; Bader, Gary D.; VandenBerg, Scott; Esparza, Lourdes Adriana; Ryzhova, Marina; Wang, Wei; Wittman, Andrea; Stark, Sebastian; Sieber, Laura; Seker-Cin, Huriye; Linke, Linda; Kratochwil, Fabian; Jäger, Natalie; Buchhalter, Ivo; Imbusch, Charles D.; Zipprich, Gideon; Raeder, Benjamin; Schmidt, Sabine; Diessl, Nicolle; Wolf, Stephan; Wiemann, Stefan; Brors, Benedikt; Lawerenz, Chris; Eils, Jürgen; Warnatz, Hans-Jörg; Risch, Thomas; Yaspo, Marie-Laure; Weber, Ursula D.; Bartholomae, Cynthia C.; von Kalle, Christof; Turányi, Eszter; Hauser, Peter; Sanden, Emma; Darabi, Anna; Siesjö, Peter; Sterba, Jaroslav; Zitterbart, Karel; Sumerauer, David; van Sluis, Peter; Versteeg, Rogier; Volckmann, Richard; Koster, Jan; Schuhmann, Martin U.; Ebinger, Martin; Grimes, H. Leighton; Robinson, Giles W.; Gajjar, Amar; Mynarek, Martin; von Hoff, Katja; Rutkowski, Stefan; Pietsch, Torsten; Scheurlen, Wolfram; Felsberg, Jörg; Reifenberger, Guido; Kulozik, Andreas E.; von Deimling, Andreas; Witt, Olaf; Eils, Roland; Gilbertson, Richard J.; Korshunov, Andrey; Taylor, Michael D.; Lichter, Peter, Korbel, Jan O.; Wechsler-Reya, Robert J.;

Pfister, Stefan M., Macmillan Publishers Limited, 2014. The dissertation author was one of three primary investigators and co-first-authors of this paper. Our collaborators provided the human MB tumors and all of the corresponding genomic analysis.

Chapter 4 contains unpublished data that is part of a manuscript in preparation: Lee, Catherine; Northcott, Paul A.; Erkek, Serap; Gao, Fangjian; Tacheva-Grigorova, Silvia; Mohammed, Helai; Yu, Li J.; Hargreaves, Diana A.; Pfister, Stefan M.; Wechsler-Reya, Robert J., “Kdm1a (Lsd1) is required for growth of Gfi1-driven medulloblastoma.” The dissertation author was the primary investigator and author of this material.

VITA

2010	Bachelor of Science, University of California, Los Angeles
2011-2013	Faculty Student Retreat Coordinator, Student Lunch Talk Coordinator Biomedical Sciences Graduate Student Council, University of California, San Diego
2012-2014	Student Mentor, Undergraduate Work Study Program University of California, San Diego
2013	Teaching Assistant, Division of Biological Sciences University of California, San Diego
2013-2014	Student Mentor, Canyon Crest Academy High School Internship Program
2015-2016	Project Leader, Project Member Advanced Professional Degree Consulting Club, University of California, San Diego
2016	Doctor of Philosophy, University of California, San Diego

PUBLICATIONS

Liu A, Fong A, Becket E, Yuan J, Tamae C, Medrano L, Maiz M, Wahba C, **Lee C**, Lee K, Tran KP, Yang H, Hoffman RM, Salih A, Miller JH. Selective advantage of resistant strains at trace levels of antibiotics: a simple and ultrasensitive color test for detection of antibiotics and genotoxic agents. *Antimicrob Agents Chemother.* 55(3):1204-10, 2011.

Northcott PA*, **Lee C***, Zichner T, et. al. Enhancer hijacking activates GFI1 family oncogenes in medulloblastoma. *Nature* 511:428-34, 2014.

*equal contribution

ABSTRACT OF THE DISSERTATION

The Role of Gfi1 Family Oncogenes in Medulloblastoma

by

Catherine Lee

Doctor of Philosophy in Biomedical Sciences

University of California, San Diego 2016

Professor Robert J. Wechsler-Reya, Chair

Professor Steven F. Dowdy, Co-Chair

Medulloblastoma (MB) is the most common malignant brain tumor in children. Recent studies have divided MB into four molecular subgroups: WNT, SHH, Group 3, and Group 4. While WNT and SHH tumors have relatively favorable prognoses, Group 3 tumors (characterized by amplification

or overexpression of the *MYC* oncogene) are frequently fatal. The first mouse models of Group 3 MB combine *Myc* overexpression and *p53* loss of function, but they do not precisely recapitulate the disease genetics, as human Group 3 tumors rarely exhibit mutation or loss of *p53*. Thus, the goal of my research has been to identify secondary hits that can cooperate with MYC and are relevant to human MB.

Collaborating with a MB genomics group, we utilized whole genome sequencing (WGS) data and identified two chromosomal loci that are hotspots for rearrangement in Group 3 MB. Using histone chromatin immunoprecipitation sequencing (ChIP-seq) and expression profiling, we found that rearrangements at these loci activate the zinc-finger transcriptional repressors *GFI1* and *GFI1B* by repositioning them adjacent to super-enhancers. Importantly, we demonstrated their functional relevance in an orthotopic transplantation model, where overexpression of either *Gfi1* or *Gfi1b* cooperated strongly with *Myc* to drive MB formation in mice. These studies highlight a new mechanism for oncogene activation in MB and reveal *GFI1/1B* as highly prevalent drivers of Group 3 MB.

Although the oncogenic potentials of *GFI1/1B* have previously been studied in blood malignancies, their roles in MB are not well understood. We proceeded to identify the chromatin modifier Lysine demethylase 1 (Lsd1) as a key mediator of Gfi1 function in MB, and integration of ChIP-seq and gene expression data revealed a number of putative target genes and signaling pathways that may be co-regulated by Gfi1/1b and Lsd1. Given the critical

interaction between Gfi1 and Lsd1 in these tumors, we tested several small molecule inhibitors of Lsd1 and found that they specifically reduced Gfi1-driven tumor cell growth both in vitro and in vivo. Together these studies confirm the importance of Lsd1 in Gfi1-driven MB and suggest that targeting Lsd1 pharmacologically may be a promising therapeutic strategy.

CHAPTER 1 – Introduction

1.1 Medulloblastoma

Cancers of the brain and nervous system have the second highest incidence and the highest mortality rate of all pediatric cancers[1,2]. Of these, medulloblastoma (MB) is the most widespread malignant tumor. Occurring most frequently in children between five and ten years of age, MB arises in the posterior fossa from neuroectodermal progenitors in or around the cerebellum. There is a slightly higher incidence in males compared to females (1.5 to 1 ratio)[3], and although it is largely a pediatric tumor, 10-25% of cases happen in adolescents and adults[4]. Patients usually present with symptoms such as increased intracranial pressure, headaches, recurrent vomiting, and ataxia[5].

Over the years, the classification and treatment of MB as a single disease has evolved significantly. The vast intertumoral heterogeneity of MB was initially recognized with respect to histopathology and response to treatment, so historically, MB has been classified based on morphological characteristics. In 2007, the World Health Organization (WHO) recognized five histological variants of MB: classic, nodular/desmoplastic, anaplastic, large-cell, and medulloblastoma with extensive nodularity (MBEN)[6]. Classic tumors are the most common, making up about 65% of all MB, while only 2-4% are large-cell, 10-22% are anaplastic, 7% are nodular/desmoplastic, and 3% are MBEN[6]. The large-cell and anaplastic tumors lie on a continuum, so they are

often referred to collectively as large-cell/anaplastic (LCA). This approach associates the classic, nodular/desmoplastic, and MBEN tumors with favorable outcomes and large-cell anaplastic (LCA) MB with aggressive behavior and poorer prognosis[6]. Although this method of classification has some prognostic value, it lacks true biological understanding of MB disease origins and pathogenesis.

1.2 Molecular subgroups and genetic drivers of MB

Within the last decade, the need for more informative MB classification and patient stratification has been acknowledged by both researchers and clinicians. Several groups have consequently analyzed gene expression and DNA copy number variation of large cohorts of human MB samples[7-12], generating an immense amount of genomic data. The general consensus from these studies is that MB is comprised of at least four main molecular subgroups: Wingless (WNT), Sonic hedgehog (SHH), Group 3, and Group 4[12]. In addition to differences in gene expression, these subgroups have distinct mutational profiles, epidemiology, and prognosis. As of 2016, the WHO has restructured the classification of MB to reflect these molecular features[13].

WNT and SHH are the best studied subgroups, and as their names suggest, they are driven by activation of the WNT and SHH pathways, respectively. WNT tumors only represent 10% of MB and have the best outlook (>90% survival). Germline mutations of the Wnt pathway inhibitor APC

(predispose Turcot syndrome) and somatic mutations in *CTNNB1* (encoding β-catenin) have both been observed in WNT tumors[12,14]. SHH tumors account for about 22% of MBs and generally have an intermediate prognosis (60-80% survival). Germline mutations in the Shh receptor *PTCH* (Gorlin syndrome) and in the Shh inhibitor *SUFU*, *as well as* somatic mutations in *PTCH*, *SMO*, or *SUFU*, and somatic amplifications of *GLI1* and *GLI2* have been frequently reported in these tumors[12,14]. Around 20% of SHH tumors also exhibit *TP53* mutations, and these patients have a much poorer overall survival (41%) compared to those without *TP53* mutations[15].

Group 3 and 4 tumors make up the majority of MBs (28% Group 3, 37% Group 4), yet they are the least understood in terms of underlying biology. Group 4 MBs have intermediate prognosis and in some cases display recurrent amplifications of *MYCN* and cyclin-dependent kinase 6 (*CDK6*)[12,14]. The roles of these genes as drivers is still unclear, however, and preclinical mouse models for Group 4 have not yet been established. Group 3 MBs, which commonly exhibit amplification (20%) or overexpression of the *MYC* oncogene, have the worst prognosis, due in part to a higher incidence of metastasis through the cerebrospinal fluid (CSF) and recurrence after initial treatment[12,14]. Group 3 tumors also commonly exhibit LCA histology. The first mouse models of Group 3 MB have only been developed within the last five years, and are described in depth below.

1.3 Animal models of Group 3 MB

A critical step in improving therapies is development of robust animal models of disease. The existence of distinct molecular subtypes of MB suggests that cellular transformation may occur through activation of different oncogenes and signaling pathways in distinct cell types. This concept has been confirmed through studies of the cellular origins and mechanisms of transformation in the WNT and SHH subtypes[6,16-18], and the resulting animal models have been invaluable for the development of new approaches to treatment[19,20]. Group 3 tumors remain very poorly understood, and until recently, lacked any animal models to study the disease.

Our lab previously identified and described a protocol for isolating a population of Prominin1+ (CD133+) neural stem cells (NSCs) from the neonatal cerebellum[21] and hypothesized that these cells could give rise to some subtypes of MB. Infection of NSCs with retroviruses encoding a stabilized form of *Myc* (T58A)[22] increased their proliferation in vitro, but did not allow them to form tumors in vivo following orthotopic transplantation into immunocompromised mice. Co-infection with *Myc* and a dominant negative mutant of *p53* (*DNp53*)[23], however, transformed the cells into aggressive tumors with histological characteristics and gene expression profiles (GEPs) similar to those of human Group 3 tumors[24]. Notably, another group showed that overexpression of Myc in p53-null cerebellar progenitors also resulted in

tumors resembling Group 3 MB[25]. While these two models have allowed us and others to begin studying the biology of Group 3 MB, they share one major caveat: very few cases of primary human Group 3 MB show loss or mutation of *TP53*[15]. In fact, *TP53* mutations are much more frequent in the WNT and SHH subtypes at diagnosis, although these mutations have been detected in Group 3 and Group 4 at relapse[26-28]. Based on this, it is believed that genes other than p53 cooperate with *MYC* to promote primary tumorigenesis.

We sought to identify genetic drivers relevant to human Group 3 MB that could cooperate with Myc to promote tumorigenesis in mice. In the process of screening a set of genes found to be deleted in human Group 3 MB, we and our collaborators discovered that about a third of all Group 3 tumors exhibited structural rearrangements leading to the mutually exclusive activation of the growth factor independent 1 family proto-oncogenes, *GFI1* and *GFI1B*.The details of these studies are discussed below in Chapter 3.

1.4 Treatment and targeted therapies for MB

The current standard of care for MB patients is multimodal, and consists of surgical resection followed by cranio-spinal radiation (for patients ≥ 3 years of age) and high-dose chemotherapy. Advancements in treatment protocols have increased overall MB survival rates from about 50% to 70%, but one-third of patients still die from the disease, and survivors often suffer severe long-term consequences from treatment, including debilitating

neurologic and endocrine disorders[1,2]. Development of more effective and safer MB therapies undoubtedly hinges upon the implementation of tumor molecular genetics in patient stratification methods and subsequent treatment plans.

At this time, patients generally undergo risk stratification based on three criteria: age at diagnosis, extent of tumor resection, and presence of metastatic disease. Children who are at least 3 years old, have less than 1.5 cm^2 of residual tumor after surgery, and have no metastases are considered average-risk, while the remainder are considered high-risk[29,30]. Risk stratification allows for some tailoring of radiation and chemotherapy doses; average-risk patients can receive less radiation, thereby reducing potential neurocognitive side effects[31], while high-risk patients receive increased doses of both chemotherapy and radiation in an effort to treat their more aggressive disease[29,32].

In light of the recent molecular subgrouping of MB, the ability to better stratify patients beyond just average- and high-risk is becoming more promising. Successful application of MB genetics in the clinic depends heavily on accurate analysis of tumor prognosticators and molecular subtype; incorrect classification could lead to under-treatment or over-treatment and severely influence patient outcome[33]. Most clinicians agree that tumor resection should still be the primary treatment, regardless of molecular subgroup. However, subgroup-specific risk stratification could reduce adjuvant radiation or chemotherapy for some patients (WNT) and administer new

targeted therapies for others (SHH, Group 3).

Clinical implementation of targeted therapies for MB has so far mostly been limited to the SHH subtype, where Smoothened inhibitors (Vismodegib, Sonidegib/LDE-225) have shown promise in Phase I and II clinical trials[34-36]. Because of the extremely poor prognosis and lack of treatments available for Group 3 MB, there has been a greater emphasis on identifying drugs specific for these tumors. Two independent high-throughput drug screens for compounds working on Group 3 tumor cells of mouse origin have yielded candidates for combinatory therapy[37,38]. One study combines a histone deacetylase (HDAC) inhibitor (panobinostat) with a PI3K inhibitor (BKM-120)[37], while the other identified a folate pathway inhibitor (Pemetrexed) and a DNA/RNA synthesis inhibitor (Gemcitabine), which is currently recruiting patients for a Phase II clinical trial[3,38].

CHAPTER 2 – Materials and Methods

2.1 Materials and methods for Chapter 3

General statistical methods

All statistical tests were performed in the R Statistical Environment (R version 3.0.0) unless otherwise specified. The Kolmogorov–Smirnov test was used to compare candidate gene expression in chr9q34 SV cases to non-SV cases. Differential expression of GFI1 and GFI1B across MB subgroups was calculated using ANOVA. Enrichment of underlying locus-specific SVs in GFI1/GFI1B-expressing cases was calculated using Fisher's exact test. Mutual exclusivity of GFI1 and GFI1B expression in group 3 and group 4 MBs was determined using Fisher's exact test. Survival analyses were performed in GraphPad Prism 5 using the log-rank (Mantel-Cox) test to compare survival differences between groups.

Sample collection and preparation

An Institutional Review Board ethical vote (Ethics Committee of the Medical Faculty of Heidelberg) was obtained according to ICGC guidelines (http://www.icgc.org), along with informed consent for all participants. No patient underwent chemotherapy or radiotherapy before surgical removal of the primary tumor. Tumor tissues were subjected to neuropathological review for confirmation of histology and for tumor cell content >80%. Analytes were

isolated as previously described[39]. Cells were cultured at 37°C with 5% CO_2. D425 Med MB cells (D425; a gift from Professor Darrell D. Bigner) were cultured in DMEM with 10% FCS (Life Technologies) and regularly authenticated and tested for mycoplasma (Multiplexion, Heidelberg, Germany). Validation samples for WGS were obtained in accordance with the Research Ethics Board at The Hospital for Sick Children (Toronto, Canada).

High-throughput sequencing data generation

Short-insert paired-end sequencing –

Samples were processed and libraries sequenced as previously described[39]. Medulloblastoma and germline WGS data[40] generated by the Pediatric Cancer Genome Project (http://explore.pediatriccancergenomeproject.org/) was accessed from The European Genome-phenome Archive (Study ID EGAS00001000347). The original alignments of this WGS data were performed against either reference genome hg18 or hg19. For comparability with our data, the alignment files in hg18 have been converted to FASTQ files using Picard tools (http://picard.sourceforge. net) providing the 'SamToFastq' option. For the alignment of the FASTQ files, the same reference genome as used in the creation of the original hg19 BAM files has been used along with BWA for alignment and Picard for merging and duplicate read filtering.

Long-range paired-end sequencing data generation –

Long-range (or ‘Mate-pair’) DNA library preparation was carried out as previously described[39] or using the newer Nextera Mate Pair Sample Preparation Kit (Illumina). In brief, 4 mg of high-molecular- mass genomic DNA were fragmented by the Tagmentation reaction in 400 ml, followed by the strand displacement and AMPure XP (Agencourt) clean-up reaction. Samples were size selected to 4–6 kb with a gel step following the Gel-Plus path of the protocol. 300–550 ng of size-selected DNA were circularized in 400 ml for 16 h at 30°C. The library was then constructed after an exonuclease digestion step to get rid of remaining linear DNA, fragmentation to 300–700 bp with a Covaris S2 instrument (LGC Genomics), binding to streptavidin beads and Illumina Truseq adaptor ligation. Final library was obtained after PCR for 1 min at 98°C, followed by 9 cycles of 30s at 98°C, 30s at 60°C, 1min at 72°C and a final 5min at 72°C step. Deep sequencing was carried out with the Illumina HiSeq2000 (2 x 101 bp) instrument to reach an average physical coverage of 20x303.

ChIP sequencing –

Chromatin extraction, immunoprecipitation and library preparation for ChIP-seq were performed at Active Motif (Carlsbad, CA) according to proprietary methods. Briefly, 15 mg of chromatin were used as input for ChIP with ChIP-grade antibodies recognizing H3K27ac (AM#39133, Active Motif), H3K9ac (AM#39918, Active Motif), or H3K27me3 (#07-449, Millipore).

Libraries were sequenced on the Illumina HiSeq 2000 platform using 2 x 101 cycles according to the manufacturer's instructions.

Histone ChIP-seq data for H3K27ac, H3K9ac and H3K27me3 was processed by the Illumina analysis pipeline (version 1.8.3) and aligned to the Human Reference Genome (assembly hg19, GRCh37) using BWA version 0.5.9- r16[41]. Putative PCR duplicates were filtered using Picard MarkDuplicates (http://picard.sourceforge.net). For downstream analyses, we generated whole-genome coverage tracks with reads normalized to all properly paired reads (RPM, paired-end reads/fragments per million). We used igvtools version 2.2.2 (http:// www.broadinstitute.org/igv/igvtools) and the non-default parameter–pairs and a window size of 25. For peak-calling of histone marks, ChIP-seq data for each histone modification (H3K27ac or H3K9ac) was used to generate individual BED files for analysed samples using BEDTools[42]. Individual BED files were then combined for each histone modification and peaks were called using the Bioconductor BayesPeak package in R[43]. Super-enhancers were identified using the ROSE algorithm with default parameters (stitching distance of 12,500 bp and promoter exclusion region of 62,000 bp around TSS)[44]. Briefly, peaks called via BayesPeak were used as constituent enhancers to run the algorithm and super-enhancers were called by ranking of H3K27ac signal at stitched constituent enhancers.

Whole-genome bisulphite sequencing –

Whole-genome bisulphite library preparation was carried out as recently

described[45], with modifications to a previously published protocol[46]. In brief, 5 mg of genomic DNA were sheared using a Covaris device (Covaris Inc.). After adaptor ligation, DNA fragments with insert lengths of 200–250 bp were isolated using an E-Gel electrophoresis system (Life Technologies) and bisulphite converted using the EZ DNA Methylation kit (Zymo Research). PCR amplification of the fragments was performed in six parallel reactions per sample using the FastStart High Fidelity PCR kit (Roche). Library aliquots were then pooled per sample and sequenced on an Illumina HiSeq 2000 machine.

RNA sequencing –

RNA quality control was performed using the 2100 Bioanalyzer platform (Agilent). RNA sequencing libraries were prepared using the TruSeq stranded protocol with Ribo-Zero Gold (Illumina) and sequenced on the Illumina HiSeq 2000 platform with 2 x 51 cycles according to the manufacturer's instructions. High-throughput sequencing data analysis. Whole-genome sequencing. Short-insert WGS data was analyzed as previously described[39]. Long-range paired-end sequencing reads were aligned to the hg19 assembly of the human reference genome using the Illumina-provided alignment software (ELAND, version 2).

Structural variant discovery and filtering –

Deletions, tandem duplications, inversion, translocations, as well as

complex rearrangements resulting in the corresponding paired-end signatures were inferred using DELLY v0.0.11 (ref. 36). We considered all those predictions as somatic that were not present in a set of 1,000 Genomes Project (1000GP; http://1000genomes.org)[47] samples corresponding to germline samples taken from normal healthy individuals. Specifically, we used DELLY to infer variants in 1,106 healthy samples belonging to phase 1 of the 1000GP. Furthermore, we inferred variants in the germline samples belonging to the studied tumors. For a given tumor sample, we considered all those variants as somatic that were present neither in any of the 1000GP samples nor in any of the additional germline samples. Two SVs were considered as identical if their start and end coordinates differed by less than 5.0 kb (approximate insert size of a long-range paired- end library) and if their reciprocal overlap was larger than 50%. Variants that were present in the control samples were either true germline variants or represented artefacts caused by misalignment of reads (for example, due to inaccuracies within the human reference genome). To consider a variant prediction as high-confidence we further required at least four supporting read pairs with a minimum median mapping quality of 20 for each event to exclude false-positive predictions caused by randomly mapping low-quality reads.

Region identification. We divided the human reference genome into overlapping 1-Mb windows (100-kb offset). For each window, we counted the number of samples with at least one SV breakpoint in the given region (based on short-insert as well as long-insert paired-end sequencing data). Only focal

high-confidence SV predictions were used in this analysis (20 kb to 10 Mb in size). Windows affected in at least five samples were investigated manually.

Copy-number analysis –

We determined the number of sequencing reads per non-overlapping genomic window of size 250 bp (high-coverage paired-end data) or 1,000 bp (low-coverage long-range paired-end data) for tumor samples with chr9q34 or chr1p22 SV and their corresponding controls. Tumor values were normalized by the ratio of read counts between tumor and controls within a 500-kb region. Subsequently, for each window, the $\log_2$ ratio between normalized tumor and control counts was determined. These values were averaged along a sliding window of 5 kb (short-insert paired-end data) or 10 kb (long-range paired-end data). For tumor samples without a matching control sample, the control of ICGC_ MB230 was used.

Whole-genome bisulphite sequencing –

WGBS sequencing data was analyzed using methylCtools[48]. In brief, methylCtools builds on BWA and adds functionality for aligning bisulphite treated DNA to a reference genome in a similar manner as described previously[49]. Sequencing reads were adaptor-trimmed using SeqPrep (https://github.com/jstjohn/SeqPrep) and translated to a fully C-to-T converted state. Alignments were performed against a single index of both in silico bisulphite-converted strands of the human reference genome (hg19, NCBI

build 37.1) using BWA version 0.6.1-r104[41] and the non-default parameters -q 20 -s. Previously translated bases were translated back to their original state, and reads mapping antisense to the respective reference strand were removed. Putative PCR duplicates were filtered using Picard MarkDuplicates (http://picard.sourceforge.net). Non-conversion rates were estimated on the basis of lambda phage genome spike-ins. Single base pair methylation ratios (beta-values) were determined by quantifying evidence for methylated (unconverted) and unmethylated (converted) cytosines at all CpG positions. Only properly paired or singleton reads with mapping quality of >/1 and bases with Phred-scaled quality score of >/20 were considered. To account for population variability, we filtered CpGs for which more than 25% of reads at a given position (on either strand) were not supportive of this CpG being in fact a CpG in the sample being analyzed. Subsequently, information from both strands was combined and CpGs with coverage less than five reads were set as NA.

RNA sequencing –

Demultiplexed FASTQ files were generated using the Bcl2FastQ conversion software (Illumina, version 1.8.4). The resulting sequencing reads were aligned to the human genome reference build hg19 (version human_g1k_v37 – 1,000 Genomes Project Phase 1) using BWA version 0.5.9-r16[41] with default parameters. Only the chromosomes 1–22, X, Y and M were used for the mapping. Read coverage plots were prepared using the

UCSC Genome Browser showing the number of aligned reads for each genomic position per million mapped reads (RPM) with mapping quality MAPQ .1. The sequencing reads were also used as input for the TopHat2-Fusion algorithm[50] for detection of gene fusion breakpoints. Allelic analysis. Germline SNPs were determined using Samtools and BCFtools. For each SNP, the number of reads in the tumour DNA-, RNA-, and ChIP-seq data supporting the alternative or the reference allele were counted using Samtools mpileup. Only bases with phred score .20 were considered. Only heterozygous SNPs covered by at least 4 sequencing reads in each data set were included in the final summary.

PCR and Sanger sequencing validation of structural variants

PCR experiments were performed as follows: 10 ng of genomic DNA were used with the SequalPrep Long PCR Kit (Invitrogen) in 20 ml volumes using the following PCR conditions in a MJ Mini thermocycler (BioRad): 94°C for 3 min, followed by 10 cycles of 94°C for 10s, 62°C for 30s and 68°C for 6 min and 25 cycles of 94°C for 10s, 60°C for 30 s and 68°C for 7 min, followed by a final cycle of 72°C for 10 min. PCR products were analyzed on a 1% agarose gel stained with Sybr Safe Dye (Invitrogen). Gel-extracted bands using the NucleoSpin Gel and PCR Clean-up Kit (Macherey-Nagel) were capillary sequenced at GATC Biotech AG to analyze SV breakpoints.

Expression array processing and data analysis

General array processing –

For gene expression array profiling of human medulloblastomas and normal cerebellar controls, high-quality RNAs were processed and hybridized to either (i) the Affymetrix Gene 1.1 ST array at The Centre for Applied Genomics (TCAG, Toronto, Canada) or (ii) the Affymetrix U133 Plus2.0 expression array at the Microarray Department of the University of Amsterdam (Amsterdam, the Netherlands). Sample library preparation, hybridization, and quality control were performed according to protocols recommended by the manufacturer. The CEL files were quantile normalized using Expression Console (v1.1.2; Affymetrix, USA) and signal estimates determined using the RMA algorithm.

Mouse medulloblastomas, non-neoplastic cerebellar stem cells (NSCs), and normal mouse cerebella were analyzed using the Affymetrix Mouse Genome 430 2.0 expression array according to the manufacturer's instructions at the DKFZ Genomics and Proteomics Core Facility (Heidelberg, Germany). The CEL files were quantile normalized using Expression Console (v1.1.2; Affymetrix, USA) and signal estimates determined using the RMA algorithm. Merging of expression array platforms. Gene expression array data generated using the Affymetrix Gene 1.1 ST array and U133 Plus2.0 array platforms was merged in order to generate a combined series that would facilitate more streamlined down- stream analyses. For each platform, a contrast value per gene was calculated by subtracting the mean expression of

that gene across all samples hybridized on that platform from each individual sample (see formula below), and the resulting contrast values of the two platforms were then combined.

$Contrast_{geneA\ in\ SampleX}$ = $Gene_A$ expression in $Sample_X$ – mean ($Gene_A$ expression)

This method minimized possible batch effects existing between the two array platforms and allowed for downstream analyses containing the combined series. Identification of GFI1- and GFI1B-activated medulloblastomas. After combining the gene expression data for the two expression array platforms, for both GFI1 and GFI1B, expression values were modelled by fitting two normal distributions to the data using the R package 'mclust'[51]. With a P value cut-off of $P<0.0001$, threshold expressions for GFI1 and GFI1B were identified as contrast scores of 0.64 and 0.65, respectively. Samples having expression greater than or equal to the thresholds were called as GFI1- or GFI1B-activated.

Pathway analysis –

Medulloblastoma expression array profiles (Affymetrix Gene 1.1 ST) were used to fit a linear model for each gene using group 3 status, GFI1 expression, and GFI1B expression as covariates. The R package 'limma' was used to perform these fits. The average rank of the statistical significance of

the GFI1 and GFI1B coefficients was used to perform a Mann–Whitney U-test for a given collection of genes (the null hypothesis being that the genes in a gene set are not ranked any higher than those which are not). In cases where multiple probes matched a single gene, the higher-ranking probe was used. The gene sets contained in the c2-c6 collections from the Molecular Signatures Database (MSigDB) were tested[52]. The P values obtained for each gene set in a collection underwent a Benjamini–Hochberg correction to correct for multiple testing.

Cross-species comparisons of human and mouse medulloblastomas

Human medulloblastoma samples were analyzed on the Affymetrix U133Plus2 platform and normalized by the MAS5 algorithm. Mouse tumours were analysed on the Affymetrix Mouse Genome 430 2.0 platform and similarly normalized by MAS5 using the 'affy' (v1.38) package within the R Statistical Environment (v 3.0.2). Human and mouse expression profiles were matched by homologues using official gene symbols and filtered for genes that exhibit conserved expression across 32 matched human and mouse tissues[53] as determined by Pearson correlation tests with multiple hypotheses correction using the Benjamini–Hochberg false discovery rate method (FDR ,0.1). Mouse adult cerebellum, fetal cerebellum and Ptch1$^{+/-}$ medulloblastoma samples were matched against the most similar human adult cerebellum, fetal cerebellum and SHH medulloblastoma samples, respectively, by Pearson correlation of expression profiles. Subsequently, these matched

sample pairs were designated as replicate samples for cross-platform calibration by the Linear Cross-Platform Integration of Microarray Data (LTR) algorithm[54] as implemented in the 'LTR' package (v 1.0.0).

Following gene filtering and expression calibration, the human and mouse expression profiles were combined and analyzed by multidimensional scaling. The first two dimensions were disregarded, as expression differences between human and mouse dominated them. The third dimension was identified as the medulloblastoma subgroup spectrum, as the coordinate values discriminate samples from different human medulloblastoma subgroups. Using this molecular subgroup spectrum, mouse samples were classified using a Bayesian classifier initialized with a uniform prior. The posterior probabilities were calculated as the normalized product of the prior and the likelihood of Gaussian distribution parameters with mean and variance estimates from each of the human medulloblastoma subgroups.

Luciferase enhancer assays

Candidate enhancer regions were amplified by PCR using the primer sets listed below (Table 1) and cloned into the pGL4.24[luc2P/minP] Vector (Promega) containing a multiple cloning region for insertion of a response element of interest upstream of a minimal promoter and the luciferase reporter gene, luc2P.

For evaluation of enhancer activity, D425 group 3 medulloblastoma cells were plated on 6-well plates. At 50% confluence, cells were transfected

in triplicate with 2.25 mg of the pGL4.24 reporters carrying the DDX31 DNA fragments plus 0.25 mg of phRL-TK encoding Renilla luciferase. Two days post-transfection, the cells were harvested, followed by measurement of luciferase activities using the Dual-Glo Luciferase Assay System (Promega). As a control, the pGL4.24 empty vector was included for calibration of activity obtained with the experimental constructs. The luminescence of the Firefly Luciferase was normalized to the Renilla Luciferase signal obtained from the phRL-TK vector and data was presented as the mean delta-fold activity (Firefly Luciferase/Renilla Luciferase) of experimental transfectants compared to the pGL4.24 empty vector transfectants.

Table 1: Primer sequences for cloning of super-enhancer response elements

Target	Sequence
BARHL1/DDX31 SE: region 1, forward	GAAGGTACCATCCCCACTTCCTGGTAAGG
BARHL1/DDX31 SE: region 1, reverse	GAAGGTACCTTCTTTGGGGAAATCATTGG
BARHL1/DDX31 SE: region 2, forward	GAAGGTACCCTGAGAGTTTGGGCTTCAGG
BARHL1/DDX31 SE: region 2, reverse	GAAGGTACCGCCTGCCAATTTTTATGTGG
BARHL1/DDX31 SE: region 3, forward	GAAGGTACCTGTCTCCAAGTGTGGTTTCG
BARHL1/DDX31 SE: region 3, reverse	GAAGGTACCTGAGCAGGGGATTTAACAGG
BARHL1/DDX31 SE: region 4, forward	GAAGGTACCAGGGGTATCGTGGTCTTGG
BARHL1/DDX31 SE: region 4, reverse	GAAGGTACCGGAAAGCACACGTGAAAAGG
BARHL1/DDX31 SE: region 5, forward	AAGGTACCAGTGTGTCAACCACCCACAA
BARHL1/DDX31 SE: region 5, reverse	AAGAGCTCGGATGGAGTGCAGTCACCTT
BARHL1/DDX31 SE: region 6, forward	AAGGTACCGAAATTCCCCAGGAGGAGAG
BARHL1/DDX31 SE: region 6, reverse	AAGAGCTCCCAATGCACCCTACGTTTCT
BARHL1/DDX31 SE: region 7, forward	AAGGTACCCACCCAGCTCTTCTCCAGTC
BARHL1/DDX31 SE: region 7, reverse	AAGAGCTCCTCCTCCAGCACAACACTGA
BARHL1/DDX31 SE: region 8, forward	AAGGTACCCTGTAGCCTCGACCTTCTGG
BARHL1/DDX31 SE: region 8, reverse	AAGAGCTCCCTTCAGAGCACTTGTAGGAGAA

Immunohistochemical and FISH analysis of human medulloblastoma samples

Immunohistochemistry (IHC) and FISH were performed on formalin-fixed paraffin-embedded (FFPE) MB sections as previously described[7]. Monoclonal GFI1 (clone 3G8, Sigma) and polyclonal GFI1B (HPA007012, Sigma) antibodies were used at working dilutions of 1:100 with an incubation

time of 1hr @ 32°C using the Ventana protocol cc1.

Mouse models

Mice –

C57BL/6 mice (males and females) were used as a source of cerebellar neural stem cells and immunocompromised (NOD-*scid* IL2Rgamma^{null}, NSG) female mice were used as transplantation hosts. Mice were bred and maintained at the Sanford Burnham and Sanford Consortium Animal Facilities. Experiments were performed in accordance with national regulations using procedures approved by the Institutional Animal Care and use Committees at SBMRI and the University of California San Diego. No a priori calculations related to sample size were performed. No specific randomization or blinding was performed.

Isolation of cerebellar neural stem cells –

Cerebellar stem cells were isolated as previously described[21]. Briefly, neonatal (p4-p6) cerebella from wildtype C57BL/6 mice were dissected out, enzymatically digested with 10 U/ml papain (cat #LS003126, Worthington Biochemical Corporation) and 240 U/ml DNase (cat #D5025, Sigma or cat # LS002007, Worthington Biochemical Corporation), and mechanically dissociated into single cell suspension. Cells were subjected to 35-65% Percoll fractionation (GE Healthcare Life Sciences #17-0891-02) and stained (anti-mouse CD133 PE, eBioscience #12-4301-82) and sorted for the

Prominin1+ (CD133+) population (approximately 3-4%) using the FACSAria III (BD Biosciences).

Retroviral constructs –

Retroviruses used in this study included, MSCV-c-Myc T58A-IRES-GFP[24], MSCV-Gfi1-IRES-GFP, MSCV-Gfi1-IRES-Luc, MSCV-Gfi1b-IRES-GFP, and MSCV-Gfi1b-IRES-Luc. To create the *Gfi1* and *Gfi1b* viral constructs, cDNAs were PCR-amplified from pCMV6-Gfi1 (#MC208542, OriGene) and pCMV6-Gfi1b (#MC201880, OriGene), respectively, and EcoRI and XhoI restriction sites were added to the cDNA ends. The PCR-amplified products were blunt-end-ligated in pJET1.2 (CloneJET PCR Cloning Kit, Thermo Scientific #K1231) and then cut with EcoRI and XhoI. The sticky-ended fragments were then ligated into the EcoRI/XhoI-digested MSCV-IRES-GFP and MSCV-IRES-Luc vectors. The primers for amplifying *Gfi1* and *Gfi1b* cDNAs are listed below in Table 2.

Table 2: Primer sequences for cloning mouse Gfi1 and Gfi1b

Target	Sequence
Gfi1 forward	GAATTCACCATGCCGCGCTCATTCCTGGTC
Gfi1 reverse	CTCGAGTCATTTGAGTCCATGCTGAGTCTC
Gfi1b forward	GAATTCACCATGCCACGGTCCTTTCTAGTG
Gfi1b reverse	CTCGAGTCACTTGAGATTGTGTTGACTCTC

Orthotopic transplantation and tumor formation –

Prior to transplantation, cerebellar stem cells (Prominin1+ cells) were infected overnight with retroviruses encoding Myc^{T58A} and *Gfi1* or *Gfi1b*. Next, transduced cells were re-suspended ($1x10^5$ cells per 4 ul) in Neurocult NSC

Basal medium (Stem Cell Technologies, cat #05700) with Neurocult NSC Proliferation Supplement (Stem Cell Technologies, cat #05701). NSG mice (6-8 weeks old) were anesthetized with Avertin (0.015 mg/kg, SBMRI) or isofluorane (2.5% in oxygen at 2 L/min, VetOne, UCSD) and placed into a stereotactic frame equipped with mouse adaptor (David Kopf Instruments). Upon exposing the skull, an 18G needle was used to drill a 1 mm diameter hole in the skull over the cerebellum. Using a 5 µl Hamilton syringe with an unbeveled 24G needle, 4 µl of the cell suspension was slowly injected into the cerebellum at a depth of 1.5-2mm. Incision sites were closed with Vetbond tissue adhesive. Animals were monitored weekly and sacrificed when they showed symptoms of MB. At time of sacrifice, brains were removed for tumor dissection and dissociation or for embedding and sectioning.

Tissue sectioning and staining –

Animals were perfused with PBS followed by 4% paraformaldehyde (PFA) (Affymetrix). Brains were then removed and drop fixed in 4% PFA overnight.

Samples for frozen sectioning were cryopreserved in 30% sucrose and frozen in TissueTek-O.C.T. (Sakura Finetek). Frozen samples were cut into 12 micron sagittal sections using a Leica CM3050S cryostat. Cryosections were rehydrated in PBS, then blocked and permeabilized with PBS containing 0.1% Triton X-100 and 1% normal goat serum, stained overnight with primary antibodies against proliferation (anti-Ki67, Abcam ab15580) and lineage

markers (anti-GFAP, Novus Biologicals NB300-141; anti-β3-Tubulin, Cell Signaling #5568), and stained for 1 hour with fluorescent secondary antibodies (Alexa Fluor 568 Donkey Anti-Rabbit IgG, Invitrogen A10042). Sections were then counter-stained with DAPI (Cell Signaling #4083), mounted using Fluoromount G (Southern Biotech #0100-01), and imaged on a confocal fluorescent microscope (Zeiss LSM700).

Samples for histological analysis were paraffin-embedded, sectioned, and stained with H&E by the Sanford Burnham Histopathology Core Facility.

In vivo bioluminescent imaging –

Mice were anesthetized with isofluorane and given intraperitoneal (i.p.) injections of 150 ng/g D-Luciferin (Caliper Life Sciences, cat #12279). Five minutes after injection, animals were imaged using the Xenogen Spectrum (IVIS-200) imaging system (Sanford Burnham and Sanford Consortium Animal Facilities).

2.2 Materials and methods for Chapter 4

General statistical methods

Survival analyses were performed in GraphPad Prism 7 using the log-rank (Mantel-Cox) test to compare survival differences between groups. Unpaired, two-tail t-test was used to compare thymidine incorporation in GFP-infected and Fbxo5-infected MG cells. Unpaired, one-tail t-test was used to

compare final tumor weights of vehicle- and GSK-LSD1-treated mice. Drug IC_{50} was calculated in GraphPad Prism 7 using nonlinear regression analysis (3 parameter log(inhibitor) vs. response).

Virus production

$8x10^6$ HEK 293T/17 cells (ATCC CRL-11268) were plated in T150 cell culture flasks one day prior to Calcium Phosphate transfection. On the day of transfection, media was exchanged 0.5-2 hrs before transfection. Sterile distilled H_2O, plasmids (VSVG, Gag/Pol, and vector of interest), and 2M $CaCl_2$ were prepared in one tube. 2x HEPES (280 mM NaCl, 1.5 mM Na_2HPO_4, 50 mM HEPES free acid; pH 7.0-7.1) was added dropwise to the tube containing H_2O/plasmids/$CaCl_2$ and incubated for 1 min at room temperature. Mixture was added onto cells and swirled very gently to mix. After incubation at 37°C for at least 5 hrs, media was exchanged and cells were returned to the incubator. Viral supernatant was harvested at 24, 48, and 72 hrs after transfection and stored in 4°C until viral concentration step.

Before concentration, viral supernatants were filtered through 0.45uM filters, placed into centrifuge buckets, weighed, and balanced. Samples were centrifuged at 25,000 RPM and 4°C for 2 hrs using the SW32 rotor in an Optima L-80 XP Ultracentrifuge. After centrifugation, supernatant was removed and the viral pellets were resuspended in ~500 ul media, aliquoted, frozen on dry ice, and stored in -80°C until further use. Virus titration was carried out by infecting 293T cells with serial dilutions of virus and analyzing

expression of the vector's reporter using flow cytometry (GFP or dsRed) or a bioluminescent plate reader (luciferase).

Retroviral constructs

Retroviruses used for generation of MG and MGB tumors include: MSCV-c-Myc T58A-IRES-GFP[24], MSCV-c-Myc T58A-IRES-Lucif, MSCV-c-Myc T58A-IRES-CD2, MSCV-Gfi1-IRES-GFP, MSCV-Gfi1-IRES-Luc, MSCV-Gfi1b-IRES-GFP, MSCV-Gfi1b-IRES-Luc, and MSCV-loxp-Gfi1-loxp-IRES-GFP. *Gfi1* and *Gfi1b* viral constructs were cloned as described earlier in section 2.1. To clone MSCV-loxp-Gfi1-loxp-IRES-GFP, *Gfi1* was PCR amplified using primers with loxp sites and EcoRI/XhoI sites added to the ends.

Retroviruses used for testing the Gfi1 domain functions include pSF91-Gfi1-dsRed (wildtype), pSF91-Gfi1 P2A-dsRed (SNAG mutant), and pSF91-Gfi1 N382S-dsRed (Zinc finger mutant). These vectors were shared with us by Dr. H. Leighton Grimes, PhD, from Cincinnati Children's.

Retroviruses used for validating Gfi1/1b and Lsd1 candidate target genes include: MSCV-Nfia-IRES-GFP, MSCV-Bmpr1a-IRES-GFP, MSCV-Smad4-IRES-GFP, MSCV-Fbxo5-IRES-GFP, MSCV-Lrig3-IRES-GFP, and MSCV-Cux1-IRES-GFP. The ChIP-seq target genes were subcloned into MSCV-IRES-GFP by PCR-amplifying cDNAs from the following plasmids: TetO-FUW-NfiA (Addgene, Plasmid #64901), MGC Mouse Bmpr1a cDNA (Dharmacon, Clone ID: 5364272), MGC Mouse Smad4 cDNA (Dharmacon,

Clone ID: 6313280), MGC Mouse Fbxo5 cDNA (Dharmacon, Clone ID: 6336178), MGC Mouse Lrig3 cDNA (Dharmacon, Clone ID: 30610561), and p110 CUX1 (gifted by Dr. Alain Nepveu, PhD, McGill University). Primers for PCR are listed in Table 3. EcoRI and/or XhoI restriction sites were added to the appropriate cDNA ends and ligated into MSCV-IRES-GFP.

Table 3: Primer sequences for cloning Gfi1/1b and Lsd1 candidate target genes

Target	Sequence
Nfia forward	GCATGAATTCACCATGTATTCTCCGCTCTGTCTC
Nfia reverse	GCATCTCGAGTTATCCCAGGTACCAGGA
Bmpr1a forward	GCATGAATTCACCATGACTCAGCTATACACTTAC
Bmpr1a reverse	GCATCTCGAGTCAAATCTTTACATCCTG
Smad4 forward	GCATGAATTCACCATGGACAATATGTCTATAACA
Smad4 reverse	GCATCTCGAGTCAGTCTAAAGGCTGTGG
Fbxo5 forward	GCATGAATTCACCATGAGCCGGCGCACC
Fbxo5 reverse	GCATCTCGAGTCACAATCTTTGTAAGTTCTTTTTACTCTT
Lrig3 forward	GCATCTCGAGACCATGGGTGCTCCCGGACT
Lrig3 reverse	GCATCTCGAGCTATGTGTCTGAATCACAAGGC
p110 CUX1 forward	GCATGAATTCACCATGTCCACCTCGCCCATGCCCA
p110 CUX1 reverse	GCATCTCGAGTCAGAACTCCCATTCGATAGGTTCCTC

Co-immunoprecipitations

MG tumor cell pellets of at least $3x10^6$ cells were lysed in lysis buffer (150mM NaCl, 20mM Tris, 1% Triton X-100) with protease inhibitor (Roche, cat #1836153). Lysates were precleared for 30 minutes with Protein G beads (Millipore #16-201D). 10% of the sample was saved as input, and the rest was split in half for IP and isotype control. Samples were incubated with Gfi1 antibody (1ug, Santa Cruz sc-8558), Lsd1 antibody (1ug, Abcam ab17721), coREST antibody (1ug, Millipore cat #07-455), or isotype control antibody (1ug, Santa Cruz sc-2028) for 1 hour. Protein G beads were added to the

samples and washed three times before preparing for Western blot by adding 4x SDS sample buffer and boiling.

Western blotting

Co-IP protein samples were run on 10% SDS-PAGE, transferred to nitrocellulose membranes, blocked with 5% nonfat milk (Apex) in Tris-buffered saline with 0.1% Tween-20 (TBST), and stained overnight with anti-Gfi1 (1:500, Abcam ab21061), anti-Lsd1 (1:800, Abcam ab17721), anti-coREST (1:2000, Millipore cat #07-455), anti-HDAC1 (1:1000, Cell Signaling cat #5356), or anti-HDAC2 (1:1000, Cell Signaling cat #5113) antibodies. Membranes were incubated for 1 hr with anti-rabbit HRP-conjugated secondary antibody (1:1000, Cell Signaling #7074) followed by visualization with Clarity Western ECL (Bio-Rad, cat #170-5060) on the ChemiDoc MP Imaging System (Bio-Rad).

All other Western samples were lysed in 1X RIPA buffer (Millipore, cat # 20-188) and quantified using the Pierce BCA protein assay kit (ThermoFisher cat #23225). Protein separation, transfer, and blocking were as described above. In addition to anti-Gfi1, anti-Lsd1, and anti-coREST antibodies mentioned above, other primary antibodies used include anti-Gapdh (1:1000 Cell Signaling #2118), anti-p21 (1:200, Santa Cruz sc-6246), and anti-p53 (1:1000, Cell Signaling #2524). Membranes were incubated with anti-rabbit HRP-conjugated secondary (1:1000, Cell Signaling #7074) or anti-mouse

HRP-conjugated secondary (1:1000, Cell Signaling #7076). Protein visualization was as described above.

Induction of p53 DNA damage response

To determine if the p53 pathway could be induced in MG tumor cells, we cultured 3-5x10^6 MG tumor cells/well in 6-well plates. As a control, we isolated e14.5 mouse embryonic fibroblasts (MEFs) from C57BL6 embryos and also cultured them in 6-well plates. Cells were treated with vehicle (DMSO), 0.1 uM, or 0.5 uM of doxorubicin (Cayman Chemical cat # 15007) and collected at 4 and 12 hrs for analysis of p53 and p21 protein levels by Western blot.

Similarly, MEFs and MG tumor cells were cultured in 6-well plates and irradiated using a low-dose Cesium 137 irradiator at the Sanford Burnham Prebys Animal Facility. Cells received 0, 1, 2, 4, or 8 Gy and were collected at 4 or 5 and 12 hrs for analysis of p53 and p21 protein levels by Western blot.

Mice

Mouse strains used in these studies include: C57BL/6, Lsd1$^{fl/fl}$ [55](gifted by Drs. Jianxun Wang, PhD and Michael Geoffrey Rosenfeld, PhD, UCSD), Tg(CAG-cre/Esr1*)5Amc/J (CAG-CreERT2) (The Jackson Laboratory), and NOD-*scid* IL2Rgamma^{null} (NSG). Lsd1$^{fl/f}$ mice were bred with CAG-CreERT2 mice to produce mice with a CAG-CreERT2 Lsd1$^{fl/fl}$ genotype. C57BL/6, Lsd1$^{fl/fl}$, CAG-CreERT2, and CAG-CreERT2 Lsd1$^{fl/fl}$ pups were all used as

sources of cerebellar neural stem cells (as described in section 2.1). NSG mice were used as transplantation hosts (as described in section 2.1)

Mice were bred and maintained at the Sanford Burnham Prebys Medical Discovery Institute (SBP) and Sanford Consortium Animal Facilities. Experiments were performed in accordance with national regulations using procedures approved by the Institutional Animal Care and use Committees at SBP Discovery and the University of California San Diego. No a priori calculations related to sample size were performed.

Isolation of cerebellar neural stem cells

Neural stem cells were isolated as described in section 2.1.

Orthotopic transplantation and tumor formation

MG and MGB tumors were generated in mice as described in section 2.1. At the time of sacrifice, brains were removed for tumor dissection and dissociation. The method for tumor dissociation is the same as the one used for NSC isolation (see Section 2.1), but the Percoll gradient and subsequent steps are not required.

In vivo bioluminescent imaging

Mice were imaged as described in section 2.1.

Genetic deletion of Gfi1 or Lsd1 from MG tumor

To delete Lsd1 in vivo from CAG-CreERT2 Lsd1$^{fl/fl}$ MG tumors, tumors were first dissociated into single cell suspension and orthotopically re-transplanted into new NSGs. After 1 week, mice were imaged using the Xenogen Spectrum imaging system. Based on tumor size determined from imaging, mice were randomized into two groups, and these were treated with either vehicle (corn oil) or 4 mg of tamoxifen (Sigma cat #T5648) via intraperitoneal (i.p.) injections. Mice were treated Monday, Wednesday, and Friday for 1 week or for 3 weeks. Tumors were collected to check Lsd1 protein levels by Western blot.

Since in vivo treatment of tamoxifen did not result in efficient deletion, we chose to pre-treat tumor cells in vitro with 4-hydroxytamoxifen (4OHT) prior to transplanting the tumor cells back into new NSG hosts. To delete Gfi1 from CAG-CreERT2 MG flox tumors and Lsd1 from CAG-CreERT2 Lsd1$^{fl/fl}$ MG tumors, we dissociated tumors into single cell suspension and cultured them overnight in DMEM (with L-glut, 4.5g/L glucose and sodium pyruvate), 10% FBS, and 1x Pen/Strep supplemented with either vehicle (DMSO) or 5 μM 4OHT. The following day, we washed and counted the cells. Some cells were used for orthotopic re-transplantation into NSGs to assess growth changes in vivo, while the majority of cells were re-plated in fresh media without vehicle or 4OHT for an additional 72 hours, and then collected for analysis of protein expression by Western blot.

ChIP-seq peak finding

Again, chromatin extraction, immunoprecipitation, and library preparation for ChIP-seq were all performed at Active Motif (Carlsbad, CA). Peak calling for Gfi1, Gfi1B, Lsd1 (MG) and Lsd1 (MGB) were done using MACS with default parameters and using the appropriate input chromatin controls, used in the preparation of the respective factor ChIPs. To identify the high confidence peak set for each factor, initially the peaks with the upper 20^{th} percentile enrichments were identified separately for the two replicates of the respective factor. Afterwards, resulting peaks were overlapped (at least 50% overlap) and the overlapping peaks were referred as the high confidence peak set of the respective factor.

Comparison of Gfi1, Gfi1B and Lsd1 signal at Gfi1 peaks

We quantified the coverage of Gfi1, Gfi1B, Lsd1 (MG) and Lsd1 (MGB) at each base pair in the region surrounding ± 3kb midpoint Gfi1 high confidence peaks. Read coverage was averaged in 200-bp windows along the regions and the values were scaled to arrange between 0–1. After ordering the values according to descending Gfi1 signal intensity, resulting values were represented as heat maps.

Quantitative PCR (Real-time PCR)

To validate expression of Gfi1/1b and Lsd1 target genes, mRNA was isolated from cells using an RNAeasy Plus Mini kit (Qiagen). RNA was reverse

transcribed to cDNA using iScript Reverse Transcription Supermix (Bio-Rad, cat #1708841), and duplicate no RT reactions were also prepared to confirm absence of genomic contamination. Then qPCR reactions were performed in triplicate using iQ SYBR Supermix (Bio-Rad, cat #1708882) on the Bio-Rad C1000 Thermocycler and CFX96/CFX384 systems. Relative gene expression was calculated using the ΔΔCT method and normalized to Actin. 95% confidence intervals for each sample were calculated using the sum of the squares method.

Table 4: Primer sequences for qPCR of Gfi1/1b and Lsd1 candidate target genes

Target	Sequence
Apc- Forward	CTTGTGGCCCAGTTAAAATCTGA
Apc- Reverse	CGCTTTTGAGGGTTGATTCCT
Arhgdia- Forward	AAGGACGATGAAAGCCTCCG
Arhgdia- Reverse	GGTCAGTCGAGTCACAATGACA
Bmpr1a- Forward	AACAGCGATGAATGTCTTCGAG
Bmpr1a- Reverse	GTCTGGAGGCTGGATTATGGG
Cux1- Forward	TGACCTGAGCGGTCCTTACA
Cux1- Reverse	TGGGGCCATGCCATTTACATC
Fbxo5- Forward	TTCCTACAGTCCCGTGTGTTT
Fbxo5- Reverse	AGCTCTTCTGTTTCGTTTGAACT
Gadd45g- Forward	GGGAAAGCACTGCACGAACT
Gadd45g- Reverse	AGCACGCAAAAGGTCACATTG
Gse1- Forward	CTCCCGCTTCCAACCACTC
Gse1- Reverse	AGCTTCTCAAGTAGTCCTCAGTC
Irf2bp1- Forward	GGTGCGTGAATTTCGAGGG
Irf2bp1- Reverse	CTAGGTCCTTGGAAGTCGGGT
Lrig3- Forward	CTCGGCTGAACTGGACGAAAG
Lrig3- Reverse	GCCAAGGGTATTGGACATCTCA
Nfia- Forward	TTCCAACGTCACCCATCATCC
Nfia- Reverse	CAGCATCAGGACAGACAAGTT
Smad4- Forward	ACACCAACAAGTAACGATGCC
Smad4- Reverse	GCAAAGGTTTCACTTTCCCCA
Tacc3- Forward	ACTTCCTCGTTTAAGGAGTCGG
Tacc3- Reverse	GCTCAGCTTCTGTCGGCTTT
Tgif2- Forward	ATGTCGGACAGCGATCTAGG
Tgif2- Reverse	TCCCGGAGGATCTTTACTGAC
Zmiz1- Forward	CCCCGCCAACTTCCACAAT
Zmiz1- Reverse	AGCCAAGAGTCTGTAGCCCA
Actin- Forward	CCGAGCGTGGCTACAGCTTC
Actin- Reverse	ACCTGGCCGTCAGGCAGCTC

Thymidine incorporation

MG tumor cells were cultured in 96-well plates at $5x10^4$ cells/well or 96-well half-area plates at $2.5x10^4$ cells/well. For drug treatment experiments, cells were treated with different concentrations of Cayman Chemical, cat #16439), ORY-1001 (Roche), or RN-1 (EMD Millipore, cat #489479) for 48 hrs before being pulsed with [methyl-^{3}H] thymidine (Perkin Elmer,

NET027A250UC). After 16-18 hours, cells were frozen at -80°C to stop incorporation and later harvested using a Mach IIIM manual harvester 96 (Tomtec). Incorporated radioactivity was quantitated using a Wallac MicroBeta TriLux microplate scintillation counter (Perkin Elmer). For drug treatment experiments, compound IC50s were determined using nonlinear regression analysis.

Cell TiterGlo viability assay

To determine whether Lsd1 inhibitors had toxic effects on post-mitotic neurons, we isolated granule neuron precursors from p7 C57BL6 pups and cultured $2x10^5$ cells/well in 96-well plates in differentiation media (NB/NS-21 containing 25mM glucose and 25mM potassium chloride) for 5 days. Cells were then treated with different concentrations of GSK-LSD1 (Cayman Chemical, cat #16439), ORY-1001 (Roche), or RN-1 (EMD Millipore, cat #489479) for 48 hrs. To assess viability, we used the Cell TiterGlo luminescent assay (Promega, cat #G7570) and added the reagent 1:1 to cultured cells. Bioluminescence was read using the EnVision plate reader (Perkim Elmer).

In vivo drug treatment

To prepare intracranial MG tumors for drug treatment, 3,000 tumor cells were re-transplanted into the cerebella of NSG mice. One week after injection,

the tumors were measured using in vivo bioluminescent imaging using the Xenogen Spectrum imaging system as described in section 2.1. The mice were then randomized into treatment groups according to size, and we began treatment. We treated mice with either vehicle, 0.5 mg/kg GSK-LSD1 (i.p., daily), 10 mg/kg GSK-LSD1 (i.p., 4 days on, 3 days off), 20 μg/kg ORY-1001 (oral gavage, 5 days on, 2 days off), 100 μg/kg ORY-1001 (oral gavage, 2 days on, 5 days off), or 200 μg/kg ORY-1001 (oral gavage, 1 day on, 6 days off). Tumor growth was monitored weekly via bioluminescent imaging. When mice became symptomatic from tumors, they were sacrificed.

To implant subcutaneous MG tumors into mice, we dissociated MG tumors into single cell suspension and mixed them 1:1 with growth factor-reduced (GFR) matrigel (BD Biosciences, cat # 354230). We injected 100 ul of 50,000 tumor cells into the flanks of NSG mice. One week after injection, the tumors were not very palpable yet, so we measured tumor size by in vivo bioluminescent imaging using the Xenogen Spectrum imaging system as described in section 2.1. The mice were then randomized into two groups according to tumor size, and we began treatment. We treated mice with either vehicle (4% DMSO in saline) or 10 mg/kg of GSK-LSD1 (Cayman Chemical, cat #16439) in saline. Tumor growth was monitored weekly both via bioluminescent imaging and caliper measurements. When tumors reached 2 cm in diameter, we terminated the experiment and sacrificed mice in both cohorts. Tumors were collected, weighed, and photographed.

CHAPTER 3 – Enhancer hijacking activates Gfi1 family proteins in MB

3.1 Introduction

Despite being the most prevalent and having the poorest outcomes, Group 3 and 4 are the least understood in terms of underlying genetics[14]. Prior to this study, the most prevalent driver events for Group 3 and 4 were somatic *MYC* and *MYCN* amplifications, respectively, and these were still only altered in a small percentage of tumors (*MYC*: 17%, *MYCN*: 6%)[56]. While *MYC* and *MYCN* are known oncogenes, previous work from our lab[24] and others[25] showed that simply overexpressing *Myc* did not promote malignant transformation of mouse neural progenitors, suggesting the need for a second genetic hit in addition to *MYC*. Recurrent somatic mutations in human MB tumors were even rarer though, so no other obvious driver genes had been revealed[14], and the two aforementioned studies proceeded to establish independent mouse models of Group 3 MB by combining overexpression of *Myc* with loss or inactivation of *p53*[24,25]. While both models appeared to recapitulate the human disease histologically and molecularly, further inquiry into human MB genomics indicated that p53 mutations in primary MB were actually rather uncommon[15].

In order to identify more relevant genetic drivers, we analyzed existing whole-genome sequencing (WGS) data from different MB studies[39,40] and identified a series of spatially clustered somatic genomic structural variants

(SVs) in Group 3 and Group 4 MBs. Genomic and epigenomic analyses revealed unique but consistent upregulation of *GFI1* and *GFI1B* via an SV-induced enhancer hijacking mechanism. Further functional validation in mice confirmed the oncogenic potential of these genes in MB. Together, these studies established *GFI1* and *GFI1B* as novel, highly prevalent oncogenes in Group 3 and 4 MB.

3.2 Results

3.2.1 Identification of diverse somatic variants on chromosome 9q34 correlate with increased *GFI1B* expression

Whole-genome sequencing of 137 primary Group 3 and 4 MB samples by our colleagues at the DKFZ in Heidelberg permitted a high-resolution screen for potential MB driver genes targeted by somatic SVs. While examining areas of recurrent amplifications and deletions is a well-established method for identifying somatically altered cancer genes, we expanded our search to include all classes of chromosomal rearrangements (breakpoint clusters) detectable by WGS, which included deletions, insertions, tandem duplications, amplifications, inversions, translocations, and more complex variants resulting from combinations of these different SV types. Using this approach, we were able to detect genetic loci encompassing already known,

MB-related genes like *MYC* and *MYCN* (Figure 1A), confirming that the method worked.

Among the loci where SVs were found, chromosome 9q34.13a was a novel region of particular interest. 9 of 137 (6.6%) cases had SVs mapping here, but instead of showing a predilection for one class of SV, we observed a variety of SV types at this locus: focal deletion (n=4), tandem duplication (n=3), and complex variants with inversion and focal deletions (n=2) (Figure 1B). This locus contained seven genes: *BARHL1, DDX31, GTF3C4, AK8, C9orf9, TSC1,* and *GFI1B*. Upon integrating SV status with sample-matched gene expression data, we found that cases with SVs at 9q34 had highly specific transcriptional upregulation of *GFI1B* (Figure 1C). Additional analysis of *GFI1B* expression in a large cohort of human MBs (n=727) showed that tumors with *GFI1B* activation only occurred in Groups 3 (10.7%) and 4 (3.5%) (Figure 1D). For 119 Group 3 and 4 tumors where WGS and matched expression data were available, 16 of 18 (89%) *GFI1B*-activated cases had an underlying SV (Figure 1E). For the few cases in which *GFI1B* was elevated but no SV was detected, it is possible that expression is driven by an alternative mechanism.

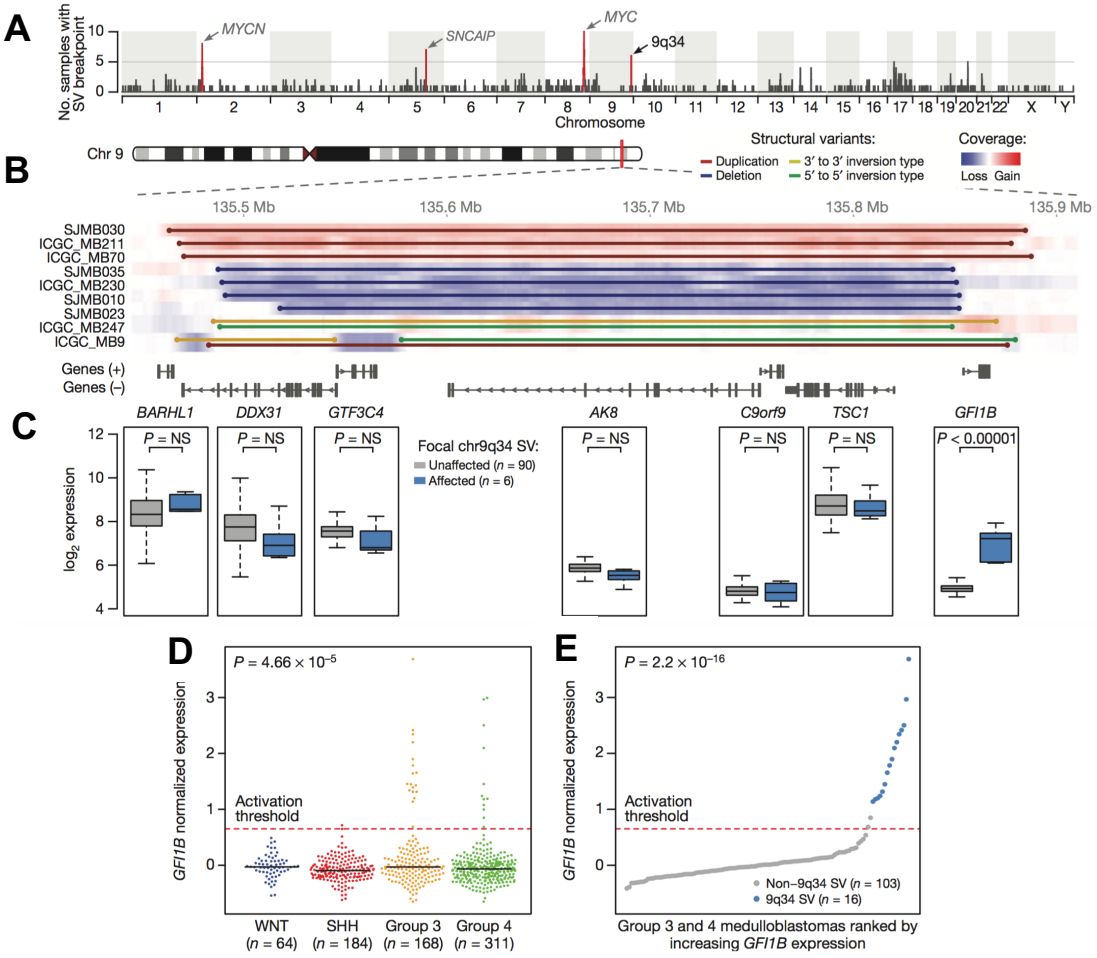

Figure 1: Recurrent SVs activate the GFI1B proto-oncogene in medulloblastoma. (A) Genome-wide SVs identified by WGS in a cohort of Group 3 and Group 4 MBs (n=137). (B) Summary of different classes of SVs affecting a common locus of aberration on chromosome 9q34. (C) Expression box-plots for the 7 genes contained within the 9q34 region of interest. Middle bar, median; lower and upper box limits, 25th and 75th percentile, respectively; whiskers, 1.5 times the interquartile range from the 25th and 75th percentiles. (D). *GFI1B* expression across medulloblastoma subgroups (n=727). Dashed indicates the threshold for detectable expression. (E) *GFI1B* expression for Group 3 and 4 MBs (n=119) colored according to 9q34 SV state. Dashed line indicates the threshold for detectable expression.

3.2.2 SV events on chromosome 9q34 reposition super-enhancer elements adjacent to *GFI1B*

To understand how SVs at 9q34 were causing *GFI1B* activation, we examined the SV-containing cases more closely. This analysis revealed that in 14 of 18 cases the SVs, irrespective of class, repositioned *GFI1B* proximal to the terminal sequence of the *DDX31* gene, which is normally located ~370 kb upstream of *GFI1B* (Figure 2A). In most samples with the SVs, *DDX31* was now just ~40 kb upstream or downstream of *GFI1B*, depending on the SV type. The pattern of SVs did not appear to indicate fusion of the promoter or coding sequence of *DDX31* to *GFI1B* as a means of transcriptional activation.

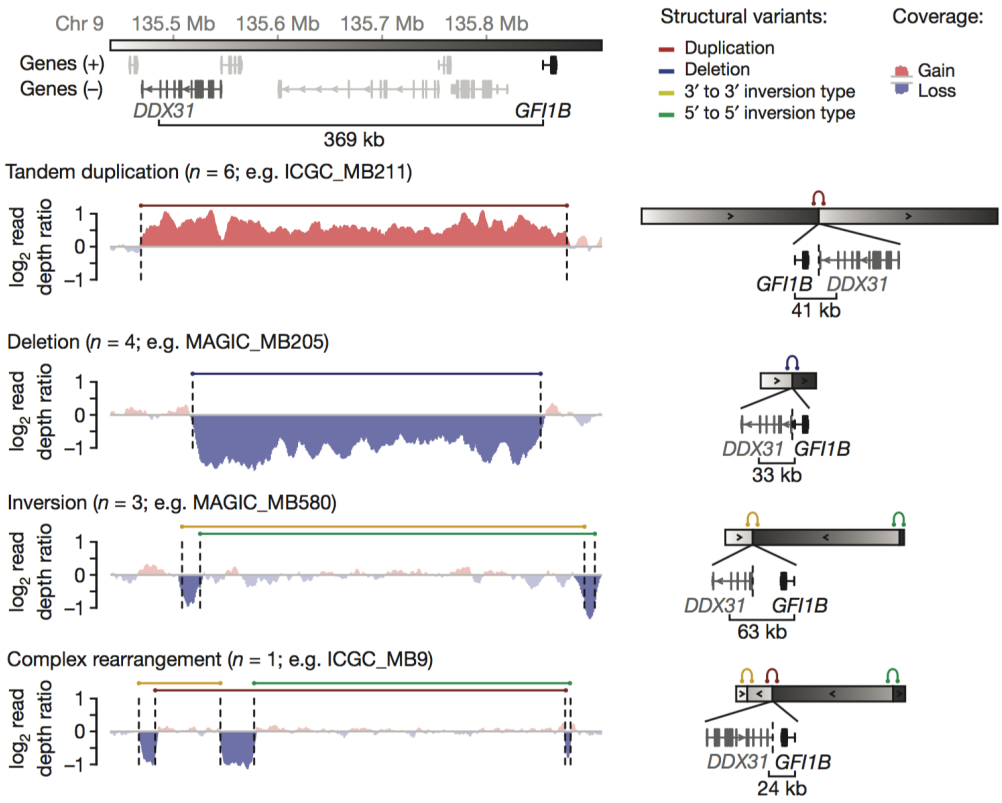

Figure 2: Summary of recurrent SVs identified in GFI1B-activated medulloblastomas. Representative WGS coverage plots and associated schematics summarizing the different SV mechanisms observed in GFI1B-activated medulloblastomas.

The repositioning of DNA elements by several hundred kilobases suggested the possibility that cis-acting regulatory elements such as enhancers might be involved. Given this possible mechanism, we examined this locus for potential enhancer activity by using chromatin immunoprecipitation sequencing for histone marks associated with active enhancers: H3K27ac and H3K9ac. In the *GFI1B*-activated tumors, strong peaks for H3K27ac and H3K9ac were seen clustered within the *DDX31* gene where the SV breakpoints occurred (Figure 3A), indicating the presence of a

super-enhancer, which has been associated with the expression of cell identity genes and master transcriptional regulators[57]. Data from whole-genome bisulfite sequencing (WGBS) also showed that DNA was hypomethylated in these super-enhancer regions, supporting the notion that the DNA in this region was in an open state and ready for transcription (Figure 3A).

To further pinpoint the enhancer region and validate its function, 2 kb fragments tiling the enhancer clusters were cloned upstream of a luciferase reporter driven by a minimal promoter. When these constructs were transfected into a Group 3 MB cell line (D425), two particular segments tested showed strong enhancer activity as they were able to upregulate luciferase reporter activity (Figure 3B). Collectively, these data suggested that SVs allowed hijacking of nearby enhancer regions within the *DDX31* gene, resulting in activation of transcription of its neighboring gene *GFI1B*.

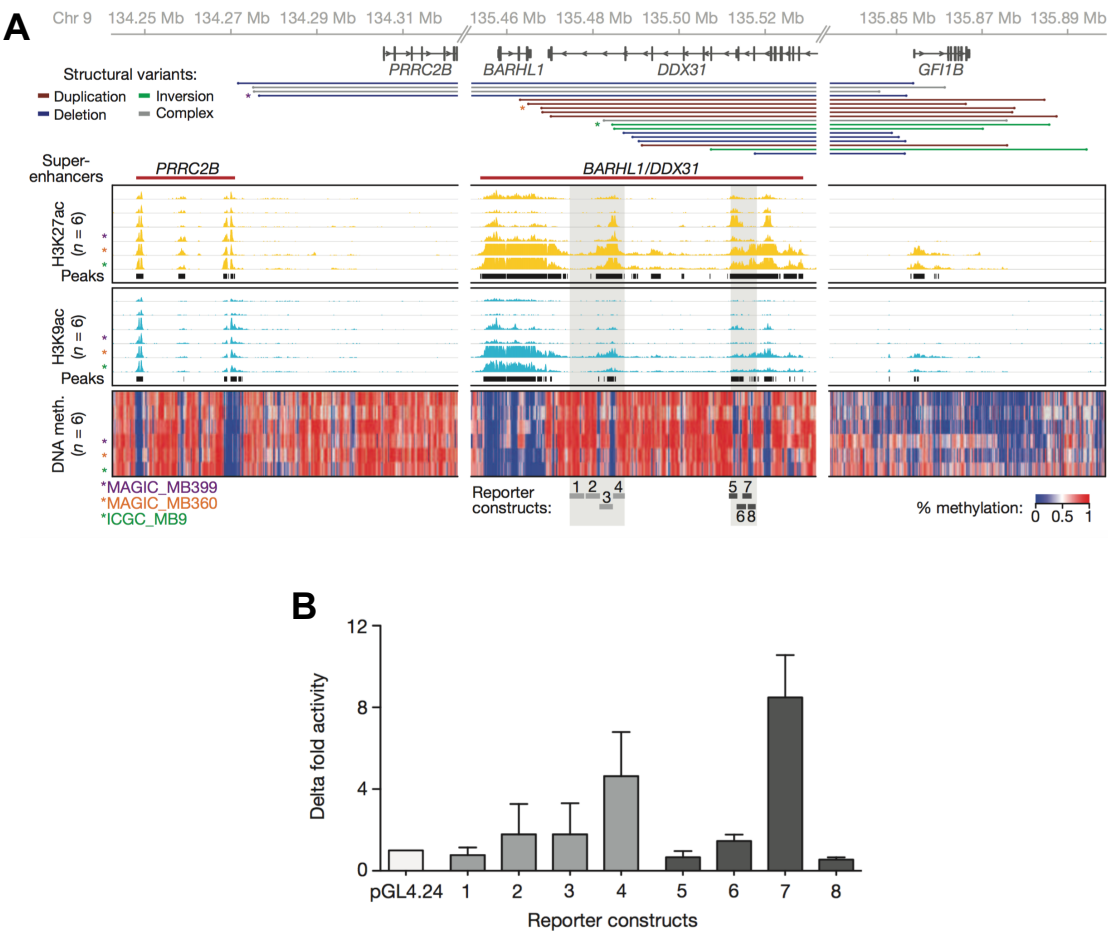

Figure 3: Recurrent SVs juxtapose GFI1B proximal to active enhancers on 9q34. (A) SV breakpoints (n=18), enhancer-histone marks (H3K27ac and H3K9ac, n=6) and whole-genome DNA methylation data (n=6) overlapping the 9q34 locus in a subset of MBs that were analyzed. (B) Luciferase reporter activity for regions within the predicted enhancers indicated in panel A. pGL4.24 is an empty vector control. Error bars are standard deviation from 3-4 independent experiments.

3.2.3 SV events also affect the *GFI1* locus

GFI1B is a close paralog of growth factor independence 1 (*GFI1*). While the two control distinct developmental processes in hematopoiesis, they have

similar molecular functions and both are potent oncogenes in certain leukemias and lymphomas[58,59]. Interestingly, analysis of expression data also uncovered activation of *GFI1* that was restricted to a subset of Group 3 MBs (29 of 724, 4.0%) (Figure 4A). Furthermore, *GFI1* and *GFI1B* expression among Group 3 and 4 tumors appeared to be mutually exclusive (Figure 4B), and together *GFI1/1B*-activated cases represented about 30% of Group 3 tumors and 5-10% of Group 4 tumors (Figure 5A, B).

To determine whether *GFI1* activation in MB could also be attributed to SV-induced enhancer hijacking, we examined WGS data around the *GFI1* locus on Chromosome 1 in Group 3 and 4 tumors (n=137). Like the *GFI1B*-activated cases, this strategy revealed 11 of 14 *GFI1*-activated cases had various SVs affecting the *GFI1* locus or surrounding genomic regions, including interchromosomal translocations (n=6), tandem duplications (n=4), and a complex rearrangement (n=1) (Figure 4C, D). Overlaying histone ChIP-seq data with breakpoint regions again revealed active enhancer-histone modification states close to the SV breakpoints (Figure 4E), suggesting that the repositioning *GFI1* into actively transcribed regions caused an increase in its expression.

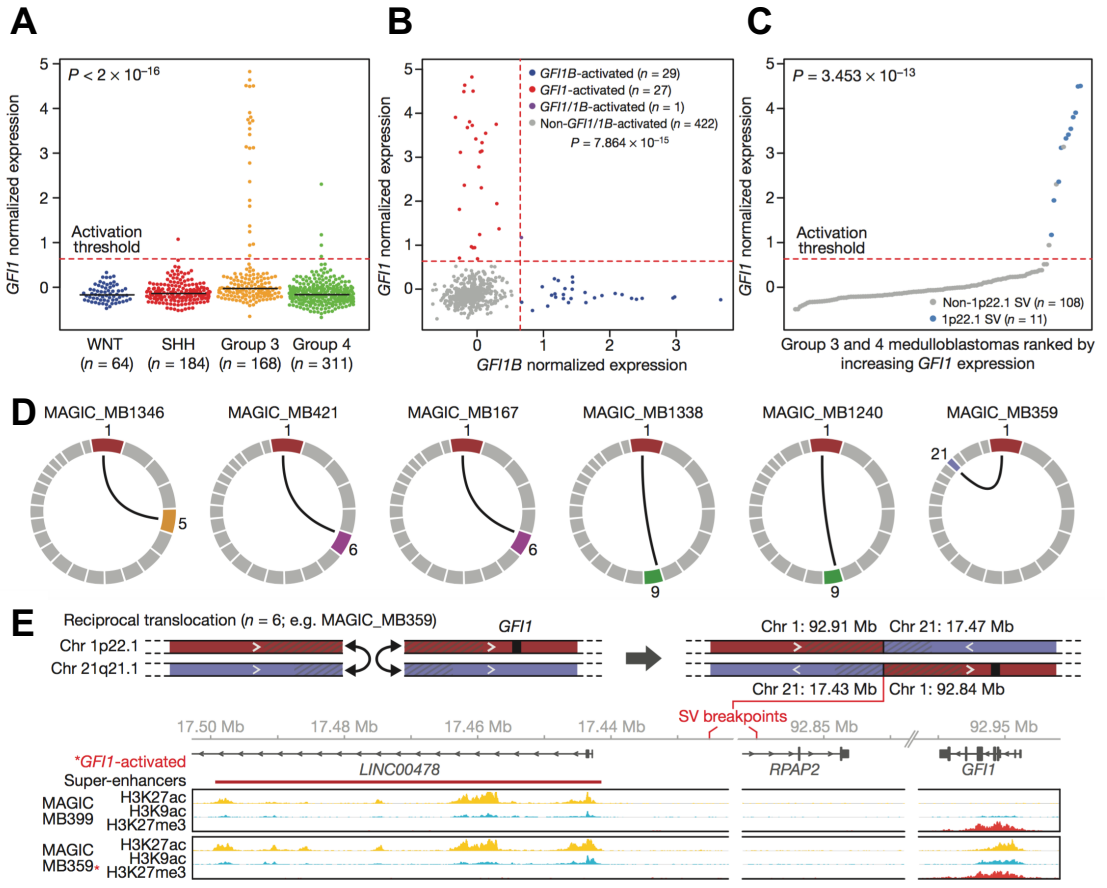

Figure 4: Mutually exclusive activation of GFI1 and GFI1B in medulloblastoma (A) *GFI1* expression is largely restricted to Group 3. (B) Expression of *GFI1* and *GFI1B* is mutually exclusive. (C) *GFI1* expression for Group 3 and 4 MBs (n=119) colored according to underlying SV state. Dashed line indicates the threshold for detectable gene expression. (D) Summary of *GFI1* translocations (n=6) observed in Group 3 MB. (E) Schematic of an example translocation observed in one *GFI1*-activated tumor (MAGIC_MB359). Histone marks overlapping the breakpoints proximal to *GFI1* and the partner chromosome translocation region for a *GFI1*-activated tumor (MAGIC_MB359) and a non-*GFI1*-activated tumor (MAGIC_MB399).

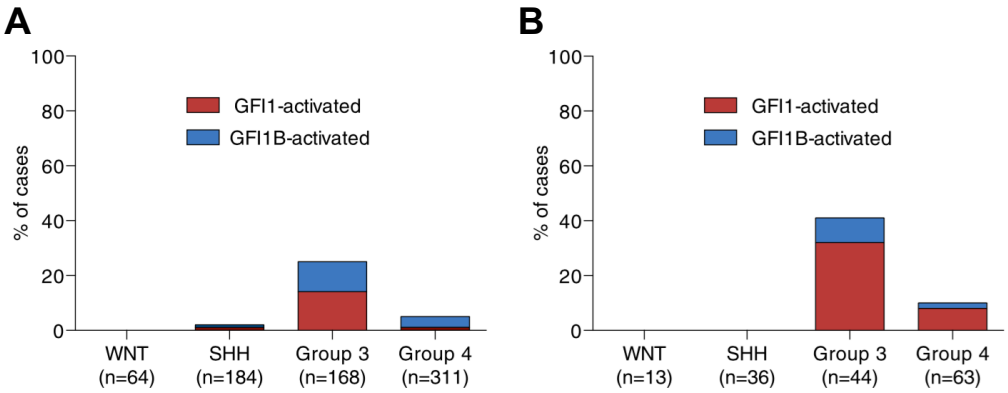

Figure 5: Frequency and distribution of GFI1/GFI1B activation in medulloblastoma subgroups. (A) Stacked bar graph shows the proportion of *GFI1/GFI1B*-activated cases in the four MB subgroups, as determined by Affymetrix gene expression profiling (n=727). (B) Stacked bar graph shows the proportion of *GFI1/GFI1B*-activated cases in the four MB subgroups, as determined by IHC with anti-GFI1 and anti-GFI1B antibodies on FFPE sections (n=156).

3.2.4 *Gfi1* and *Gfi1b* promote medulloblastoma formation in vivo

Mouse models of MB have been extremely valuable for understanding tumor biology and discovering new treatments. Currently the only two models for Group 3 involve overexpression of c-*Myc* and *Trp53* loss-of-function, which is not a combination that is typically observed in human MB, as *MYC* amplification/overexpression (Group 3) and *TP53* mutations (WNT and SHH) occur in different subgroups[14,15]. Our examination of human Group 3 tumors with *GFI1/1B* activation, however, suggested that *GFI1* and *MYC* could be a more relevant combination. Gene expression data confirmed that *GFI1/1B*-activated Group 3 tumors had upregulated *MYC* expression and *MYC* pathway

enrichment compared to that of non-*GFI1/GFI1B*-activated Group 3 tumors (Figure 6) There also appeared to be a subset of Group 3 MBs that were both *MYC* amplified and *GFI1*-activated (Figure 6). Furthermore, synergy between *Gfi1* and *Myc* has previously been observed in mouse models of T-cell lymphoma[60,61].

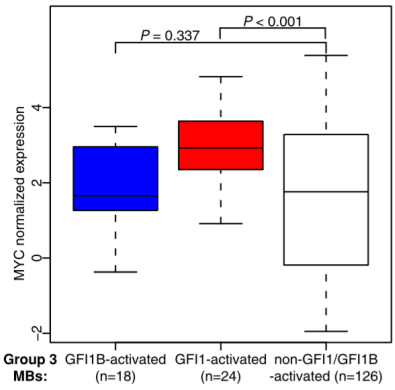

Figure 6: Association between GFI1/GFI1B activation and MYC in Group 3 medulloblastoma. *MYC* expression in Group 3 MBs (with *GFI1/1B* activation is somewhat higher than in those without *GFI1/GFI1B* activation (total n=168).

To functionally evaluate whether *GFI1* and *GFI1B* are relevant genetic drivers of MB, we used an orthotopic transplantation model, in which we isolated CD133+ neural stem cells (NSCs) from the neonatal mouse cerebellum, transduced the cells with retroviruses encoding *Gfi1* or *Gfi1b* alone or in combination with *Myc*, and transplanted them into the cerebella of immunocompromised mice (Figure 7A). Using this model, we confirmed that *Myc* overexpression alone was unable to transform NSCs into malignant tumor cells. Likewise, we found that neither *Gfi1* nor *Gfi1b* alone was sufficient to

promote tumorigenesis in this system (Figure 7C, D). When combined with *Myc*, however, both *Gfi1* and *Gfi1b* rapidly produced highly aggressive cerebellar tumors in nearly all recipient mice within 4–5 weeks (Figure 7B-D). Mice transplanted with *Myc*+*Gfi1* (MG) had a median survival of 38 days, while mice transplanted with *Myc*+*Gfi1b* (MGB) had a median survival of 26 days (Figure 7C).

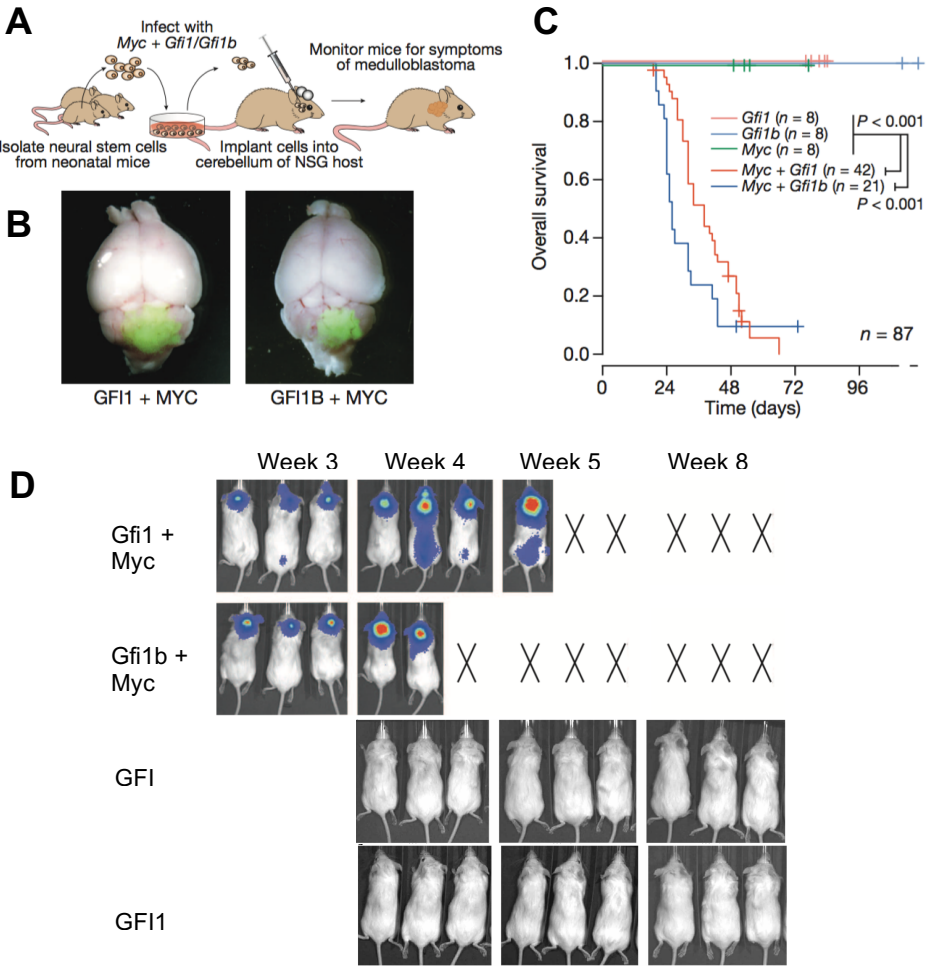

Figure 7: Gfi1 and Gfi1b cooperate with Myc to promote medulloblastoma formation in mice. (A) Strategy for evaluating *Gfi1* and *Gfi1b* as putative MB oncogenes. (B) Whole-mount images of GFP-expressing *Myc+Gfi1* (left) and *Myc+Gfi1b* (right) tumors. (C) Survival curves for animals receiving $1x10^5$ cells infected with viruses carrying the indicated genes. (D) Bioluminescent imaging of recipient animals at indicated time points. X symbols denote animals that were euthanized due to tumor symptoms.

MG and MGB tumors were collected from mice, and histological analysis showed pleomorphism, morphologically consistent with large cell, anaplastic (LCA) MB (Figure 8A, C). LCA histology is significantly more

prevalent in Group 3 medulloblastoma (20–25% of cases) than in other medulloblastoma subgroups. Metastatic dissemination was also noted in 30–50% of MG and MGB tumor-bearing mice (Figure 7D), paralleling the high frequency of metastasis seen in Group 3 MB patients. Moreover, immunofluorescence microscopy confirmed that MG and MGB tumors are highly proliferative and express neuronal but not glial lineage markers (Figure 8B, D), consistent with a MB-like phenotype. Transcriptional profiling and subsequent multidimensional scaling analysis demonstrated a notable similarity between the *Gfi1*- and *Gfi1b*-driven models and confirmed an expression signature consistent with human Group 3 MB counterparts, suggesting that these models recapitulate molecular characteristics of the human disease (Figure 8E).

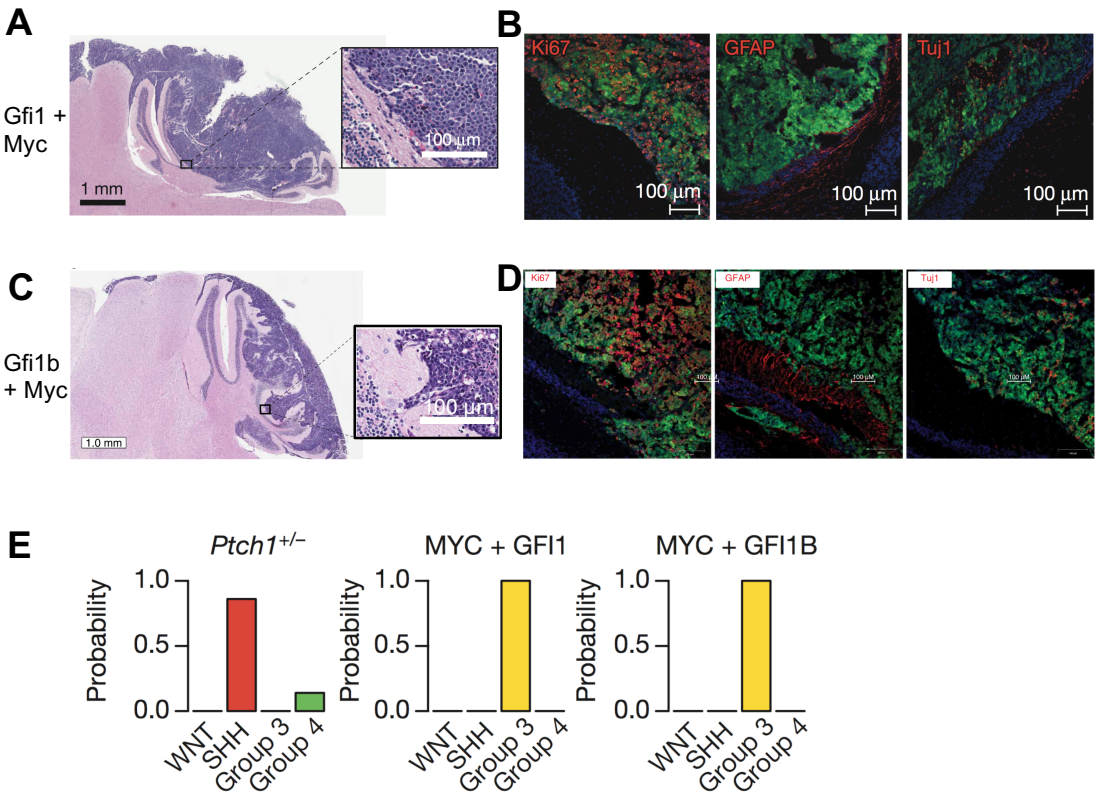

Figure 8: Myc+Gfi1 and Myc+Gfi1b tumors resemble Group 3 MB histologically and molecularly. (A, C) Hematoxylin and eosin staining of cerebellar sections derived from *Myc+Gfi1* tumor-bearing mice (A) and *Myc+Gfi1b* tumor-bearing mice (C). (B, D) Immunofluorescence imaging of *Myc+Gfi1* tumors (B) and *Myc+Gfi1b* tumors (D). (E) Subgroup probabilities for *Ptch1*$^{+/-}$*, Myc+Gfi1,* and *Myc+Gfi1b* models based on cross-species molecular classification.

3.3 Discussion

MB genomics studies have amassed a plethora of new data on human MB, but still very few recurrently mutated driver genes have been revealed for Groups 3 and 4[14], further highlighting the extensive intertumoral heterogeneity of this disease. In this study, we took advantage of whole genome sequencing

to identify somatic genomic rearrangements that were associated with mutually exclusive *GFI1* or *GFI1B* activation in about 30% of Group 3 tumors and 5-10% of Group 4 tumors. Moreover, our subsequent studies in mice functionally validated the strong oncogenic potential of *GFI1/GFI1B* as drivers of MB tumorigenesis. Together these findings now qualify *GFI1* and *GFI1B* as some of the most prevalent driver events in Group 3 MB. The common activation of these genes in Group 3 and Group 4 also reinforces the possibility that these subgroups share some biological similarities[7,8].

Identifying cancer genes that are recurrently targeted by SVs has conventionally focused on minimal common regions of aberration, and the targeted genes usually had to be included in those regions. This approach largely only accounts for genes that are either amplified or deleted, with some well-known examples in MB being *MYC* and *MYCN* amplifications[56,62]. Our current study analyzing WGS data for all types of SVs revealed a subset of MBs with alterations causing activation of *GFI1* or *GFI1B*, which unlike *MYC* and *MYCN,* are not amplified. Not only were *GFI1/GFI1B* affected by multiple classes of SVs (duplication, deletion, inversion, translocation, and complex rearrangement), but many of these SVs did not actually encompass the *GFI1* or *GFI1B* genes themselves. This raises the possibility that some oncogenic drivers may have been overlooked in other cancer genome studies, and that closer re-examination of sequencing data may yield new findings.

The fact that SVs are capable of activating *GFI1* and *GFI1B* by moving them from transcriptionally silent parts of the genome to areas with active

enhancers indicates the major effect epigenetic regulation can have on the cancer genome[44,63,64]. This mechanism is particularly interesting because it does not involve direct dysregulation of the epigenome, but rather the misappropriation or “hijacking” of an existing, normal epigenetic regulatory element. While this is the first report of SV-induced enhancer hijacking in brain tumors, similar processes of oncogene activation were first observed in various hematological neoplasms[65,66]. One of the best-studied examples occurs in follicular lymphoma, where translocations reposition *BCL2* near enhancer regions belonging to the immunoglobulin IgH gene[67,68]. Likewise, another translocation commonly observed in Burkitt’s lymphoma results in the juxtaposition of the *c-MYC* oncogene to the IgH locus[69-71]. Studies that surfaced more recently have now also begun to report oncogene activation through enhancer hijacking in other solid cancers such as lung adenocarcinoma[72], endometrial carcinoma[72], and adenoid cystic carcinoma[73].

The importance of *GFI1/1B* in normal hematopoietic development, as well as their potential for promoting leukemia[74-76] and lymphoma[58,59], has long been recognized. Lesser known functions for *GFI1* also extend into the nervous system[77,78], lung[79], and gut[80], but information on *GFI1/1B* involvement in the brain and in brain tumors has been scarce. Our finding that aberrant overexpression of *GFI1/1B* can drive some subtypes of MB is novel and substantiates the need to further understand the roles of these genes in the brain and their effects on neural progenitors. The synergy we reported between *Gfi1/1b* and *Myc* is not entirely surprising, since *Gfi1* and *Myc*

cooperation has been seen before in lymphomagenesis[61,81]. The fact that neither *Myc* nor *Gfi1/1b* expression alone was sufficient to generate MB in mice suggests they have complementary functions. Indeed, observations from the tumor model combining *Myc* and *p53* loss of function (MP) implied that *Myc* overexpression promoted proliferation but also cell death, which was dampened by the anti-apoptotic effects associated with co-expression of a dominant negative *p53*[24]. Going forward, it will be interesting to determine whether *Gfi1/1b* also regulate *p53* in the MG and MGB models.

While 30% of Group 3 and 10% of Group 4 MB are *GFI1/1B*-activated, it is clear that genetic drivers for a significant proportion of Group 3 and 4 tumors remain unaccounted for. The huge amount of data gleaned from MB genomics provides clues to potential mechanisms of tumorigenesis, but the functional relevance of so many of these indications has not been tested yet. Our study attests to the value of integrating genomic findings with functional assays, and future studies aimed at validating new candidate genes, perhaps with large-scale functional screens, will be necessary for understanding and developing unique therapies for other subsets of MB.

3.4 Acknowledgements

Chapter 3 contains material that also appears in Nature 2014: Northcott, Paul A.*; Lee, Catherine*; Zichner*, Thomas; Stütz, Adrian M.; Erkek, Serap; Kawauchi, Daisuke; Shih, David J.H.; Hovestadt, Volker;

Zapatka, Marc; Sturm, Dominik; Jones, David T.W.; Kool, Marcel; Remke, Marc; Cavalli, Florence M.G.; Zuyderduyn, Scott; Bader, Gary D.; VandenBerg, Scott; Esparza, Lourdes Adriana; Ryzhova, Marina; Wang, Wei; Wittman, Andrea; Stark, Sebastian; Sieber, Laura; Seker-Cin, Huriye; Linke, Linda; Kratochwil, Fabian; Jäger, Natalie; Buchhalter, Ivo; Imbusch, Charles D.; Zipprich, Gideon; Raeder, Benjamin; Schmidt, Sabine; Diessl, Nicolle; Wolf, Stephan; Wiemann, Stefan; Brors, Benedikt; Lawerenz, Chris; Eils, Jürgen; Warnatz, Hans-Jörg; Risch, Thomas; Yaspo, Marie-Laure; Weber, Ursula D.; Bartholomae, Cynthia C.; von Kalle, Christof; Turányi, Eszter; Hauser, Peter; Sanden, Emma; Darabi, Anna; Siesjö, Peter; Sterba, Jaroslav; Zitterbart, Karel; Sumerauer, David; van Sluis, Peter; Versteeg, Rogier; Volckmann, Richard; Koster, Jan; Schuhmann, Martin U.; Ebinger, Martin; Grimes, H. Leighton; Robinson, Giles W.; Gajjar, Amar; Mynarek, Martin; von Hoff, Katja; Rutkowski, Stefan; Pietsch, Torsten; Scheurlen, Wolfram; Felsberg, Jörg; Reifenberger, Guido; Kulozik, Andreas E.; von Deimling, Andreas; Witt, Olaf; Eils, Roland; Gilbertson, Richard J.; Korshunov, Andrey; Taylor, Michael D.; Lichter, Peter; Korbel, Jan O.; Wechsler-Reya, Robert J.; Pfister, Stefan M., Macmillan Publishers Limited, 2014. The dissertation author was one of three primary investigators and co-first-authors of this paper. Our collaborators provided the human MB tumors and all of the corresponding genomic analysis.

CHAPTER 4 – Kdm1a (Lsd1) is required for growth of Gfi1-driven medulloblastoma

4.1 Introduction

While the majority of Group 3 tumors exhibit amplification or overexpression of the *MYC* oncogene, previous reports in mice have indicated that *Myc* overexpression is insufficient to promote MB tumorigenesis by itself[24,25]. As described in Chapter 3, we recently identified a subset of Group 3 tumors that upregulate the Growth factor independence 1 (*GFI1*) family genes via an enhancer hijacking mechanism. We furthermore confirmed that overexpression of *Myc* and either *Gfi1* or *Gfi1b* was sufficient to transform mouse neural progenitors into tumors resembling Group 3 MB[82].

The GFI1 family of proteins, consisting of GFI1 and GFI1B, are known transcriptional repressors that are crucial for normal hematopoietic development[83-88]. Not surprisingly, the dysregulation of these proteins has been found to promote some types of leukemias and lymphomas[89,90]. While the oncogenic potential of Gfi1 itself is relatively low, the ability to cooperate strongly with Myc was also seen in lymphomagenesis[61]. In these systems, Gfi1/1b have been linked to possible downregulation of p53 and p53 effectors, such as p21 and Bax[89-91]. A recent study of acute lymphoblastic leukemia suggested that Gfi1 directly antagonizes p53 and that deletion of Gfi1 in the cancer cells cured mice of leukemia[89].

The transcriptional repressor activity of GFI1/1B is thought to depend on its assembly of a co-repressor complex made up of epigenetic modifiers like lysine demethylase 1A (KDM1A/LSD1) and histone deacetylases (HDACs)[92-94]. Together these proteins remove active transcriptional marks while applying repressive ones to *GFI1/1B* target genes[93,95-97]. Thus far, the roles of Gfi1/1b have not been studied in the context of MB, and we presently aim to elucidate the mechanisms by which they contribute to MB development. Understanding the basis for Gfi1/1b-mediated tumorigenesis will provide insight into MB pathogenesis as well as potential therapeutic targets for the future.

4.2 Results

4.2.1 Gfi1 is required for tumor maintenance

Although Gfi1 expression is essential for tumor initiation in combination with c-Myc[82], it is unknown whether continued expression is required following establishment of a tumor. To investigate its role in tumor maintenance, we designed a retroviral vector encoding loxp-Gfi1-loxp-IRES-GFP (floxed Gfi1), where Gfi1 is deleted upon expression of Cre protein. We isolated CD133+ cerebellar neural stem cells (NSCs)[21] from CAG-CreERT2 mice and infected them with viruses encoding c-Myc-IRES-luciferase and floxed Gfi1. Orthotopic transplantation of the cells into NSG mice led to tumor growth within 5 weeks,

which was no different compared to what was observed for normal MG tumors generated from wild type (WT) cells[82] (Figure 7C).

To delete Gfi1 in the resulting tumors, we dissociated them into single cell suspensions and cultured them overnight with vehicle (DMSO) or 4-hydroxytamoxifien (4OHT). The following day, we washed the cells and divided up the samples for in vitro and in vivo assays. The majority of cells were re-plated in fresh media without vehicle or 4OHT for an additional 72 hours, and then collected for assessment of Gfi1 protein. We found that levels of Gfi1 protein in 4OHT-treated tumor cells was significantly reduced, whereas the Gfi1 protein remained present in the vehicle-treated cells (Figure 9A).

To assay the effects of Gfi1 loss on tumor cell growth after Gfi1 deletion, we re-transplanted the treated tumor cells into new NSG hosts and monitored tumor growth. Mice that received 4OHT-treated cells no longer developed tumors whereas those that received vehicle-treated cells still quickly developed tumors (Figure 9B, C). The experiments described here have only been carried out once and still need to be repeated to ensure reproducibility, but the preliminary results suggest that MG tumors depend on Gfi1 expression for maintenance of tumor growth in vivo.

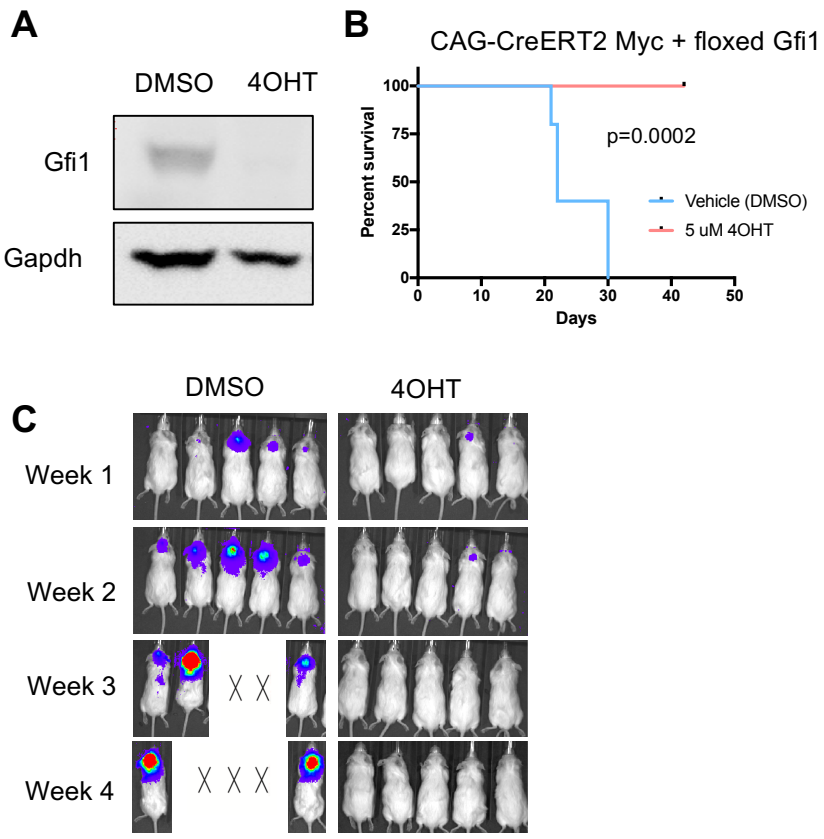

Figure 9: Gfi1 is required for maintenance of Myc+Gfi1 tumors. (A) Western blot of CAG-CreERT2 Myc + floxed Gfi1 tumor cells after treatment with vehicle or 4OHT (B) Survival curve of mice transplanted with CAG-CreERT2 Myc + floxed Gfi1 tumor cells treated with vehicle control (DMSO, n=6) or 4OHT (n=8). (C) Bioluminescent images of mice curve of mice transplanted with CAG-CreERT2 Myc+ floxed Gfi1 tumor cells treated with vehicle control (DMSO) or 4OHT.

4.2.2 Gfi1 recruits the cofactor Lysine demethylase 1 (Lsd1) in Gfi1-driven MB

The studies described above demonstrate the importance of Gfi1-family proteins in MB initiation and maintenance, but the mechanisms by which these proteins promote tumor growth remain unclear. Studies in the hematopoietic

system suggest that Gfi1/1b repress target genes via their interactions with various co-factor proteins, including the histone lysine demethylase Kdm1a (Lsd1)[92-94], the corepressor coREST[92,93], and the histone deacetylases HDAC1 and HDAC2[96,98]. These protein interactions with Gfi1 have not yet been described in MB, but we hypothesized that they may also be involved in epigenetic regulation in Gfi1-driven MB. To test this, we performed co-immunoprecipitation (coIP) experiments for these proteins in MG tumors. After immunoprecipitation (IP) of Gfi1, we detected interactions with Lsd1 and coREST by Western blot (Figure 10A), but we did not observe HDAC1 or HDAC2 (Figure 10D). The reverse IPs of Lsd1 and coREST yielded similar results, showing interactions with each other as well as with Gfi1 (Figure 10B, C). Interestingly, in all of the IPs, the amount of Gfi1 protein pulled down was comparable to the total input, suggesting the majority of Gfi1 in the tumor cells complexes with Lsd1 and coREST. This was in stark contrast to Lsd1, where the amount of Lsd1 detected in the Gfi1 and coREST IPs appeared to be only a small fraction of the total Lsd1, perhaps suggesting that Lsd1 is also occupied by partners other than Gfi1. These data confirm that Gfi1 interacts with the epigenetic coregulators Lsd1 and coREST in Gfi1-driven MB.

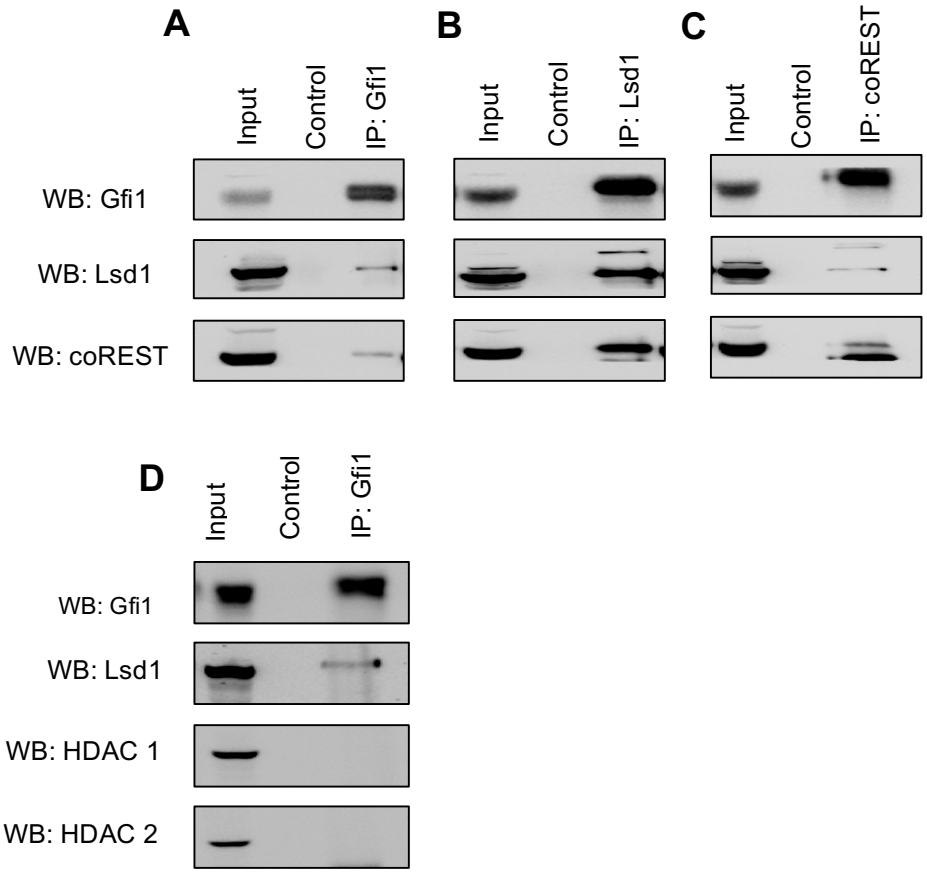

Figure 10: Gfi1 binds co-repressor proteins Lsd1 and coREST in Gfi1-driven medulloblastoma. (A-C) Co-immunoprecipitations of Gfi1 (A), Lsd1 (B), and coREST (C) from Myc+Gfi1 (MG) mouse tumor cells. (D) Immunoprecipitation of Gfi1 and detection for Lsd1 and HDACS 1 and 2 in MG tumor cells.

4.2.3 The SNAG domain is critical for Gfi1-driven tumorigenesis

Given that Gfi1 is involved in both tumor initiation and maintenance (Figure 9), we investigated the basis of its tumor-promoting properties. Previous studies have shown that the Gfi1 family proteins contain a highly

conserved N-terminal SNAG domain that is important for protein-protein interactions and six C-terminal zinc fingers that are involved in DNA binding[99,100] (Figure 11A). To determine if the functions of these domains are required for tumorigenesis, we utilized mutant *Gfi1* constructs and tested their ability to generate tumors in combination with *Myc*. The Gfi1 SNAG mutant encodes a proline to alanine change at amino acid position 2 (*Gfi1*-P2A) and results in a full-length protein (Fig 11B) with a non-functional SNAG domain[101]. We co-infected NSCs with *Myc* and the *Gfi1*-P2A mutant, transplanted them into NSG mice, and monitored for tumor growth. While *Myc* + WT *Gfi1*-transduced cells steadily expanded into tumors as expected, *Myc* + *Gfi1*-P2A-transduced cells did not. By 4-5 weeks, mice with WT *Gfi1* had to be sacrificed, whereas mice with *Gfi1*-P2A were monitored for 7 months with no signs of tumor development (Figure 12A, B).

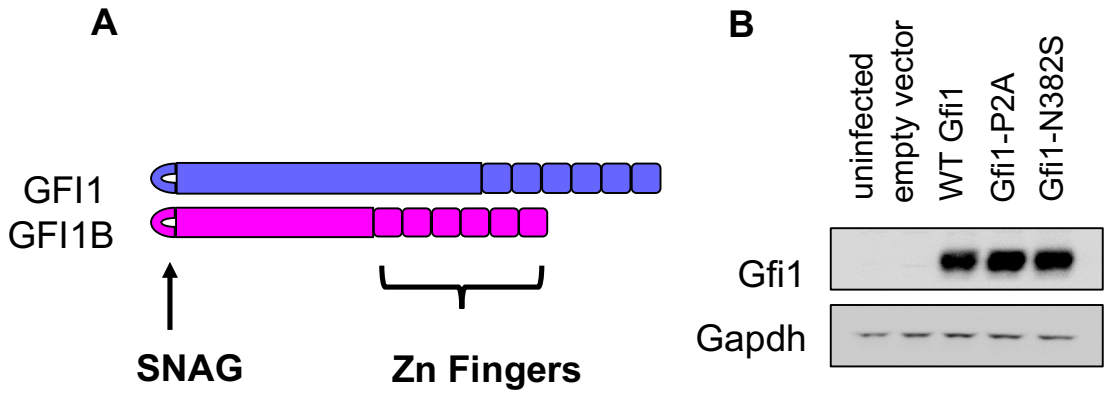

Figure 11: Gfi1 and Gfi1 contain a SNAG domain and a zinc finger domain. (A) Illustration showing the highly conserved SNAG and Zinc finger domains of Gfi1 and Gfi1b. (B) Retroviral constructs encoding the wildtype (WT), the SNAG mutant (Gfi1-P2A), and the zinc finger mutant (Gfi1-N382S) encode full-length Gfi1 proteins at similar levels of overexpression.

We simultaneously tested a Gfi1 zinc finger mutant that encodes an asparagine to serine change at amino acid position 382 (*Gfi1*-N382S). This mutation results in a full-length protein (Figure 11B) that can no longer bind DNA[102,103]. NSCs were infected with *Myc* + *Gfi1*-N382S and orthotopically transplanted into mice. Instead of completely abrogating tumor growth as seen with the *Gfi1*-P2A construct, *Gfi1*-N382S was still capable of cooperating with Myc to transform NSCs into tumors, albeit with a slightly longer latency (median survival= 43 days) than WT Gfi1 (median survival= 27 days, Figure 12A, B). These results strongly suggest that the ability of Gfi1 to recruit and interact with other proteins is essential for its oncogenic activity, while its DNA-binding activity is not necessarily required. Furthermore, the different results in tumor development and latency do not appear to be due to unequal levels of protein expression, since Western blot analysis of cells infected with equal amounts of virus confirmed similar levels of protein overexpression (Figure 3B).

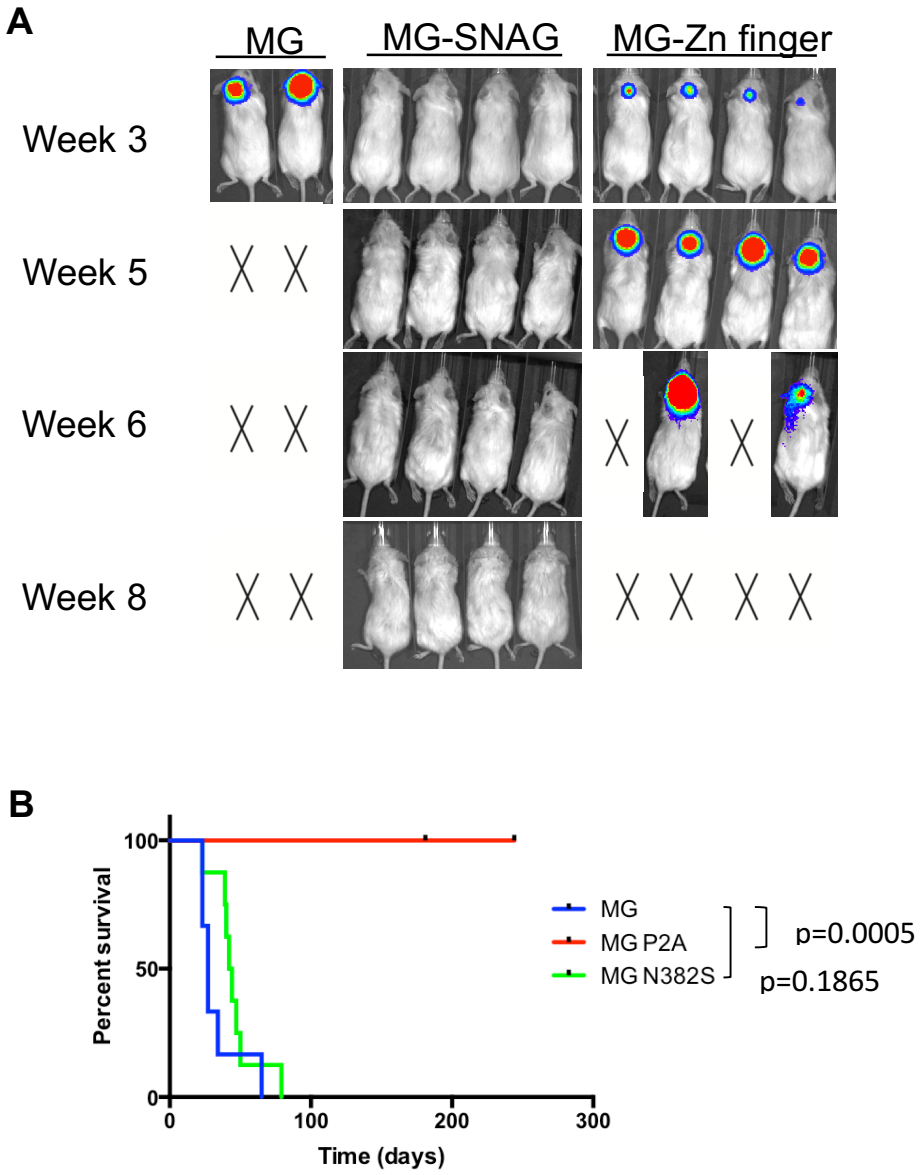

Figure 12: The SNAG domain of Gfi1 is critical for Gfi1-driven tumorigenesis in mice. (A) Bioluminescent images of mice transplanted with Myc+Gfi1 (MG), Myc+Gfi1 P2A (MG P2A), and Myc+Gfi1 N382S (MG N382S). (B) Survival of mice transplanted with MG (n=6), MG P2A (n=6), and MG N382S (n=8).

4.2.4 Genetic deletion of Lsd1 impairs growth of Gfi1-driven MB

The findings described above demonstrate that the SNAG domain is required for Gfi1-driven tumorigenesis and that Lsd1 is found to physically interact with Gfi1. Because the SNAG domain is responsible for recruiting proteins like Lsd1, we were interested in determining whether Lsd1 was required for growth of MG tumors. To genetically control Lsd1 expression in tumors, we bred CAG-CreERT2 mice with $Lsd1^{fl/fl}$ mice[55] to yield CAG-CreERT2; $Lsd1^{fl/fl}$ pups. We isolated NSCs from the pups and transduced them with *Myc* and *Gfi1* to generate CAG-CreERT2; $Lsd1^{fl/fl}$ MG tumors. We initially attempted to activate CreERT2 by administering tamoxifen directly to tumor-bearing mice via intraperitoneal (i.p.) injections. But while there was a delay in tumor growth in tamoxifen-treated mice, these animals did develop tumors, and the difference in survival between control and tamoxifen-treated mice was not as significant as we had expected ($p=0.0104$) (Figure 13A). Moreover, when mice were sacrificed, all tumors were found to express similar levels of Lsd1 protein regardless of treatment (Figure 13B). We suspected that in vivo treatment with tamoxifen was not efficiently reaching tumor cells in the brain and therefore not efficiently deleting Lsd1.

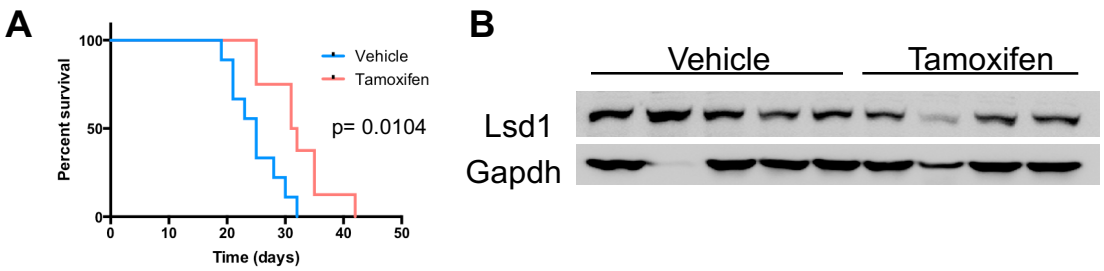

Figure 13: In vivo tamoxifen treatment does not efficiently delete Lsd1 or inhibit the growth of MG tumors. (A) Survival curve of mice with CAG-CreERT2 Lsd1$^{fl/fl}$ MG cells treated with vehicle (corn oil) (n=10) or tamoxifen (n=10) via i.p. injections. (D) Western blot for Lsd1 in tumors resulting after 3 weeks of treatment.

To be sure that tamoxifen was working, we conducted a follow-up experiment in which we administered three doses of vehicle or tamoxifen to tumor-bearing mice at two-day intervals (0, 48, and 96 hours) and sacrificed them at two time points (72 and 120 hours) (Figure 14A). Analyzing the tumors by Western blot confirmed that tamoxifen treatment was working to delete Lsd1 but that residual Lsd1 protein remained (Figure 14B). Presumably, the cells that had escaped deletion continued to grow, allowing tamoxifen-treated mice to develop tumors and diminishing the overall difference in survival between groups.

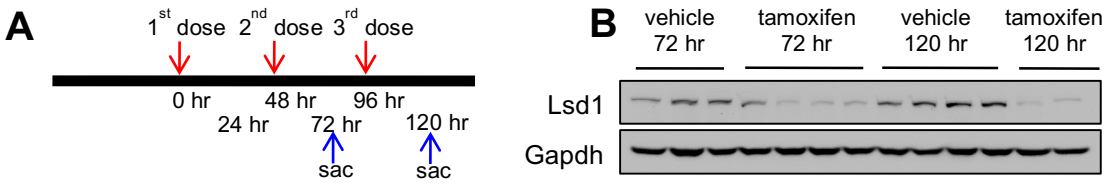

Figure 14: In vivo, short-term tamoxifen treatment deletes Lsd1. (A) Timeline of tamoxifen treatments and sacrifice of mice for tumor collection. (B) Western blot for Lsd1 in tumors harvested at 72 and 120 hrs after first tamoxifen treatment.

Since in vivo tamoxifen treatment did not efficiently eliminate Lsd1, we tested the effects of treating with tamoxifen in vitro. We harvested CreERT2; $Lsd1^{fl/fl}$ MG tumor cells and cultured them overnight with either vehicle (DMSO) or 4-hydroxytamoxifen (4OHT). Assaying the cells at 96 hours showed significantly less Lsd1 protein in 4OHT-treated cells compared to DMSO-treated cells (Figure 15A). After initiating deletion of Lsd1 in vitro, we transplanted the cells back into NSG mice to monitor effects on tumor growth. All mice that received vehicle-treated tumor cells developed tumors, with a median survival of 17 days, while only about 30% of those that received 4OHT-treated tumor cells developed tumors, and did so with an increased latency (Figure 15B, C). In the tamoxifen-treated mice that did develop tumors, there was no detectable difference in Lsd1 protein levels compared to tumors from vehicle-treated mice (Figure 15D), again suggesting that the tumors that developed after being treated with 4OHT were most likely from cells that had escaped Lsd1 deletion.

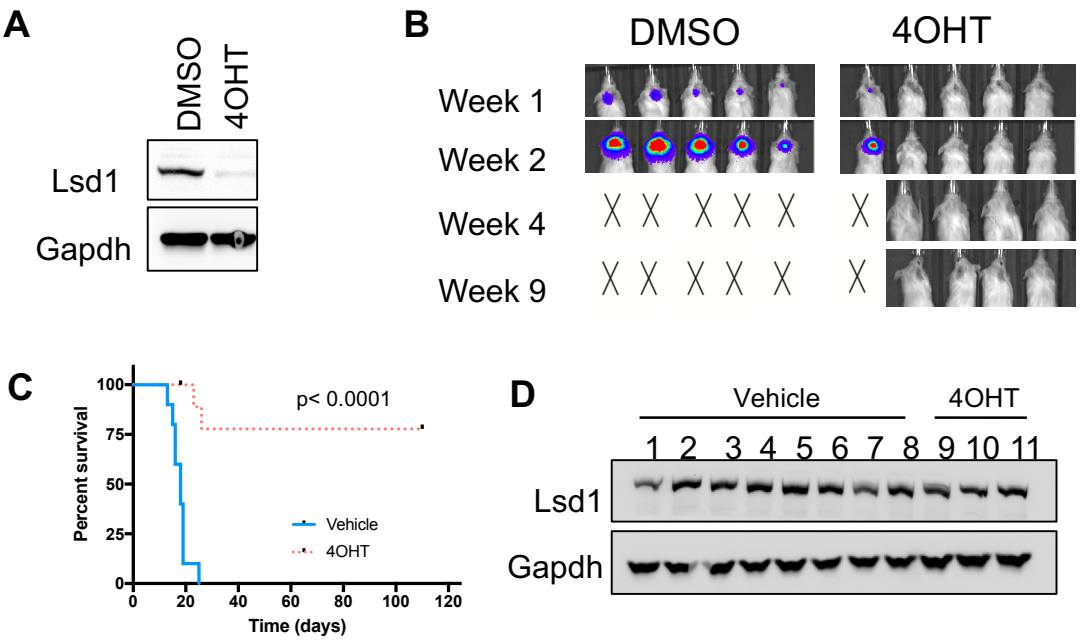

Figure 15: Genetic deletion of Lsd1 inhibits the growth of MG tumor cells in vivo. (A) Western blot for Lsd1 in CAG-CreERT2 Lsd1$^{fl/fl}$ MG tumor cells 96 hrs after treatment with vehicle (DMSO) or 5uM 4OHT in vitro. (B) Bioluminescent imaging of mice re-transplanted with CAG-CreERT2 Lsd1$^{fl/fl}$ MG cells treated with vehicle or 4OHT. (C) Survival curve of mice re-transplanted with CAG-CreERT2 Lsd1$^{fl/fl}$ MG cells treated with vehicle (n=10) or 4OHT (n=10). (D) Western blot for Lsd1 in tumors resulting after re-transplant.

To rule out the possibility that the effect on tumor growth was a direct result of 4OHT treatment, as opposed to deletion of Lsd1, we carried out parallel experiments using MG tumor cells from mice carrying floxed Lsd1 but no CreERT2. Treatment of these tumor cells with 4OHT did not activate CreERT2 and consequently did not delete Lsd1 (Figure 16A). Both groups of mice receiving vehicle- or 4OHT-treated tumor cells developed tumors, with no difference in penetrance or latency (Figure 16B). Overall, these experiments show that Lsd1 plays a critical role in Gfi1-driven tumorigenesis.

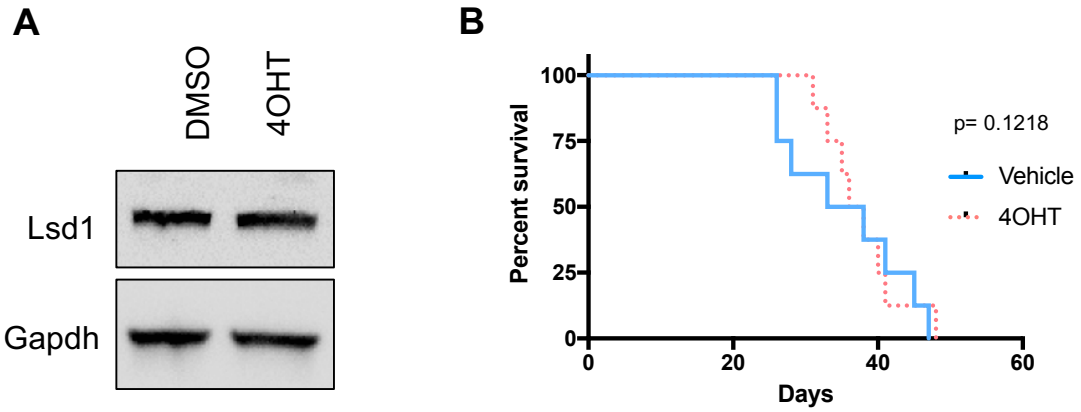

Figure 16: Tamoxifen treatment does not affect growth of Lsd1$^{fl/fl}$ MG tumors. (A) Western blot for Lsd1 in Lsd1$^{fl/fl}$ MG tumor cells 96 hrs after treatment with vehicle (DMSO) or 5uM 4OHT in vitro. (B) Survival curve of mice re-transplanted with Lsd1$^{fl/fl}$ MG cells treated with vehicle (n=8) or 4OHT (n=8).

4.2.5 Gfi1-driven tumorigenesis is not mediated by repression of the p53 pathway

The studies above indicated that Gfi1 relies on its ability to interact with Lsd1 to promote tumor formation, but the precise mechanisms and signaling pathways that are affected by Gfi1 and its cofactors remain unknown. In hematopoietic model systems, several groups have reported that Gfi1 can repress the p53 pathway[89,90,104-106]. Furthermore, two previously established models of MB showed that combining *Myc* overexpression with *p53* loss of function[24,25] resulted in tumors resembling human Group 3 MB. To assess whether Gfi1 might be suppressing the p53 pathway in the MG model, we used doxorubicin and γ-irradiation to elicit p53-dependent responses (Figure

17B, D). MG tumor cells were isolated and treated with 0, 0.1, and 0.5 μM doxorubicin (Figure 17B) or with 0, 2, and 8 Gray (Gy) of γ-irradiation (Figure 17D). All samples were analyzed by Western blotting to look for p53 pathway activity, and a dose dependent increase in levels of p53 protein and its target p21 were observed for both treatments and at both time points (Figure 17B, D). Positive control experiments carried out in mouse embryonic fibroblasts (MEFs) containing wildtype p53 confirmed that the changes observed in response to doxorubicin and γ-irradiation were representative of an active p53 pathway (Figure 17A, C). We are currently carrying out similar experiments using MP tumor cells and MG tumor cells engineered to overexpress *DNp53*; in both of these cell types, dominant negative p53 should repress p53 function, and thus we would not expect to see induction of p53 targets. The data we have so far suggest that the p53 pathway can be activated in MG tumor cells and that repression of p53 and p53 target genes may not be the underlying mechanism of Gfi1-driven tumorigenesis.

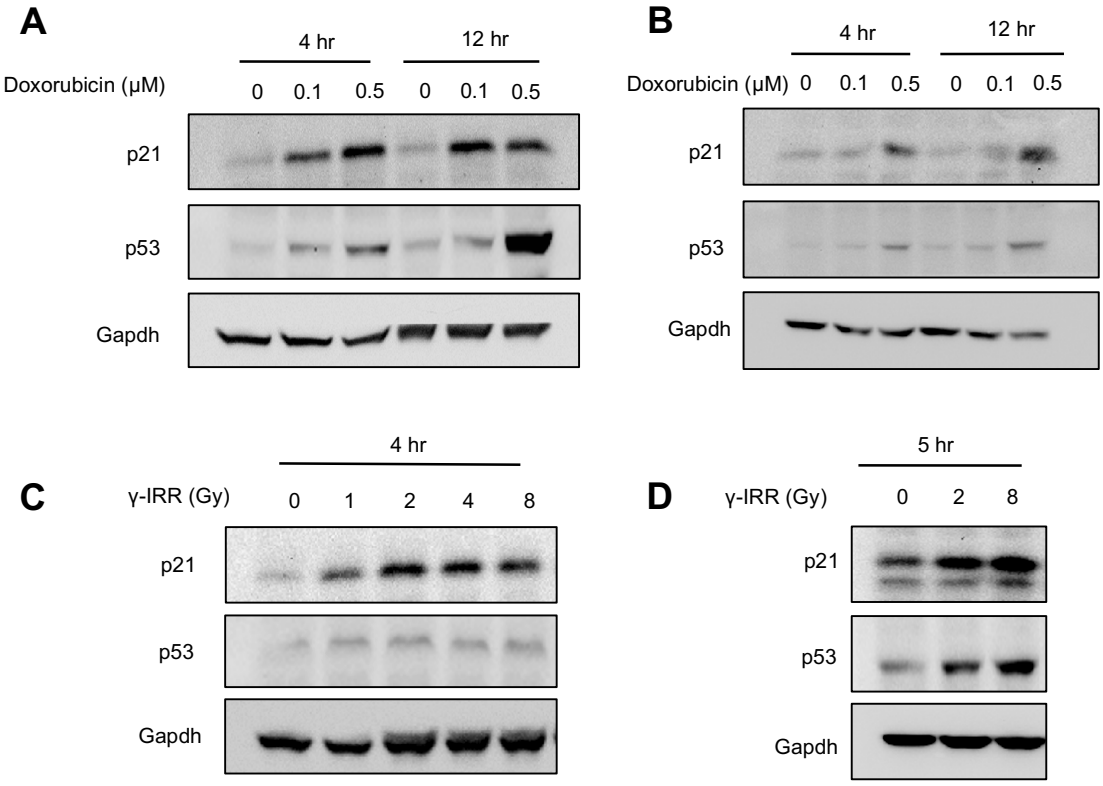

Figure 17: Gfi1-driven tumorigenesis is not mediated by repression of the p53 pathway. (A) Western blot of wildtype MEFs treated with increasing doses of doxorubicin and collected at 4 and 12 hrs. (B) Western blot of MG tumor cells treated with increasing doses of doxorubicin and collected at 4 and 12 hrs. (C). Western blot of wildtype MEFs treated with increasing doses of radiation and collected at 4 hrs. (D) Western blot of MG tumor cells treated with increasing doses of doxorubicin and collected at 5 hrs.

4.2.6 Gfi1/1b and Lsd1 co-regulate many common loci in tumor cells

Since p53 pathway activation appears to remain intact in MG tumor cells, we sought to identify other potential mechanisms by which Gfi1 might contribute to tumorigenesis. By performing ChIP-seq of Gfi1 and Gfi1b in MG and MGB tumors, respectively, we identified the genetic loci bound by these

proteins (Figure 18A-D). Because we determined that Gfi1 associates with and depends on Lsd1 in MG tumors, we also carried out Lsd1 ChIP-seq in both MG and MGB tumors (Figure 18A-D). Peak calling identified 4,311 genes bound by Gfi1, 3,222 genes bound by Gfi1b, 5,038 genes bound by Lsd1 in MG, and 6,338 genes bound by Lsd1 in MGB (Figure 18B). We presumed that Lsd1 likely regulates a wide range of target genes and may have functions independent of Gfi1, so we compared the loci that were common between Gfi1 and Lsd1 in MG tumors and between Gfi1b and Lsd1 in MGB tumors. This analysis revealed a significant overlap of genes in both models: 3,452 co-occupied genes in MG and 2,196 co-occupied genes in MGB (Figure 18B-D).

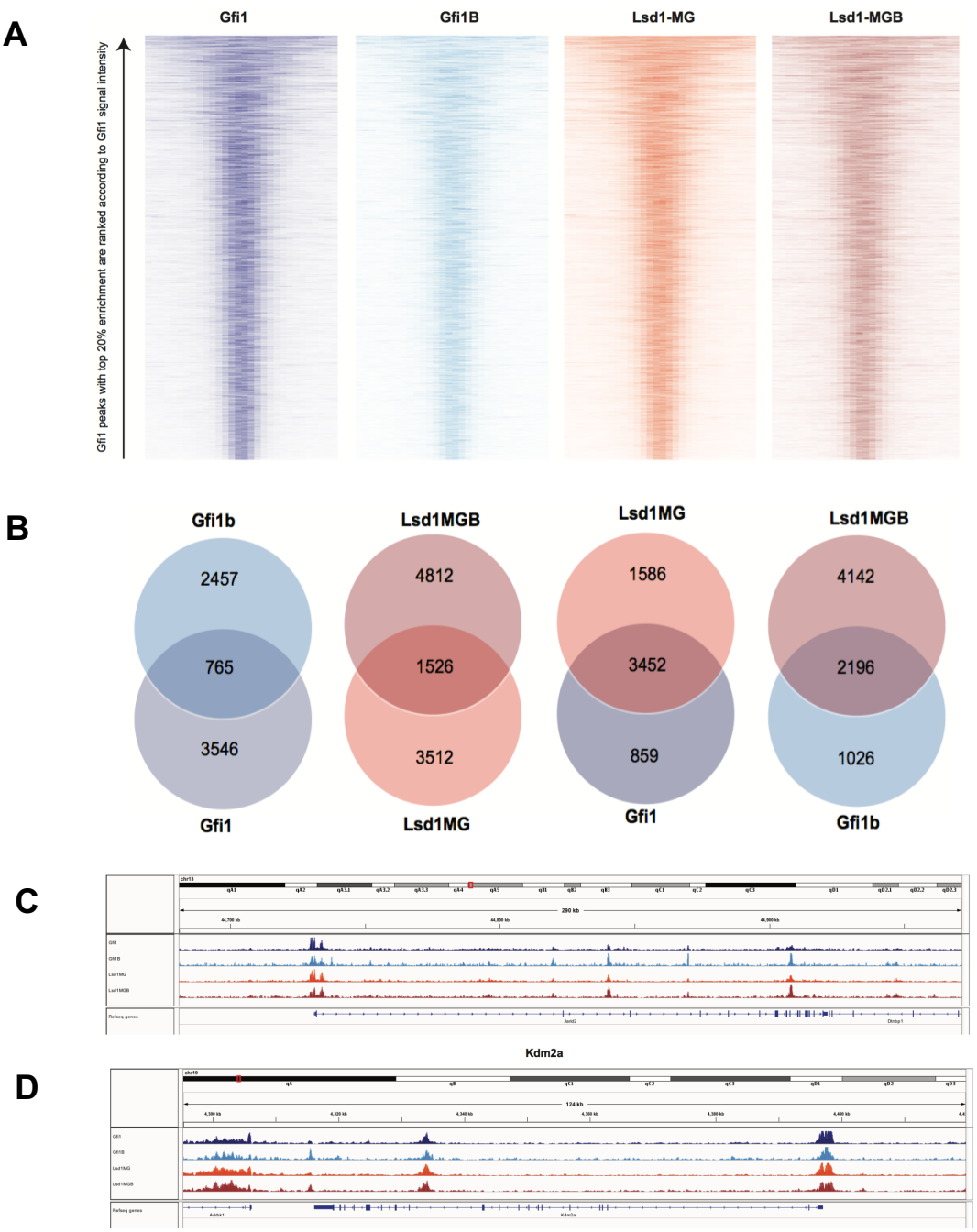

Figure 18: Gfi1/1b and Lsd1 bind to many of the same loci in MG tumor cells. (A) Heatmaps show the scaled read densities surrounding ± 3kb midpoint Gfi1 peaks for Gfi1, Gfi1B, Lsd1 (MG) and Lsd1 (MGB). Only the high confidence Gfi1 peaks are shown and ordered according to the Gfi1 signal intensity. (B) Venn diagrams show the overlap between high confidence Gfi1, Gfi1B, Lsd1 (MG) and Lsd1 (MGB) peaks. (C-D) Snapshots show the signal intensity of Gfi1, Gfi1B, Lsd1 (MG) and Lsd1 (MGB) at Jarid2 (C) and Kdm2a (D) loci.

Although ChIP-seq analysis identified genes that are bound by Gfi1/1b and Lsd1, being bound does not directly signify these genes are important for tumor growth. In order to identify those that are more likely to play functional roles in tumorigenesis, we cross-referenced the ChIP-seq genes with gene expression data for MG/MGB tumors (Figure 19A, B). By selecting genes that are bound and either >2-fold upregulated or downregulated in comparison to NSCs, we created a list of candidate targets of Gfi1/1b and Lsd1. Of these genes, GEP data indicated that the majority were repressed (Figure 19A).

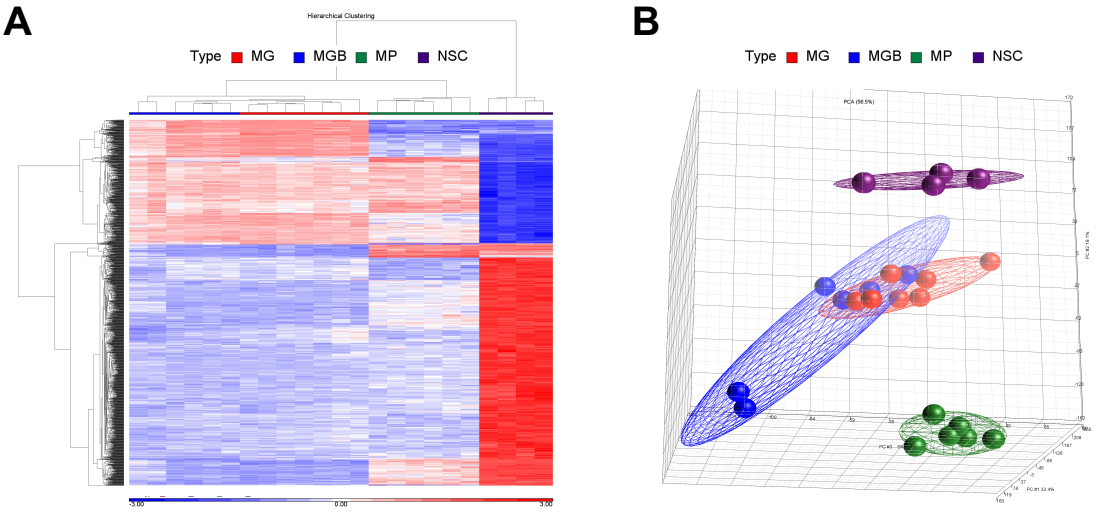

Figure 19: Gene expression profiling of MG and MG tumors indicates many genes are repressed in comparison to NSCs. (A) Hierarchical clustering of gene expression data from mouse NSCs and MG, MGB, and Myc+DNp53 (MP) tumor samples. Red indicates upregulation and blue indicates downregulation. (B) Principle component analysis (PCA)

We then chose fourteen genes (Table 5) that were predicted to be repressed for qPCR validation in additional MG and MGB samples and showed that the expression predicted by GEP was accurate for many of the

genes (Figure 20A-D, Table 5). Finally, of the genes that we validated by expression, we chose six (Table 5) for functional validation: Nfia, Smad4, Lrig3, Fbxo5, Bmpr1a, and Cux1. After cloning these genes into the MSCV-IRES-GFP vector and generating retroviral particles, we infected MG tumor cells overnight and sorted for infected cells the following day. Sorted cells were assayed for overexpression of the gene of interest, plated for thymidine incorporation experiments, and re-transplanted into (Figure 21). Five of six genes did not appear to confer any changes in tumor latency or mouse survival (Table 5), but Fbxo5 (Emi1) consistently inhibited tumor growth in vitro (Figure 22B) and in vivo (Figure 22C, D). qPCR confirmed Fbxo5 overexpression in the cells after infection and sorting (Figure 22A).

Table 5: Candidate target genes of Gfi1/1b and Lsd1.

Gene	**Expression predicted by GEP**	**Expression in MG and MGB compared to NSC (qPCR)**	**Result of forced overexpression in MG tumor cells (in vivo)**
Apc	downregulated	down in MG	n/a
Arhgdia	downregulated	upregulated	n/a
Bmpr1a	downregulated	downregulated	No change
Cux1	downregulated	downregulated	No change
Fbxo5	downregulated	downregulated	Tumor inhibition
Gadd45g	downregulated	downregulated	n/a
Gse1	downregulated	no difference	n/a
Irf2bp1	downregulated	upregulated	n/a
Lrig3	downregulated	downregulated	No change
Nfia	downregulated	downregulated	No change
Smad4	downregulated	no change	No change
Tacc3	downregulated	down in MG	n/a
Tgif2	downregulated	no difference	n/a
Zmiz1	downregulated	downregulated	n/a

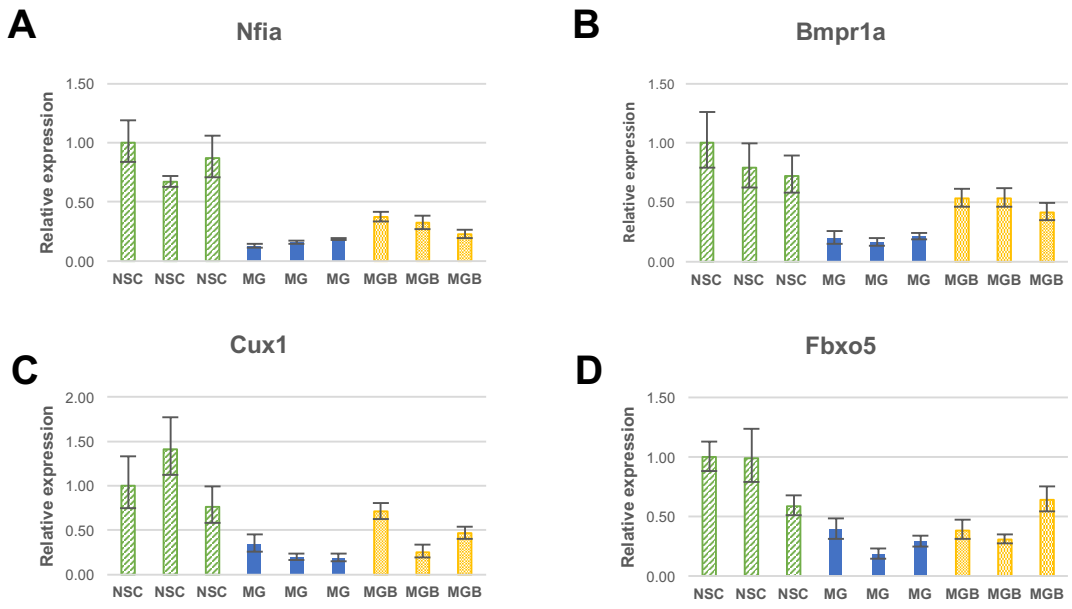

Figure 20: Target genes of Gfi1/1b and Lsd1 are downregulated in MG and MGB tumors in comparison to NSCs. (A-D) Example qPCR validation of target genes filtered from ChIP-seq and GEP analysis: (A) Nfia, (B) Bmpr1a, (C) Cux1, and (D) Fbxo5. Green striped bars are NSCs, Solid blue bars are MG tumors, and checkered yellow bars are MGB tumors. Three biological replicates are shown for each cell type.

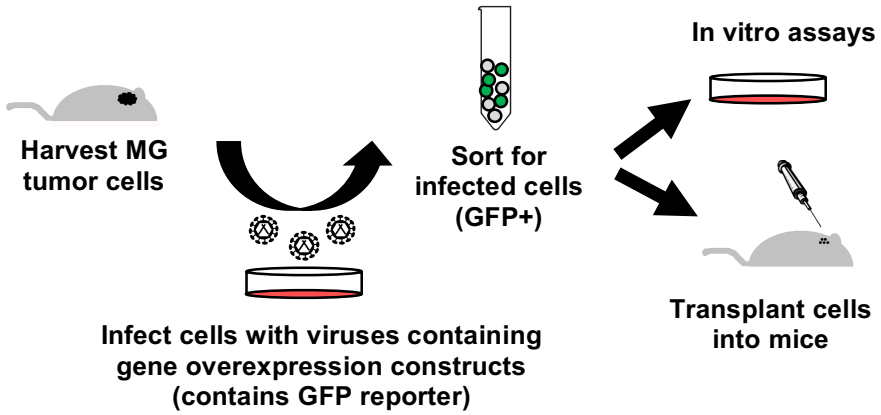

Figure 21: Experimental design for functional validation of target genes that are repressed in MG/MGB tumors.

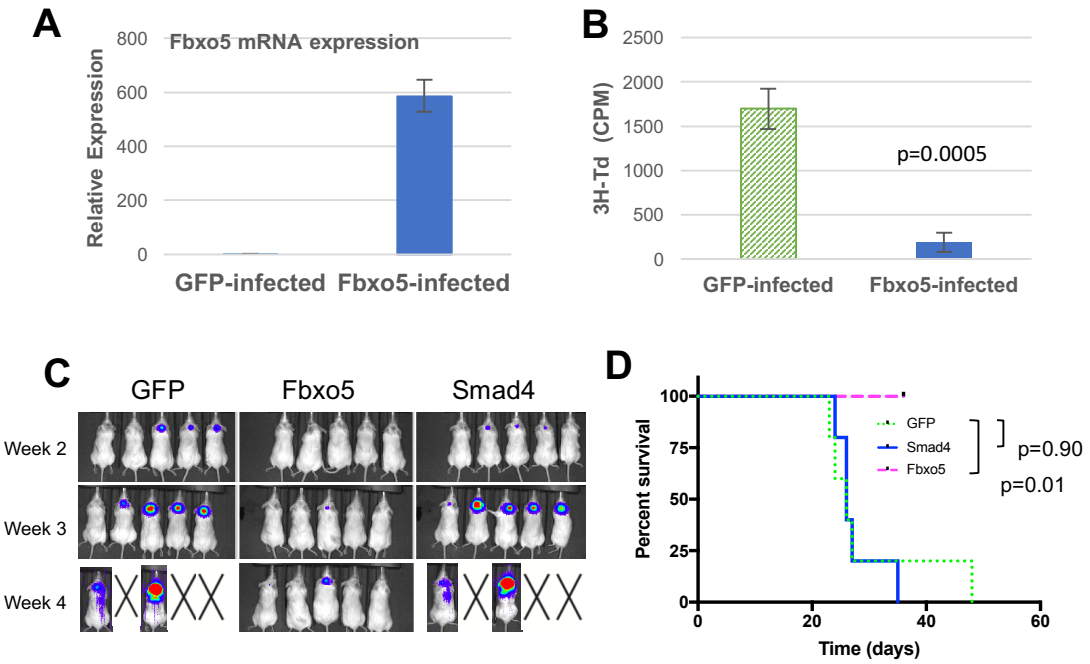

Figure 22: Overexpression of Fbxo5 inhibits MG tumor growth in vitro and in vivo. (A) Fbxo5 expression in MG tumor cells after infection with GFP (control) or Fbxo5 virus and sorting. (B) ^{3}H-Thymidine incorporation assay measuring in vitro proliferation of MG cells after overexpression of GFP (control) or Fbxo5. Striped green bar indicates GFP-infected cells, and solid blue bar indicates Fbxo5-infected cells. (C) Bioluminescent imaging of mice transplanted with MG tumor cells overexpressing GFP (control), Fbxo5, or Smad4. (D) Survival curve of mice transplanted with MG tumor cells overexpressing GFP (control), Fbxo5, or Smad4. Fbxo5 group was terminated earlier than intended, but did not have tumors. Fbxo5 experiment has been repeated and yields similar results.

4.2.7 Pharmacological inhibitors of Lsd1 as a therapeutic strategy for Gfi1-driven MB

Most MB patients are not treated with therapies specific for their tumors, but as the ability to stratify tumors based on genomics improves, employing targeted therapies is becoming a more attractive option. While inhibiting Gfi1 in Gfi1-driven tumors would be ideal, there are currently no

pharmacological inhibitors of Gfi1, and the ability to inhibit transcription factors and transcriptional repressors is difficult. Based on our findings that the interaction of Lsd1 with Gfi1 is crucial for MG tumor growth, we sought to determine whether small molecule inhibitors of Lsd1 would be effective against these tumors. We performed thymidine incorporation assays on cells treated with various concentrations of three different Lsd1 inhibitors: RN-1, GSK-LSD1, and ORY-1001 (Figure 23A). All three compounds very potently inhibited the proliferation of MG tumor cells in vitro, with IC50s ranging from 0.05-5 nM (Table 6). When the inhibitors were tested on MP tumor cells, however, their proliferation was only modestly inhibited, and only at much high concentrations (Figure 23B, Table 6), suggesting that the effect of Lsd1 inhibition was specific to Gfi1-driven tumors. Additionally, the Lsd1 inhibitors were tested on differentiated granule neurons, and they did not have significant effects on the in vitro viability as measured by the CellTiter-Glo luminescent assay (Figure 23C). These data show that pharmacological inhibition of Lsd1 potently and selectively inhibits the proliferation of MG tumor cells in vitro.

Table 6: IC_{50} values for Lsd1 inhibitors on MG tumor cells and MP tumor cells.

Compound	**IC_{50} on MG cells**	**IC_{50} on MP cells**
RN-1	4.731 nM	1.449 μM
GSK-LSD1	0.0547 nM	440.2 nM
ORY-1001	0.143 nM	401 nM

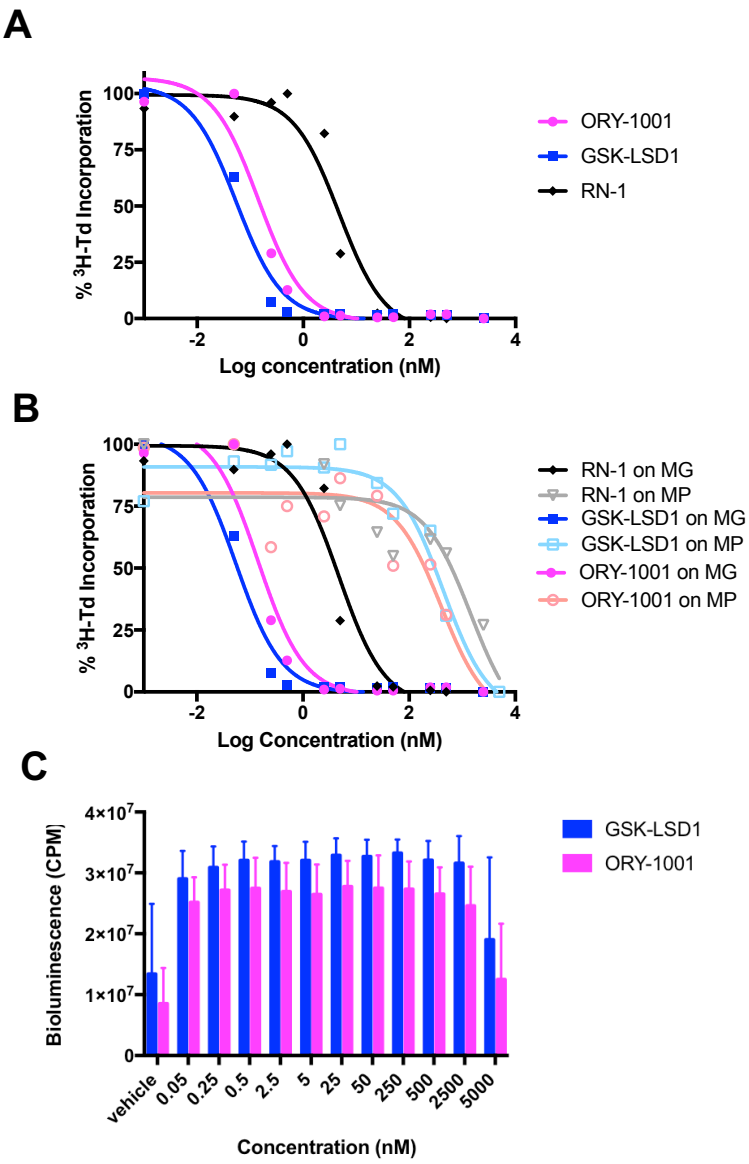

Figure 23: Pharmacological inhibition of Lsd1 selectively inhibits MG tumor cell proliferation in vitro. (A) IC_{50} curves for the inhibitory effects of RN-1, GSK-LSD1, and ORY-1001 on MG tumor cells proliferation, as determined by ^{3}H-Thymidine incorporation assay. (B) An overlay of the IC_{50} curves for the effects of RN-1, GSK-LSD1, and ORY-1001 on MP tumor cells (non-Gfi1-driven tumor model), as determined by ^{3}H-Thymidine incorporation assay. (C) Cell viability of post-mitotic granule neurons after treatment with GSK-LSD1 or ORY-1001. Viability is measured by Cell TiterGlo luminescent assay.

To test whether the Lsd1 inhibition also impairs tumor growth in vivo, we carried out several different treatment protocols on intracranial allografts of MG tumors. 3,000 MG tumor cells were injected into the cerebella of NSG mice, and tumor sizes were quantified one week later using bioluminescent imaging. Mice were randomized into vehicle or treatment groups, and treatments were started. We tried several treatment dosages and regimens: 0.5 mg/kg of GSK-LSD1 daily (i.p., Figure 24A), 10 mg/kg of GSK-LSD1 for four days on and three days off (i.p., Figure 24B), 20 μg/kg of ORY-1001 for 5 days on and 2 days off (oral gavage, Figure 24B), 100 μg/kg of ORY-1001 for 2 days on and 5 days off (oral gavage, Figure 24C), and 200 μg/kg of ORY-1001 for 1 day on and 6 days off (oral gavage, Figure 24C). Despite our efforts, none of these methods slowed intracranial tumor growth nor prolonged mouse survival (Figure 24A-C).

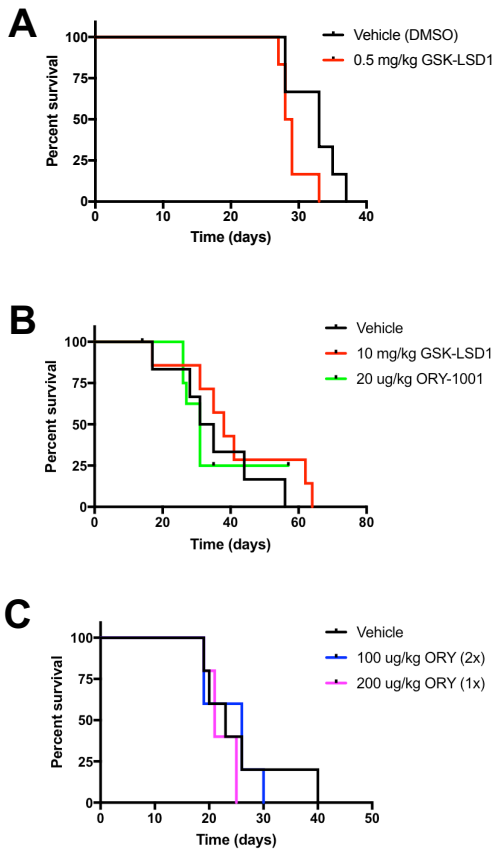

Figure 24: Pharmacological inhibition of Lsd1 does not inhibit growth of intracranial MG tumors. (A-C) MG tumor cells were re-transplanted into the cerebella of NSG mice and treated with vehicle or Lsd1 inhibitors. Survival curves for mice receiving (A) 0.5 mg/kg GSK-LSD1 daily via i.p. injections, (B) 10 mg/kg GSK-LSD1 for four days on and three days off via i.p. injections, (B) 20 µg/kg ORY-1001 for five days on and two days off via oral gavage, (C) 100 µg/kg ORY-1001 for two days on and five days off via oral gavage, and (C) 200 µg/kg ORY-1001 for one day on and six days off via oral gavage.

Because we suspected that the lack of efficacy of these drugs in vivo could be due to poor blood brain barrier (BBB) penetration or inadequate accumulation of drug in the brain, we then tested the effects of GSK-LSD1 on subcutaneous MG tumors. 50,000 MG tumor cells were suspended in growth factor-reduced matrigel and implanted into the flanks of NSG mice. Tumor

sizes were quantified using bioluminescent imaging one week after implantation and randomized into two groups based on the signal intensity of the implanted cells. Mice were administered i.p. injections of vehicle (4% DMSO in saline) or 10 mg/kg GSK-LSD1 in cycles of four days on and three days off. Tumor growth was monitored weekly via both bioluminescent imaging and caliper measurements (Figure 25A). When tumors reached a maximum size of 2 cm in diameter, the experiment was terminated and the tumors were collected, weighed (Figure 25B), and photographed (Figure 25C). Treatment with GSK-LSD1 significantly slowed tumor growth and decreased the size of MG tumors in vivo (Figure 25A-C), indicating that Lsd1 inhibitors can potently suppress tumor growth in vivo. The fact that we observed inhibition of MG tumors in the flank but not in the brain further supports the notion that the Lsd1 inhibitors we tested were not reaching the intracranial compartment. Nonetheless, the results described here are proof of concept that Lsd1 inhibition is a potential strategy for treating Gfi1-driven medulloblastoma in patients.

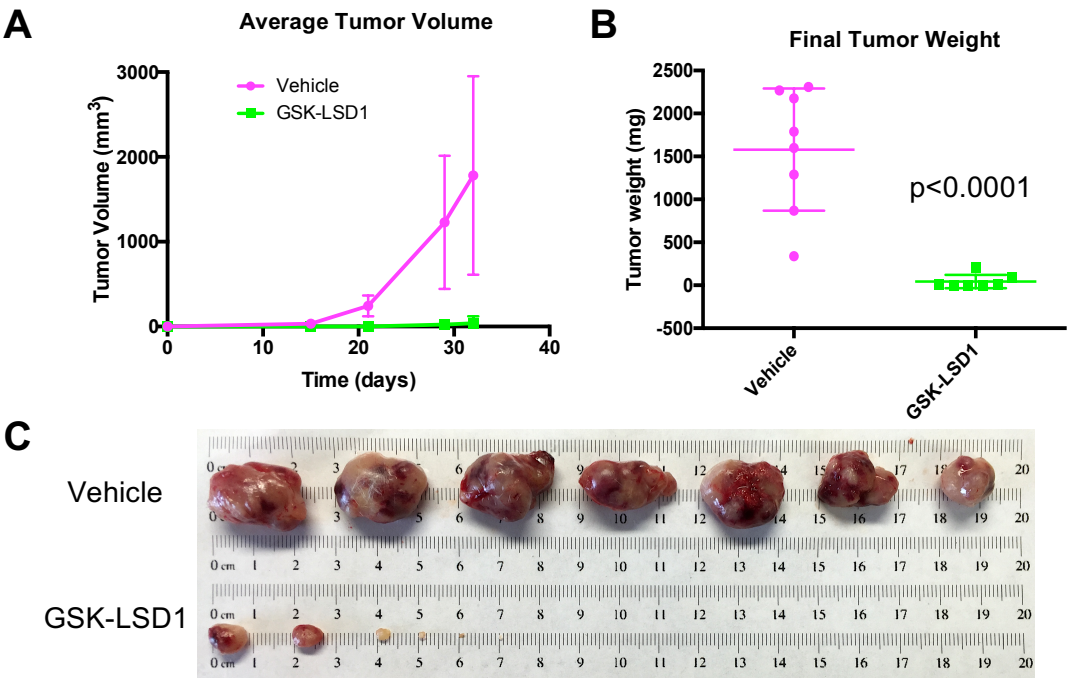

Figure 25: Pharmacological inhibition of Lsd1 inhibits Gfi1-driven tumor growth in vivo. (A-C) MG tumors were implanted subcutaneously and mice were treated with vehicle (n=9) or 10 mg/kg GSK-LSD1 (n=9). Dosing schedule was 4 days on then 3 days off. (A) Comparison of average tumor volume over time in mice receiving vehicle or 10 mg/kg GSK-LSD1. Tumor volume is calculated based on weekly caliper measurements, where V = $(\text{width})^2$ x length/2. (B) Distribution of tumor weights collected at the end of the experiment. (C) Photograph of resulting tumors collected at the end of the experiment.

4.3 Discussion

The identification of *GFI1* and *GFI1B* as novel drivers of MB has provided two new tumor models (*Myc* + *Gfi1*, *Myc* + *Gfi1b*) that accurately represent the genetics of ~30% of Group 3 MB[82], but the means by which they promote MB tumorigenesis is not well understood. In the present study, we identify Lsd1 as a critical player in Gfi1-driven tumor growth and find that Gfi1

and Lsd1 regulate many of the same target genes. We also demonstrate that targeting Lsd1 may be an effective strategy for treating Gfi1-driven MB.

In our co-immunoprecipitation studies, we detected association of Gfi1 with Lsd1 and coREST, but not with HDACs 1 or 2. The detection of some but not all of these proteins is not necessarily unusual, as the current knowledge about whether the interactions with Gfi1/1b are mutually exclusive, cell type specific, or target specific is still unclear[107]. However, studies in other systems have shown that Lsd1 and coREST form a co-repressor complex with Gfi1/1b[92,93,108], and our detection of both of these proteins associated with Gfi1 in MG tumor cells is consistent with this information. Recruitment of Lsd1 and coREST is thought to depend on the SNAG domain of Gfi1, which has been well-characterized as a transcriptional repression domain that functions by interacting with a variety of co-repressor proteins[90,99,100]. Like others before us[90,101,109], we also found the SNAG domain to be crucial for Gfi1 function and demonstrated that the Gfi1-P2A SNAG mutant did not generate tumors in combination with Myc. We inferred from these data that the oncogenic function of Gfi1/1b very likely depends on its interactions with Lsd1 and coREST.

When we evaluated the Gfi1 SNAG mutant, we also tested the Gfi1-N382S zinc finger mutant, which was identified in patients with severe congenital neutropenia (SCN)[102]. The mutation encodes an asparagine to serine change in the minor groove of the Gfi1 DNA-binding site, impairing DNA-binding function[102,103]. Given that the mutant protein has been reported to function as a dominant negative inhibitor of Gfi1[102,103], we were surprised to

discover that it could still drive tumor growth when combined with Myc. This implies that the ability of Gfi1 to bind DNA directly might not be required for tumorigenesis. We speculate that Gfi1-N382S might exert repressor activity at its targets through interaction with other transcription factors, and indeed, several groups have documented interactions of Gfi1 with other transcription factors[110-114]. To investigate this idea further, we recently prepared MG and MG-N382S samples for Gfi1 and Lsd1 ChIP-seq. Comparison of the target genes occupied by Gfi1 and Gfi1-N382S should yield some interesting insights into the mechanistic differences of their oncogenic roles. Moreover, examining the data for consensus motifs will also give us an idea of which transcription factors might mediate the effects of Gfi1-N382S.

At the moment, Lsd1 is the only known protein that interacts with both Gfi1 and Gfi1b solely at the SNAG domain, which is essential for Gfi1/1b function[92,107]. We chose to focus on Lsd1 for this reason and showed that conditionally deleting it from MG tumors impaired tumor growth, regardless of whether deletion was induced in vivo or in vitro. It is clear that Lsd1 plays an important role in MG tumors, but whether the effects of Lsd1 deletion are specific to Gfi1-driven MB remains uncertain. We have already shown that pharmacological inhibitors of Lsd1 do not affect proliferation of MP tumors (which are not driven by Gfi1), but it will be worthwhile to test the effects of genetic deletion of Lsd1 in these tumors as well. Because Lsd1 has important functions in many different cell types, it would not be entirely unprecedented to find that its deletion could affect other types of MB. Indeed, another report

found that knockdown or inhibition of Lsd1 induced apoptosis and reduced proliferation in MB cell lines[115] that, to our knowledge, do not depend on Gfi1.

Previous models of Group 3 MB demonstrated that overexpression of Myc alone increased cell death[24,25], and that this effect was abrogated by loss or inactivation of p53. This led us to speculate that the mechanism of synergy between Gfi1 and Myc might involve p53 repression. While previous studies have found Gfi1 can antagonize p53 and some of its targets[89,104,106,112], we showed that treatment of MG tumor cells with the DNA-damaging agents, doxorubicin and γ-IRR still led to increases in p53 and p21 protein levels. These data suggest that in MG tumors, Gfi1 does not function by inactivating p53. However, we cannot completely rule out the possibility that Gfi1 may regulate p53 function. Comparing transcriptome data for the presence of a p53 signature in MP and MG tumors may also shed some light on whether the pathway is active or not. Even if p53 itself is not repressed by Gfi1 in MG tumors, it is possible that Gfi1 regulates apoptotic pathways downstream or independent of p53, since Myc has been reported to induce both p53-dependent and independent mechanisms of apoptosis[116].

To identify potential Gfi1/1b target genes besides p53, we analyzed both MG and MGB tumors using a combination of gene expression profiling and ChIP-seq for Gfi1/1b and Lsd1. The analysis not only revealed significant overlaps of loci bound by Gfi1/1b and Lsd1, but showed that the majority of these genes were repressed (i.e. downregulated in tumors compared to NSCs). Although the genes bound only by Gfi1/1b could be interesting targets,

we chose to focus on those that were co-occupied by Lsd1, since the results of our Lsd1 deletion and inhibition experiments suggest that these genes are probably the most important in MG/MGB tumors. The fact that most of these genes were downregulated was not surprising, given that Gfi1/1b often function as transcriptional repressors[90,103]. Similar studies carried out in leukemia models have identified Gfi1 targets in that disease[89,92] and a comparison of their ChIP-seq results with ours could potentially reveal which Gfi1 targets are common between different cancer types or unique to MB. In addition to the Gfi1/1b and Lsd1 ChIP-seq we described, we (in collaboration with Drs. Diana Hargreaves and Fangjian Gao from the Salk Institute and Dr. Paul Northcott from St. Jude and Dr. Serap Erkek from DKFZ) are now in the process of completing ChIP-seq for various histone marks as well. The histone ChIP-seq will allow us to more closely examine chromatin states (active, repressed, or poised) surrounding candidate targets of Gfi1/1b and Lsd1.

Among the candidate Gfi1 target genes we tested so far, Fbxo5 (Emi1) was the most intriguing. We validated downregulation of its expression in both MG and MGB tumors compared to NSCs, and showed that forced overexpression of Fbxo5 in MG tumor cells reduced in vitro proliferation and consistently abolished in vivo tumor growth. Oddly enough, these findings seem to conflict with previous descriptions of Fbxo5 function. In most cases, Fbxo5 acts as a positive regulator of the cell cycle, inhibiting the anaphase-promoting complex (APC/C), which in turn promotes S-phase and mitotic entry[117-119]. Furthermore, overexpression of Fbxo5 is seen across many types

of cancer and is often correlated with higher tumor grade and poor prognosis[120-123]. The converse idea, that Fbxo5 could also function as a tumor suppressor, has been proposed before by scientists who observed that loss of one *Emi1* allele in *p53* mutated zebrafish enhanced their susceptibility to neural sheath tumorigenesis[124], but moving forward, we will need to confirm these findings and attempt to understand the mechanism for tumor inhibition. It will also be interesting to see whether loss of Fbxo5 can drive tumor growth in our system and whether expression and function of Fbxo5 are different across the molecular subtypes of human MB.

Having shown that Lsd1 expression is critical for MG tumor growth, we also tested its potential to be a therapeutic target. We demonstrated that pharmacological inhibitors of Lsd1 potently inhibit the proliferation and growth of MG tumors both in vitro and in vivo. Rather than having a global effect on multiple cell types, the negative growth effects of Lsd1 inhibitors seem to be specific for Gfi1-activated tumor cells, since the drugs have minimal effects on MP tumors. This finding suggests that Lsd1 inhibition may be a promising therapy, specifically for patients with Gfi1/1b-activated tumors. However, the fact that we saw efficacy in subcutaneous MG tumors but not in intracranial MG tumors raises the concern that the Lsd1 inhibitors we tested are limited in their ability to cross the blood brain barrier (BBB). This is somewhat surprising, since RN-1 has been reported to affect memory formation[125], and pharmacokinetic studies (performed in collaboration with GlaxoSmithKline (GSK) and Roche) suggested that ORY-1001 (but not GSK-LSD1) can be

detected in the brain after systemic delivery. It is possible that these drugs do enter intracranial tumors, but are inactive (due to metabolism or binding to proteins in the microenvironment) or do not persist long enough to exert their effects. Further studies will be necessary to determine whether alternative modes of delivery may increase the efficacy of these drugs for intracranial tumors. Alternatively, novel Lsd1 inhibitors with increased brain penetration and activity may be developed for treatment of brain tumors. If these approaches are successful, Lsd1 inhibition could be a very effective targeted therapy for MB patients with Gfi1/1b-activated tumors.

4.4 Acknowledgements

Chapter 4 contains unpublished data that is part of a manuscript in preparation: Lee, Catherine; Northcott, Paul A.; Erkek, Serap; Gao, Fangjian; Tacheva-Grigorova, Silvia; Mohammed, Helai; Yu, Li J.; Hargreaves, Diana A.; Pfister, Stefan M.; Wechsler-Reya, Robert J., “Kdm1a (Lsd1) is required for growth of Gfi1-driven medulloblastoma.” The dissertation author was the primary investigator and author of this material. The dissertation author was the primary investigator and author of this material.

CHAPTER 5 – Discussion

The work summarized in this dissertation demonstrated a unique method for identifying novel cancer genes and resulted in the development of new animal models and identification of new therapeutic targets for Group 3 MB. The findings we reported here have not only uncovered new information regarding the pathogenesis of Group 3 tumors, but have also raised major questions and considerations for future studies. Some of these concepts include: 1) approaches for identifying new driver genes, 2) enhancer hijacking and the role of epigenetics in cancer, and 3) drug discovery and challenges for drug delivery to the brain.

5.1 Identifying driver genes in cancer

Within the last decade, genome-wide technologies have advanced significantly, making many next generation sequencing (NGS) assays easier and cheaper for researchers to use. Applications in cancer biology have revealed molecular aspects of disease that were previously unknown, yet there is undoubtedly still a lot to be learned from the outcomes of these experiments. One obvious observation from all of the genomic data that has been produced is that extensive intertumoral heterogeneity exists within cancer types. The realization that no two patients are the same and the improvement in genome-wide analysis continue to promote the alluring

prospect of personalized medicine, but one of the main challenges to this is distinguishing actionable drivers of tumorigenesis from benign passenger mutations[126].

The genomic characterization of medulloblastoma has had a tremendous impact on our understanding of the disease, especially with the emergence of a molecular classification system. While driver genes for Group 3 and Group 4 medulloblastoma still remain largely elusive, the studies we described here have identified *GFI1* and *GFI1B* as novel drivers for approximately 30% of Group 3 tumors and 10% of Group 4 tumors. These findings resulted primarily from WGS analysis identifying loci containing all possible types of SVs. Previously, only recurrent amplifications or deletions had been noted, as it was presumed recurrent amplifications could signify oncogene activation, whereas recurrent deletions could denote the loss of a tumor suppressor. In the MB cases with *GFI1/1B* activation, the aberrant expression of these genes was not due to copy number increases, but rather to an alternative mechanism of spatial rearrangement of enhancer clusters. The emergence of this mode of oncogene activation in MB highlights the diversity of the cancer genome and calls for a closer examination of all detectable genetic alterations in tumors. An organized catalog of such events would facilitate a systematic search for correlation between event incidence and expression changes in potential driver genes.

As cancer genome data accumulates, and researchers continue to mine it for potential genetic drivers, the need to functionally validate these

genes grows more pressing. The functional validation experiments we conducted for *GFI1* and *GFI1B* involved testing these genes individually (alone and in combination with Myc), but going forward it may be possible to perform higher-throughput functional screens to distinguish passengers from drivers within large sets of candidate genes. One approach for validating tumor suppressors would be an RNA interference (RNAi) screen using short hairpin RNAs (shRNAs), which target homologous RNAs to stably repress gene expression in mammalian cells[127-129]. Barcoded shRNA library screens have been successful both in vitro[130,131] and in vivo[132-135], with the in vivo screens being able to assess gene activities more accurately due to the presence of cues from the tumor microenvironment. However, drawbacks of RNAi screens include incomplete gene knockdown and off-target effects[136,137]. An alternative to shRNAs that has gained prominence more recently uses CRISPR/Cas9 and DNA double-strand break (DSB) repair pathways to introduce targeted mutations or to knock out genes[138-140]. Unlike RNAi, CRISPR/Cas9-mediated screens are more consistent and have less off-target activity with clearer phenotypic effects[141,142]. Prior to the discovery of *GFI1* and *GFI1B* in MB, we had been preparing to conduct an in vivo shRNA screen of commonly deleted genes in Group 3 MB[7,8]. Since Group 3 tumors are driven in part by the *MYC* oncogene, we planned to transduce neural progenitors with *Myc* and pools of barcoded shRNAs against ~200 unique genes, orthotopically transplant the cells into mice, and sequence any tumors that arose for barcode identification. Although we have not yet completed these studies, the fact that activation of

GFI1/GFI1B only accounts for a fraction of Group 3 MBs indicates that there is still value in testing these candidate genes in the future.

The shRNA and CRISPR/Cas9 screens described above would be most useful for testing focused libraries of candidate genes based on data generated by NGS studies. Conversely, unbiased techniques like transposon mutagenesis would also be valuable tools for discovering new driver genes in cancer. Transposons are DNA elements that can jump throughout the genome, interrupting or activating genes while leaving behind a traceable footprint[143-145]. One of the most popular systems used is the Sleeping Beauty (SB) transposon, where the transposase enzyme activates SB to move randomly around the genome by a cut-and-paste mechanism[143-145]. Insertional mutagenesis can identify both tumor suppressors and oncogenes depending on where the transposon inserts itself. Insertion inside a gene can disrupt its expression, whereas insertion near a gene can affect its regulatory region and enhance gene expression. Previous studies have used SB in models of SHH MB to identify drivers of metastatic dissemination[146] as well as drivers that discriminate between the molecular subgroups[147]. To identify genes that can cooperate with *Myc* to drive Group 3 tumorigenesis, we also began a study which involved overexpressing *Myc* in NSCs with a Nestin-Cre-activated SB transposon/transposase and then transplanting them into the brains of host mice. Around 10% of the mice we transplanted developed tumors, which we collected for analysis of SB insertion sites. Our sample size has not yet reached a level where common insertion sites (CIS) are significant, but

nevertheless, the ability to generate tumors using this system confirms the potential for finding cooperating driver genes in MB.

5.2 Enhancer hijacking and the cancer epigenome

Early reports of oncogene activation by enhancer hijacking were mostly due to translocations in blood malignancies[65,66]. Newer discoveries since our report on *GFI1/1B* activation in MB have found similar mechanisms in lung[72], endometrial[72], and adenoid cystic carcinoma[73]. One study found that recurrent amplifications of noncoding DNA harboring super-enhancers were associated with overexpression of the nearby *MYC* oncogene[72], while another study found distinct chromosomal translocations brought super-enhancer regions next to the *MYB* promoter[73]. Collectively, these studies provide strong evidence for enhancer hijacking as a general mechanism for driving tumorigenesis across different types of cancer. Furthermore, the involvement of enhancers more broadly suggests that aberrant epigenetic regulation plays a role in many cancers.

In addition to our observation of aberrant enhancer activity in Group 3 tumors, a number of papers have also pointed to other mechanisms of epigenetic deregulation in MB[39,40,148-150]. Somatic copy number aberrations (SCNAs) have been found to affect various genes with roles in chromatin modification, including histone lysine methyltransferases (HMTs), histone demethylases (HDMs), histone acetyltranserases (HATs), and polycomb

group repressors[148]. Moreover, whole exome sequencing (WES) and WGS studies have indicated that the HMTs *MLL2* and *MLL3* often exhibit loss of function mutations in the WNT/SHH and Group3/4 subtypes, respectively[39,40,149,150]. Mutually exclusive mutations in *SMARCA4* (*BRG1)* and *ARID1B*, which encode proteins in the SWI/SNF chromatin-remodeling complex have also been found. In Group 4 MB, recurrent mutations and homozygous deletions of the HDM *KDM6A* have been observed[14,148], and are correlated with higher levels of the repressive histone mark H3K27me3[40,151]. While alterations of many epigenetic regulators have been seen in MB, the significance of these alterations has yet to be determined and will rely on future functional studies.

The convergence on chromatin remodeling proteins as important players in MB pathogenesis suggests that epigenetic therapy may be useful for treating these tumors. The fact that epigenetic modifications are not permanent makes targeting them a much more attractive option than trying to reverse genomic alterations. Indeed, several pharmacological agents that target epigenetic modifiers are currently being investigated for efficacy in MB[37,152-154]. Histone deacetylase (HDAC) inhibitors, such as vorinostat (SAHA) and panobinostat (LBH-589), have proven to be effective on *MYC*-driven MB cell lines[154] as well as mouse and human PDX models of the disease[37]. Another inhibitor that has gained attention in the past few years is the bromodomain inhibitor, JQ1, which prevents bromodomain-containing proteins such as HATs and HMTs from binding to acetylated lysine residues[155].

Observations that JQ1 treatment can indirectly downregulate MYC[156,157] makes it an even more promising tool for targeting Group 3/MYC-driven MB[158,159]. Furthermore, our investigations into the role of Gfi1 in Group 3 MB revealed a key relationship between Gfi1 and the HDM Lsd1, and our preclinical experiments using Lsd1 inhibitors support targeted epigenetic therapy of these tumors. An important detail to note for many of the drug treatment studies referenced here is that they were largely conducted in cell lines or mouse models. Moving forward, it will be valuable to test such epigenetic inhibitors in more regularly in patient-derived xenograft (PDX) models of MB before moving into human trials.

5.3 Drug discovery and drug delivery to the brain

As discussed above, an important developing area of MB therapeutics involves targeting various epigenetic modifiers. Given the heterogeneity of MB and the ability of cancers to develop drug resistance, however, there is a constant need to find better and alternative treatment strategies. A widely-used approach for identifying new drugs is high-throughput drug screening of compound libraries. Since patients with Group 3 tumors have the worst prognosis, and animal models have only just become available for this subtype, screening efforts to identify drugs for these tumors have recently been completed. Our lab published results from a screen of 3,642 compounds on the *Myc+DNp53* (MP) model and a *MYC*-driven PDX model of Group 3

MB[37]. Interestingly, HDAC inhibitors were among the most potent inhibitors of cell viability, and the authors observed a synergistic effect when panobinostat treatment was combined with the PI3K inhibitor BKM-120. A similar high-throughput screen of ~7,000 compounds on neurospheres from another Group 3 mouse model[25] yielded a different combination of drugs: gemcitabine and pemetrexed[38], which are a DNA/RNA synthesis inhibitor and a folate pathway inhibitor, respectively. This drug combination also inhibited growth of two Group 3 PDXs with *MYC* amplification, and clinicians have since begun recruiting patients for a phase II clinical trial[3].

Despite the fact that many compounds are promising when tested in the laboratory, there are many reasons (absorption, distribution, metabolism, excretion, toxicity), that most of them never make it into clinical trials, let alone clinical practice. This is even more true for drugs meant to treat central nervous system (CNS) diseases, since achieving high enough levels of drug in the brain is a formidable challenge. Our data suggest that Lsd1 inhibitors can potently block MG tumor growth in the periphery but not in the intracranial setting. Factors that may impede successful uptake include plasma protein binding, compound molecular weight, and drug efflux[160]. Many drugs are often bound up by proteins in the blood plasma[161], which leaves very little free drug to even reach the BBB. If intact, the BBB is a complex structure that controls the exchange of molecules from the blood into the brain. It generally blocks molecules larger than 180 daltons (most chemotherapeutics are well over 400 daltons), and it expresses high levels of efflux pumps, which actively transport

molecules out of the brain[160]. Even though the BBB may be compromised in brain tumors due to disordered and leaky tumor vasculature[162], many regions of the tumor remain behind an intact barrier, and are not exposed to therapeutically relevant doses of drug. Moreover, diffusion of drug into the tumor is limited because the high interstitial pressure within the tumor creates a gradient that causes drugs to diffuse outward into the surrounding normal tissue[163,164].

For Lsd1 inhibitors and other epigenome-modifying drugs to be useful for treatment of MB in the clinic, it will be necessary to find effective ways to deliver them to the tumor site. The development of effective drug delivery techniques is an exploding area of research, and general strategies for targeting the brain include modulating the BBB, exploiting cellular transport systems, and avoiding the BBB altogether[165,166]. Methods aimed at directly regulating the BBB include: disruption by hyperosmotic mannitol infusion[167], disruption by focused ultrasound (FUS)[168], inhibition of efflux pumps (P-glycoprotein)[169-171], and stimulation of tight junction opening[172,173]. Other technologies focused on exploiting receptor-mediated transport utilize drug modifications and delivery vehicles like tumor-homing peptides[174-177] and nanoparticles (NPs)[178,179]. Currently, one of the most promising types of NPs are those made of biocompatible and biodegradable poly(lactic-co-glycolic acid) (PLGA)[180,181]. Encapsulation of the chemotherapy drug camptothecin in PLGA NPs have shown increased drug accumulation and efficacy on intracranial glioma models[181], and similar PLGA NP experiments in MB are

currently underway in our laboratory. Approaches for circumventing the BBB, in particular convection enhanced delivery (CED), deliver drugs directly into the tumor cavity and have worked in preclinical animal models[182-184]. Unfortunately, results from glioma clinical trials have so far been disappointing, largely due to sub-therapeutic drug concentrations in tumor cells[185,186]. It is conceivable that effective drug delivery to the brain will require a combination of the techniques outlined here, which will be important to keep in mind as researchers move forward with drug discovery and clinical trial design.

The successful treatment of MB and other CNS tumors will depend on several aspects of cancer research and drug development that we have touched on in this discussion. Systematic approaches for the identification and validation of novel tumor drivers will provide a more complete understanding of MB tumor biology and shed light on actionable therapeutic targets. Simultaneously, improvements in drug delivery across the BBB will be crucial in order for many targeted therapies to be considered for future clinical use in MB.

REFERENCES

1 Smith, M. A., Seibel, N. L., Altekruse, S. F., Ries, L. A., Melbert, D. L., O'Leary, M., Smith, F. O. & Reaman, G. H. Outcomes for children and adolescents with cancer: challenges for the twenty-first century. *J Clin Oncol* **28**, 2625-2634, doi:10.1200/JCO.2009.27.0421 (2010).

2 Polkinghorn, W. R. & Tarbell, N. J. Medulloblastoma: tumorigenesis, current clinical paradigm, and efforts to improve risk stratification. *Nat Clin Pract Oncol* **4**, 295-304, doi:10.1038/ncponc0794 (2007).

3 Coluccia, D., Figuereido, C., Isik, S., Smith, C. & Rutka, J. T. Medulloblastoma: Tumor Biology and Relevance to Treatment and Prognosis Paradigm. *Curr Neurol Neurosci Rep* **16**, 43, doi:10.1007/s11910-016-0644-7 (2016).

4 Smoll, N. R. & Drummond, K. J. The incidence of medulloblastomas and primitive neurectodermal tumours in adults and children. *J Clin Neurosci* **19**, 1541-1544, doi:10.1016/j.jocn.2012.04.009 (2012).

5 Park, T. S., Hoffman, H. J., Hendrick, E. B., Humphreys, R. P. & Becker, L. E. Medulloblastoma: clinical presentation and management. Experience at the hospital for sick children, toronto, 1950-1980. *J Neurosurg* **58**, 543-552, doi:10.3171/jns.1983.58.4.0543 (1983).

6 Gilbertson, R. J. & Ellison, D. W. The origins of medulloblastoma subtypes. *Annu Rev Pathol* **3**, 341-365, doi:10.1146/annurev.pathmechdis.3.121806.151518 (2008).

7 Northcott, P. A., Korshunov, A., Witt, H., Hielscher, T., Eberhart, C. G., Mack, S., Bouffet, E., Clifford, S. C., Hawkins, C. E., French, P., Rutka, J. T., Pfister, S. & Taylor, M. D. Medulloblastoma comprises four distinct molecular variants. *J Clin Oncol* **29**, 1408-1414, doi:10.1200/JCO.2009.27.4324 (2011).

8 Cho, Y. J., Tsherniak, A., Tamayo, P., Santagata, S., Ligon, A., Greulich, H., Berhoukim, R., Amani, V., Goumnerova, L., Eberhart, C. G., Lau, C. C., Olson, J. M., Gilbertson, R. J., Gajjar, A., Delattre, O., Kool, M., Ligon, K., Meyerson, M., Mesirov, J. P. & Pomeroy, S. L. Integrative genomic analysis of medulloblastoma identifies a molecular subgroup that drives poor clinical outcome. *J Clin Oncol* **29**, 1424-1430, doi:10.1200/JCO.2010.28.5148 (2011).

9 Kool, M., Koster, J., Bunt, J., Hasselt, N. E., Lakeman, A., van Sluis, P., Troost, D., Meeteren, N. S., Caron, H. N., Cloos, J., Mrsic, A., Ylstra,

B., Grajkowska, W., Hartmann, W., Pietsch, T., Ellison, D., Clifford, S. C. & Versteeg, R. Integrated genomics identifies five medulloblastoma subtypes with distinct genetic profiles, pathway signatures and clinicopathological features. *PLoS One* **3**, e3088, doi:10.1371/journal.pone.0003088 (2008).

10 Remke, M., Hielscher, T., Northcott, P. A., Witt, H., Ryzhova, M., Wittmann, A., Benner, A., von Deimling, A., Scheurlen, W., Perry, A., Croul, S., Kulozik, A. E., Lichter, P., Taylor, M. D., Pfister, S. M. & Korshunov, A. Adult medulloblastoma comprises three major molecular variants. *J Clin Oncol* **29**, 2717-2723, doi:10.1200/JCO.2011.34.9373 (2011).

11 Thompson, M. C., Fuller, C., Hogg, T. L., Dalton, J., Finkelstein, D., Lau, C. C., Chintagumpala, M., Adesina, A., Ashley, D. M., Kellie, S. J., Taylor, M. D., Curran, T., Gajjar, A. & Gilbertson, R. J. Genomics identifies medulloblastoma subgroups that are enriched for specific genetic alterations. *J Clin Oncol* **24**, 1924-1931, doi:10.1200/JCO.2005.04.4974 (2006).

12 Taylor, M. D., Northcott, P. A., Korshunov, A., Remke, M., Cho, Y. J., Clifford, S. C., Eberhart, C. G., Parsons, D. W., Rutkowski, S., Gajjar, A., Ellison, D. W., Lichter, P., Gilbertson, R. J., Pomeroy, S. L., Kool, M. & Pfister, S. M. Molecular subgroups of medulloblastoma: the current consensus. *Acta Neuropathol* **123**, 465-472, doi:10.1007/s00401-011-0922-z (2012).

13 Louis, D. N., Perry, A., Reifenberger, G., von Deimling, A., Figarella-Branger, D., Cavenee, W. K., Ohgaki, H., Wiestler, O. D., Kleihues, P. & Ellison, D. W. The 2016 World Health Organization Classification of Tumors of the Central Nervous System: a summary. *Acta Neuropathol* **131**, 803-820, doi:10.1007/s00401-016-1545-1 (2016).

14 Northcott, P. A., Jones, D. T., Kool, M., Robinson, G. W., Gilbertson, R. J., Cho, Y. J., Pomeroy, S. L., Korshunov, A., Lichter, P., Taylor, M. D. & Pfister, S. M. Medulloblastomics: the end of the beginning. *Nat Rev Cancer* **12**, 818-834, doi:10.1038/nrc3410 (2012).

15 Zhukova, N., Ramaswamy, V., Remke, M., Pfaff, E., Shih, D. J., Martin, D. C., Castelo-Branco, P., Baskin, B., Ray, P. N., Bouffet, E., von Bueren, A. O., Jones, D. T., Northcott, P. A., Kool, M., Sturm, D., Pugh, T. J., Pomeroy, S. L., Cho, Y. J., Pietsch, T., Gessi, M., Rutkowski, S., Bognar, L., Klekner, A., Cho, B. K., Kim, S. K., Wang, K. C., Eberhart, C. G., Fevre-Montange, M., Fouladi, M., French, P. J., Kros, M., Grajkowska, W. A., Gupta, N., Weiss, W. A., Hauser, P., Jabado, N.,

Jouvet, A., Jung, S., Kumabe, T., Lach, B., Leonard, J. R., Rubin, J. B., Liau, L. M., Massimi, L., Pollack, I. F., Shin Ra, Y., Van Meir, E. G., Zitterbart, K., Schuller, U., Hill, R. M., Lindsey, J. C., Schwalbe, E. C., Bailey, S., Ellison, D. W., Hawkins, C., Malkin, D., Clifford, S. C., Korshunov, A., Pfister, S., Taylor, M. D. & Tabori, U. Subgroup-specific prognostic implications of TP53 mutation in medulloblastoma. *J Clin Oncol* **31**, 2927-2935, doi:10.1200/JCO.2012.48.5052 (2013).

16 Schuller, U., Heine, V. M., Mao, J., Kho, A. T., Dillon, A. K., Han, Y. G., Huillard, E., Sun, T., Ligon, A. H., Qian, Y., Ma, Q., Alvarez-Buylla, A., McMahon, A. P., Rowitch, D. H. & Ligon, K. L. Acquisition of granule neuron precursor identity is a critical determinant of progenitor cell competence to form Shh-induced medulloblastoma. *Cancer Cell* **14**, 123-134, doi:10.1016/j.ccr.2008.07.005 (2008).

17 Gibson, P., Tong, Y., Robinson, G., Thompson, M. C., Currle, D. S., Eden, C., Kranenburg, T. A., Hogg, T., Poppleton, H., Martin, J., Finkelstein, D., Pounds, S., Weiss, A., Patay, Z., Scoggins, M., Ogg, R., Pei, Y., Yang, Z. J., Brun, S., Lee, Y., Zindy, F., Lindsey, J. C., Taketo, M. M., Boop, F. A., Sanford, R. A., Gajjar, A., Clifford, S. C., Roussel, M. F., McKinnon, P. J., Gutmann, D. H., Ellison, D. W., Wechsler-Reya, R. & Gilbertson, R. J. Subtypes of medulloblastoma have distinct developmental origins. *Nature* **468**, 1095-1099, doi:10.1038/nature09587 (2010).

18 Yang, Z. J., Ellis, T., Markant, S. L., Read, T. A., Kessler, J. D., Bourboulas, M., Schuller, U., Machold, R., Fishell, G., Rowitch, D. H., Wainwright, B. J. & Wechsler-Reya, R. J. Medulloblastoma can be initiated by deletion of Patched in lineage-restricted progenitors or stem cells. *Cancer Cell* **14**, 135-145, doi:10.1016/j.ccr.2008.07.003 (2008).

19 Buonamici, S., Williams, J., Morrissey, M., Wang, A., Guo, R., Vattay, A., Hsiao, K., Yuan, J., Green, J., Ospina, B., Yu, Q., Ostrom, L., Fordjour, P., Anderson, D. L., Monahan, J. E., Kelleher, J. F., Peukert, S., Pan, S., Wu, X., Maira, S. M., Garcia-Echeverria, C., Briggs, K. J., Watkins, D. N., Yao, Y. M., Lengauer, C., Warmuth, M., Sellers, W. R. & Dorsch, M. Interfering with resistance to smoothened antagonists by inhibition of the PI3K pathway in medulloblastoma. *Sci Transl Med* **2**, 51ra70, doi:10.1126/scitranslmed.3001599 (2010).

20 Romer, J. T., Kimura, H., Magdaleno, S., Sasai, K., Fuller, C., Baines, H., Connelly, M., Stewart, C. F., Gould, S., Rubin, L. L. & Curran, T. Suppression of the Shh pathway using a small molecule inhibitor eliminates medulloblastoma in Ptc1(+/-)p53(-/-) mice. *Cancer Cell* **6**, 229-240, doi:10.1016/j.ccr.2004.08.019 (2004).

21 Lee, A., Kessler, J. D., Read, T. A., Kaiser, C., Corbeil, D., Huttner, W. B., Johnson, J. E. & Wechsler-Reya, R. J. Isolation of neural stem cells from the postnatal cerebellum. *Nat Neurosci* **8**, 723-729, doi:10.1038/nn1473 (2005).

22 Chang, D. W., Claassen, G. F., Hann, S. R. & Cole, M. D. The c-Myc transactivation domain is a direct modulator of apoptotic versus proliferative signals. *Mol Cell Biol* **20**, 4309-4319 (2000).

23 Bowman, T., Symonds, H., Gu, L., Yin, C., Oren, M. & Van Dyke, T. Tissue-specific inactivation of p53 tumor suppression in the mouse. *Genes Dev* **10**, 826-835 (1996).

24 Pei, Y., Moore, C. E., Wang, J., Tewari, A. K., Eroshkin, A., Cho, Y. J., Witt, H., Korshunov, A., Read, T. A., Sun, J. L., Schmitt, E. M., Miller, C. R., Buckley, A. F., McLendon, R. E., Westbrook, T. F., Northcott, P. A., Taylor, M. D., Pfister, S. M., Febbo, P. G. & Wechsler-Reya, R. J. An animal model of MYC-driven medulloblastoma. *Cancer Cell* **21**, 155-167, doi:10.1016/j.ccr.2011.12.021 (2012).

25 Kawauchi, D., Robinson, G., Uziel, T., Gibson, P., Rehg, J., Gao, C., Finkelstein, D., Qu, C., Pounds, S., Ellison, D. W., Gilbertson, R. J. & Roussel, M. F. A mouse model of the most aggressive subgroup of human medulloblastoma. *Cancer Cell* **21**, 168-180, doi:10.1016/j.ccr.2011.12.023 (2012).

26 Ramaswamy, V., Nor, C. & Taylor, M. D. p53 and Meduloblastoma. *Cold Spring Harb Perspect Med* **6**, a026278, doi:10.1101/cshperspect.a026278 (2015).

27 Morrissy, A. S., Garzia, L., Shih, D. J., Zuyderduyn, S., Huang, X., Skowron, P., Remke, M., Cavalli, F. M., Ramaswamy, V., Lindsay, P. E., Jelveh, S., Donovan, L. K., Wang, X., Luu, B., Zayne, K., Li, Y., Mayoh, C., Thiessen, N., Mercier, E., Mungall, K. L., Ma, Y., Tse, K., Zeng, T., Shumansky, K., Roth, A. J., Shah, S., Farooq, H., Kijima, N., Holgado, B. L., Lee, J. J., Matan-Lithwick, S., Liu, J., Mack, S. C., Manno, A., Michealraj, K. A., Nor, C., Peacock, J., Qin, L., Reimand, J., Rolider, A., Thompson, Y. Y., Wu, X., Pugh, T., Ally, A., Bilenky, M., Butterfield, Y. S., Carlsen, R., Cheng, Y., Chuah, E., Corbett, R. D., Dhalla, N., He, A., Lee, D., Li, H. I., Long, W., Mayo, M., Plettner, P., Qian, J. Q., Schein, J. E., Tam, A., Wong, T., Birol, I., Zhao, Y., Faria, C. C., Pimentel, J., Nunes, S., Shalaby, T., Grotzer, M., Pollack, I. F., Hamilton, R. L., Li, X. N., Bendel, A. E., Fults, D. W., Walter, A. W., Kumabe, T., Tominaga, T., Collins, V. P., Cho, Y. J., Hoffman, C., Lyden, D., Wisoff, J. H., Garvin, J. H., Jr., Stearns, D. S., Massimi, L.,

Schuller, U., Sterba, J., Zitterbart, K., Puget, S., Ayrault, O., Dunn, S. E., Tirapelli, D. P., Carlotti, C. G., Wheeler, H., Hallahan, A. R., Ingram, W., MacDonald, T. J., Olson, J. J., Van Meir, E. G., Lee, J. Y., Wang, K. C., Kim, S. K., Cho, B. K., Pietsch, T., Fleischhack, G., Tippelt, S., Ra, Y. S., Bailey, S., Lindsey, J. C., Clifford, S. C., Eberhart, C. G., Cooper, M. K., Packer, R. J., Massimino, M., Garre, M. L., Bartels, U., Tabori, U., Hawkins, C. E., Dirks, P., Bouffet, E., Rutka, J. T., Wechsler-Reya, R. J., Weiss, W. A., Collier, L. S., Dupuy, A. J., Korshunov, A., Jones, D. T., Kool, M., Northcott, P. A., Pfister, S. M., Largaespada, D. A., Mungall, A. J., Moore, R. A., Jabado, N., Bader, G. D., Jones, S. J., Malkin, D., Marra, M. A. & Taylor, M. D. Divergent clonal selection dominates medulloblastoma at recurrence. *Nature* **529**, 351-357, doi:10.1038/nature16478 (2016).

28 Hill, R. M., Kuijper, S., Lindsey, J. C., Petrie, K., Schwalbe, E. C., Barker, K., Boult, J. K., Williamson, D., Ahmad, Z., Hallsworth, A., Ryan, S. L., Poon, E., Robinson, S. P., Ruddle, R., Raynaud, F. I., Howell, L., Kwok, C., Joshi, A., Nicholson, S. L., Crosier, S., Ellison, D. W., Wharton, S. B., Robson, K., Michalski, A., Hargrave, D., Jacques, T. S., Pizer, B., Bailey, S., Swartling, F. J., Weiss, W. A., Chesler, L. & Clifford, S. C. Combined MYC and P53 defects emerge at medulloblastoma relapse and define rapidly progressive, therapeutically targetable disease. *Cancer Cell* **27**, 72-84, doi:10.1016/j.ccell.2014.11.002 (2015).

29 Gajjar, A., Chintagumpala, M., Ashley, D., Kellie, S., Kun, L. E., Merchant, T. E., Woo, S., Wheeler, G., Ahern, V., Krasin, M. J., Fouladi, M., Broniscer, A., Krance, R., Hale, G. A., Stewart, C. F., Dauser, R., Sanford, R. A., Fuller, C., Lau, C., Boyett, J. M., Wallace, D. & Gilbertson, R. J. Risk-adapted craniospinal radiotherapy followed by high-dose chemotherapy and stem-cell rescue in children with newly diagnosed medulloblastoma (St Jude Medulloblastoma-96): long-term results from a prospective, multicentre trial. *Lancet Oncol* **7**, 813-820, doi:10.1016/S1470-2045(06)70867-1 (2006).

30 Gajjar, A., Bowers, D. C., Karajannis, M. A., Leary, S., Witt, H. & Gottardo, N. G. Pediatric Brain Tumors: Innovative Genomic Information Is Transforming the Diagnostic and Clinical Landscape. *J Clin Oncol* **33**, 2986-2998, doi:10.1200/JCO.2014.59.9217 (2015).

31 Packer, R. J. Risk-adapted craniospinal radiotherapy followed by high-dose chemotherapy and stem-cell rescue in children with newly diagnosed medulloblastoma. *Curr Neurol Neurosci Rep* **7**, 130, 132 (2007).

32 Tarbell, N. J., Friedman, H., Polkinghorn, W. R., Yock, T., Zhou, T., Chen, Z., Burger, P., Barnes, P. & Kun, L. High-risk medulloblastoma: a pediatric oncology group randomized trial of chemotherapy before or after radiation therapy (POG 9031). *J Clin Oncol* **31**, 2936-2941, doi:10.1200/JCO.2012.43.9984 (2013).

33 Goschzik, T., Zur Muhlen, A., Kristiansen, G., Haberler, C., Stefanits, H., Friedrich, C., von Hoff, K., Rutkowski, S., Pfister, S. M. & Pietsch, T. Molecular stratification of medulloblastoma: comparison of histological and genetic methods to detect Wnt activated tumours. *Neuropathol Appl Neurobiol* **41**, 135-144, doi:10.1111/nan.12161 (2015).

34 Rodon, J., Tawbi, H. A., Thomas, A. L., Stoller, R. G., Turtschi, C. P., Baselga, J., Sarantopoulos, J., Mahalingam, D., Shou, Y., Moles, M. A., Yang, L., Granvil, C., Hurh, E., Rose, K. L., Amakye, D. D., Dummer, R. & Mita, A. C. A phase I, multicenter, open-label, first-in-human, dose-escalation study of the oral smoothened inhibitor Sonidegib (LDE225) in patients with advanced solid tumors. *Clin Cancer Res* **20**, 1900-1909, doi:10.1158/1078-0432.CCR-13-1710 (2014).

35 Robinson, G. W., Orr, B. A., Wu, G., Gururangan, S., Lin, T., Qaddoumi, I., Packer, R. J., Goldman, S., Prados, M. D., Desjardins, A., Chintagumpala, M., Takebe, N., Kaste, S. C., Rusch, M., Allen, S. J., Onar-Thomas, A., Stewart, C. F., Fouladi, M., Boyett, J. M., Gilbertson, R. J., Curran, T., Ellison, D. W. & Gajjar, A. Vismodegib Exerts Targeted Efficacy Against Recurrent Sonic Hedgehog-Subgroup Medulloblastoma: Results From Phase II Pediatric Brain Tumor Consortium Studies PBTC-025B and PBTC-032. *J Clin Oncol* **33**, 2646-2654, doi:10.1200/JCO.2014.60.1591 (2015).

36 Ransohoff, K. J., Sarin, K. Y. & Tang, J. Y. Smoothened Inhibitors in Sonic Hedgehog Subgroup Medulloblastoma. *J Clin Oncol* **33**, 2692-2694, doi:10.1200/JCO.2015.62.2225 (2015).

37 Pei, Y., Liu, K. W., Wang, J., Garancher, A., Tao, R., Esparza, L. A., Maier, D. L., Udaka, Y. T., Murad, N., Morrissy, S., Seker-Cin, H., Brabetz, S., Qi, L., Kogiso, M., Schubert, S., Olson, J. M., Cho, Y. J., Li, X. N., Crawford, J. R., Levy, M. L., Kool, M., Pfister, S. M., Taylor, M. D. & Wechsler-Reya, R. J. HDAC and PI3K Antagonists Cooperate to Inhibit Growth of MYC-Driven Medulloblastoma. *Cancer Cell* **29**, 311-323, doi:10.1016/j.ccell.2016.02.011 (2016).

38 Morfouace, M., Shelat, A., Jacus, M., Freeman, B. B., 3rd, Turner, D., Robinson, S., Zindy, F., Wang, Y. D., Finkelstein, D., Ayrault, O., Bihannic, L., Puget, S., Li, X. N., Olson, J. M., Robinson, G. W., Guy, R.

K., Stewart, C. F., Gajjar, A. & Roussel, M. F. Pemetrexed and gemcitabine as combination therapy for the treatment of Group3 medulloblastoma. *Cancer Cell* **25**, 516-529, doi:10.1016/j.ccr.2014.02.009 (2014).

39 Jones, D. T., Jager, N., Kool, M., Zichner, T., Hutter, B., Sultan, M., Cho, Y. J., Pugh, T. J., Hovestadt, V., Stutz, A. M., Rausch, T., Warnatz, H. J., Ryzhova, M., Bender, S., Sturm, D., Pleier, S., Cin, H., Pfaff, E., Sieber, L., Wittmann, A., Remke, M., Witt, H., Hutter, S., Tzaridis, T., Weischenfeldt, J., Raeder, B., Avci, M., Amstislavskiy, V., Zapatka, M., Weber, U. D., Wang, Q., Lasitschka, B., Bartholomae, C. C., Schmidt, M., von Kalle, C., Ast, V., Lawerenz, C., Eils, J., Kabbe, R., Benes, V., van Sluis, P., Koster, J., Volckmann, R., Shih, D., Betts, M. J., Russell, R. B., Coco, S., Tonini, G. P., Schuller, U., Hans, V., Graf, N., Kim, Y. J., Monoranu, C., Roggendorf, W., Unterberg, A., Herold-Mende, C., Milde, T., Kulozik, A. E., von Deimling, A., Witt, O., Maass, E., Rossler, J., Ebinger, M., Schuhmann, M. U., Fruhwald, M. C., Hasselblatt, M., Jabado, N., Rutkowski, S., von Bueren, A. O., Williamson, D., Clifford, S. C., McCabe, M. G., Collins, V. P., Wolf, S., Wiemann, S., Lehrach, H., Brors, B., Scheurlen, W., Felsberg, J., Reifenberger, G., Northcott, P. A., Taylor, M. D., Meyerson, M., Pomeroy, S. L., Yaspo, M. L., Korbel, J. O., Korshunov, A., Eils, R., Pfister, S. M. & Lichter, P. Dissecting the genomic complexity underlying medulloblastoma. *Nature* **488**, 100-105, doi:10.1038/nature11284 (2012).

40 Robinson, G., Parker, M., Kranenburg, T. A., Lu, C., Chen, X., Ding, L., Phoenix, T. N., Hedlund, E., Wei, L., Zhu, X., Chalhoub, N., Baker, S. J., Huether, R., Kriwacki, R., Curley, N., Thiruvenkatam, R., Wang, J., Wu, G., Rusch, M., Hong, X., Becksfort, J., Gupta, P., Ma, J., Easton, J., Vadodaria, B., Onar-Thomas, A., Lin, T., Li, S., Pounds, S., Paugh, S., Zhao, D., Kawauchi, D., Roussel, M. F., Finkelstein, D., Ellison, D. W., Lau, C. C., Bouffet, E., Hassall, T., Gururangan, S., Cohn, R., Fulton, R. S., Fulton, L. L., Dooling, D. J., Ochoa, K., Gajjar, A., Mardis, E. R., Wilson, R. K., Downing, J. R., Zhang, J. & Gilbertson, R. J. Novel mutations target distinct subgroups of medulloblastoma. *Nature* **488**, 43-48, doi:10.1038/nature11213 (2012).

41 Li, H. & Durbin, R. Fast and accurate short read alignment with Burrows-Wheeler transform. *Bioinformatics* **25**, 1754-1760, doi:10.1093/bioinformatics/btp324 (2009).

42 Quinlan, A. R. & Hall, I. M. BEDTools: a flexible suite of utilities for comparing genomic features. *Bioinformatics* **26**, 841-842, doi:10.1093/bioinformatics/btq033 (2010).

43 Cairns, J., Spyrou, C., Stark, R., Smith, M. L., Lynch, A. G. & Tavare, S. BayesPeak--an R package for analysing ChIP-seq data. *Bioinformatics* **27**, 713-714, doi:10.1093/bioinformatics/btq685 (2011).

44 Hnisz, D., Abraham, B. J., Lee, T. I., Lau, A., Saint-Andre, V., Sigova, A. A., Hoke, H. A. & Young, R. A. Super-enhancers in the control of cell identity and disease. *Cell* **155**, 934-947, doi:10.1016/j.cell.2013.09.053 (2013).

45 Richter, J., Schlesner, M., Hoffmann, S., Kreuz, M., Leich, E., Burkhardt, B., Rosolowski, M., Ammerpohl, O., Wagener, R., Bernhart, S. H., Lenze, D., Szczepanowski, M., Paulsen, M., Lipinski, S., Russell, R. B., Adam-Klages, S., Apic, G., Claviez, A., Hasenclever, D., Hovestadt, V., Hornig, N., Korbel, J. O., Kube, D., Langenberger, D., Lawerenz, C., Lisfeld, J., Meyer, K., Picelli, S., Pischimarov, J., Radlwimmer, B., Rausch, T., Rohde, M., Schilhabel, M., Scholtysik, R., Spang, R., Trautmann, H., Zenz, T., Borkhardt, A., Drexler, H. G., Moller, P., MacLeod, R. A., Pott, C., Schreiber, S., Trumper, L., Loeffler, M., Stadler, P. F., Lichter, P., Eils, R., Kuppers, R., Hummel, M., Klapper, W., Rosenstiel, P., Rosenwald, A., Brors, B., Siebert, R. & Project, I. M.-S. Recurrent mutation of the ID3 gene in Burkitt lymphoma identified by integrated genome, exome and transcriptome sequencing. *Nat Genet* **44**, 1316-1320, doi:10.1038/ng.2469 (2012).

46 Lister, R., Pelizzola, M., Kida, Y. S., Hawkins, R. D., Nery, J. R., Hon, G., Antosiewicz-Bourget, J., O'Malley, R., Castanon, R., Klugman, S., Downes, M., Yu, R., Stewart, R., Ren, B., Thomson, J. A., Evans, R. M. & Ecker, J. R. Hotspots of aberrant epigenomic reprogramming in human induced pluripotent stem cells. *Nature* **471**, 68-73, doi:10.1038/nature09798 (2011).

47 Genomes Project, C., Abecasis, G. R., Auton, A., Brooks, L. D., DePristo, M. A., Durbin, R. M., Handsaker, R. E., Kang, H. M., Marth, G. T. & McVean, G. A. An integrated map of genetic variation from 1,092 human genomes. *Nature* **491**, 56-65, doi:10.1038/nature11632 (2012).

48 Hovestadt, V., Jones, D. T., Picelli, S., Wang, W., Kool, M., Northcott, P. A., Sultan, M., Stachurski, K., Ryzhova, M., Warnatz, H. J., Ralser, M., Brun, S., Bunt, J., Jager, N., Kleinheinz, K., Erkek, S., Weber, U. D., Bartholomae, C. C., von Kalle, C., Lawerenz, C., Eils, J., Koster, J., Versteeg, R., Milde, T., Witt, O., Schmidt, S., Wolf, S., Pietsch, T., Rutkowski, S., Scheurlen, W., Taylor, M. D., Brors, B., Felsberg, J., Reifenberger, G., Borkhardt, A., Lehrach, H., Wechsler-Reya, R. J., Eils, R., Yaspo, M. L., Landgraf, P., Korshunov, A., Zapatka, M.,

Radlwimmer, B., Pfister, S. M. & Lichter, P. Decoding the regulatory landscape of medulloblastoma using DNA methylation sequencing. *Nature* **510**, 537-541, doi:10.1038/nature13268 (2014).

49 Krueger, F. & Andrews, S. R. Bismark: a flexible aligner and methylation caller for Bisulfite-Seq applications. *Bioinformatics* **27**, 1571-1572, doi:10.1093/bioinformatics/btr167 (2011).

50 Kim, D. & Salzberg, S. L. TopHat-Fusion: an algorithm for discovery of novel fusion transcripts. *Genome Biol* **12**, R72, doi:10.1186/gb-2011-12-8-r72 (2011).

51 Yeung, K. Y., Fraley, C., Murua, A., Raftery, A. E. & Ruzzo, W. L. Model-based clustering and data transformations for gene expression data. *Bioinformatics* **17**, 977-987 (2001).

52 Subramanian, A., Tamayo, P., Mootha, V. K., Mukherjee, S., Ebert, B. L., Gillette, M. A., Paulovich, A., Pomeroy, S. L., Golub, T. R., Lander, E. S. & Mesirov, J. P. Gene set enrichment analysis: a knowledge-based approach for interpreting genome-wide expression profiles. *Proc Natl Acad Sci U S A* **102**, 15545-15550, doi:10.1073/pnas.0506580102 (2005).

53 Su, A. I., Wiltshire, T., Batalov, S., Lapp, H., Ching, K. A., Block, D., Zhang, J., Soden, R., Hayakawa, M., Kreiman, G., Cooke, M. P., Walker, J. R. & Hogenesch, J. B. A gene atlas of the mouse and human protein-encoding transcriptomes. *Proc Natl Acad Sci U S A* **101**, 6062-6067, doi:10.1073/pnas.0400782101 (2004).

54 Boutros, P. C. LTR: Linear Cross-Platform Integration of Microarray Data. *Cancer Inform* **9**, 197-208 (2010).

55 Wang, J., Scully, K., Zhu, X., Cai, L., Zhang, J., Prefontaine, G. G., Krones, A., Ohgi, K. A., Zhu, P., Garcia-Bassets, I., Liu, F., Taylor, H., Lozach, J., Jayes, F. L., Korach, K. S., Glass, C. K., Fu, X. D. & Rosenfeld, M. G. Opposing LSD1 complexes function in developmental gene activation and repression programmes. *Nature* **446**, 882-887, doi:10.1038/nature05671 (2007).

56 Northcott, P. A., Shih, D. J., Peacock, J., Garzia, L., Morrissy, A. S., Zichner, T., Stutz, A. M., Korshunov, A., Reimand, J., Schumacher, S. E., Beroukhim, R., Ellison, D. W., Marshall, C. R., Lionel, A. C., Mack, S., Dubuc, A., Yao, Y., Ramaswamy, V., Luu, B., Rolider, A., Cavalli, F. M., Wang, X., Remke, M., Wu, X., Chiu, R. Y., Chu, A., Chuah, E., Corbett, R. D., Hoad, G. R., Jackman, S. D., Li, Y., Lo, A., Mungall, K.

L., Nip, K. M., Qian, J. Q., Raymond, A. G., Thiessen, N. T., Varhol, R. J., Birol, I., Moore, R. A., Mungall, A. J., Holt, R., Kawauchi, D., Roussel, M. F., Kool, M., Jones, D. T., Witt, H., Fernandez, L. A., Kenney, A. M., Wechsler-Reya, R. J., Dirks, P., Aviv, T., Grajkowska, W. A., Perek-Polnik, M., Haberler, C. C., Delattre, O., Reynaud, S. S., Doz, F. F., Pernet-Fattet, S. S., Cho, B. K., Kim, S. K., Wang, K. C., Scheurlen, W., Eberhart, C. G., Fevre-Montange, M., Jouvet, A., Pollack, I. F., Fan, X., Muraszko, K. M., Gillespie, G. Y., Di Rocco, C., Massimi, L., Michiels, E. M., Kloosterhof, N. K., French, P. J., Kros, J. M., Olson, J. M., Ellenbogen, R. G., Zitterbart, K., Kren, L., Thompson, R. C., Cooper, M. K., Lach, B., McLendon, R. E., Bigner, D. D., Fontebasso, A., Albrecht, S., Jabado, N., Lindsey, J. C., Bailey, S., Gupta, N., Weiss, W. A., Bognar, L., Klekner, A., Van Meter, T. E., Kumabe, T., Tominaga, T., Elbabaa, S. K., Leonard, J. R., Rubin, J. B., Liau, L. M., Van Meir, E. G., Fouladi, M., Nakamura, H., Cinalli, G., Garami, M., Hauser, P., Saad, A. G., Iolascon, A., Jung, S., Carlotti, C. G., Vibhakar, R., Ra, Y. S., Robinson, S., Zollo, M., Faria, C. C., Chan, J. A., Levy, M. L., Sorensen, P. H., Meyerson, M., Pomeroy, S. L., Cho, Y. J., Bader, G. D., Tabori, U., Hawkins, C. E., Bouffet, E., Scherer, S. W., Rutka, J. T., Malkin, D., Clifford, S. C., Jones, S. J., Korbel, J. O., Pfister, S. M., Marra, M. A. & Taylor, M. D. Subgroup-specific structural variation across 1,000 medulloblastoma genomes. *Nature* **488**, 49-56, doi:10.1038/nature11327 (2012).

57 Whyte, W. A., Orlando, D. A., Hnisz, D., Abraham, B. J., Lin, C. Y., Kagey, M. H., Rahl, P. B., Lee, T. I. & Young, R. A. Master transcription factors and mediator establish super-enhancers at key cell identity genes. *Cell* **153**, 307-319, doi:10.1016/j.cell.2013.03.035 (2013).

58 Gilks, C. B., Bear, S. E., Grimes, H. L. & Tsichlis, P. N. Progression of interleukin-2 (IL-2)-dependent rat T cell lymphoma lines to IL-2-independent growth following activation of a gene (Gfi-1) encoding a novel zinc finger protein. *Mol Cell Biol* **13**, 1759-1768 (1993).

59 Scheijen, B., Jonkers, J., Acton, D. & Berns, A. Characterization of pal-1, a common proviral insertion site in murine leukemia virus-induced lymphomas of c-myc and Pim-1 transgenic mice. *J Virol* **71**, 9-16 (1997).

60 Zornig, M., Schmidt, T., Karsunky, H., Grzeschiczek, A. & Moroy, T. Zinc finger protein GFI-1 cooperates with myc and pim-1 in T-cell lymphomagenesis by reducing the requirements for IL-2. *Oncogene* **12**, 1789-1801 (1996).

61 Schmidt, T., Karsunky, H., Gau, E., Zevnik, B., Elsasser, H. P. & Moroy, T. Zinc finger protein GFI-1 has low oncogenic potential but cooperates strongly with pim and myc genes in T-cell lymphomagenesis. *Oncogene* **17**, 2661-2667, doi:10.1038/sj.onc.1202191 (1998).

62 Rausch, T., Jones, D. T., Zapatka, M., Stutz, A. M., Zichner, T., Weischenfeldt, J., Jager, N., Remke, M., Shih, D., Northcott, P. A., Pfaff, E., Tica, J., Wang, Q., Massimi, L., Witt, H., Bender, S., Pleier, S., Cin, H., Hawkins, C., Beck, C., von Deimling, A., Hans, V., Brors, B., Eils, R., Scheurlen, W., Blake, J., Benes, V., Kulozik, A. E., Witt, O., Martin, D., Zhang, C., Porat, R., Merino, D. M., Wasserman, J., Jabado, N., Fontebasso, A., Bullinger, L., Rucker, F. G., Dohner, K., Dohner, H., Koster, J., Molenaar, J. J., Versteeg, R., Kool, M., Tabori, U., Malkin, D., Korshunov, A., Taylor, M. D., Lichter, P., Pfister, S. M. & Korbel, J. O. Genome sequencing of pediatric medulloblastoma links catastrophic DNA rearrangements with TP53 mutations. *Cell* **148**, 59-71, doi:10.1016/j.cell.2011.12.013 (2012).

63 Plass, C., Pfister, S. M., Lindroth, A. M., Bogatyrova, O., Claus, R. & Lichter, P. Mutations in regulators of the epigenome and their connections to global chromatin patterns in cancer. *Nat Rev Genet* **14**, 765-780, doi:10.1038/nrg3554 (2013).

64 Shen, H. & Laird, P. W. Interplay between the cancer genome and epigenome. *Cell* **153**, 38-55, doi:10.1016/j.cell.2013.03.008 (2013).

65 Korsmeyer, S. J. Chromosomal translocations in lymphoid malignancies reveal novel proto-oncogenes. *Annu Rev Immunol* **10**, 785-807, doi:10.1146/annurev.iy.10.040192.004033 (1992).

66 Nambiar, M., Kari, V. & Raghavan, S. C. Chromosomal translocations in cancer. *Biochim Biophys Acta* **1786**, 139-152, doi:10.1016/j.bbcan.2008.07.005 (2008).

67 Bakhshi, A., Wright, J. J., Graninger, W., Seto, M., Owens, J., Cossman, J., Jensen, J. P., Goldman, P. & Korsmeyer, S. J. Mechanism of the t(14;18) chromosomal translocation: structural analysis of both derivative 14 and 18 reciprocal partners. *Proc Natl Acad Sci U S A* **84**, 2396-2400 (1987).

68 Cleary, M. L. & Sklar, J. Nucleotide sequence of a t(14;18) chromosomal breakpoint in follicular lymphoma and demonstration of a breakpoint-cluster region near a transcriptionally active locus on chromosome 18. *Proc Natl Acad Sci U S A* **82**, 7439-7443 (1985).

69 Taub, R., Kirsch, I., Morton, C., Lenoir, G., Swan, D., Tronick, S., Aaronson, S. & Leder, P. Translocation of the c-myc gene into the immunoglobulin heavy chain locus in human Burkitt lymphoma and murine plasmacytoma cells. *Proc Natl Acad Sci U S A* **79**, 7837-7841 (1982).

70 Hecht, J. L. & Aster, J. C. Molecular biology of Burkitt's lymphoma. *J Clin Oncol* **18**, 3707-3721, doi:10.1200/jco.2000.18.21.3707 (2000).

71 Leder, P., Battey, J., Lenoir, G., Moulding, C., Murphy, W., Potter, H., Stewart, T. & Taub, R. Translocations among antibody genes in human cancer. *Science* **222**, 765-771 (1983).

72 Zhang, X., Choi, P. S., Francis, J. M., Imielinski, M., Watanabe, H., Cherniack, A. D. & Meyerson, M. Identification of focally amplified lineage-specific super-enhancers in human epithelial cancers. *Nat Genet* **48**, 176-182, doi:10.1038/ng.3470 (2016).

73 Drier, Y., Cotton, M. J., Williamson, K. E., Gillespie, S. M., Ryan, R. J., Kluk, M. J., Carey, C. D., Rodig, S. J., Sholl, L. M., Afrogheh, A. H., Faquin, W. C., Queimado, L., Qi, J., Wick, M. J., El-Naggar, A. K., Bradner, J. E., Moskaluk, C. A., Aster, J. C., Knoechel, B. & Bernstein, B. E. An oncogenic MYB feedback loop drives alternate cell fates in adenoid cystic carcinoma. *Nat Genet* **48**, 265-272, doi:10.1038/ng.3502 (2016).

74 Khandanpour, C., Thiede, C., Valk, P. J., Sharif-Askari, E., Nuckel, H., Lohmann, D., Horsthemke, B., Siffert, W., Neubauer, A., Grzeschik, K. H., Bloomfield, C. D., Marcucci, G., Maharry, K., Slovak, M. L., van der Reijden, B. A., Jansen, J. H., Schackert, H. K., Afshar, K., Schnittger, S., Peeters, J. K., Kroschinsky, F., Ehninger, G., Lowenberg, B., Duhrsen, U. & Moroy, T. A variant allele of Growth Factor Independence 1 (GFI1) is associated with acute myeloid leukemia. *Blood* **115**, 2462-2472, doi:10.1182/blood-2009-08-239822 (2010).

75 Huang, M., Hu, Z., Chang, W., Ou, D., Zhou, J. & Zhang, Y. The growth factor independence-1 (Gfi1) is overexpressed in chronic myelogenous leukemia. *Acta Haematol* **123**, 1-5, doi:10.1159/000253856 (2010).

76 Vassen, L., Khandanpour, C., Ebeling, P., van der Reijden, B. A., Jansen, J. H., Mahlmann, S., Duhrsen, U. & Moroy, T. Growth factor independent 1b (Gfi1b) and a new splice variant of Gfi1b are highly expressed in patients with acute and chronic leukemia. *Int J Hematol* **89**, 422-430, doi:10.1007/s12185-009-0286-5 (2009).

77 Wallis, D., Hamblen, M., Zhou, Y., Venken, K. J., Schumacher, A., Grimes, H. L., Zoghbi, H. Y., Orkin, S. H. & Bellen, H. J. The zinc finger transcription factor Gfi1, implicated in lymphomagenesis, is required for inner ear hair cell differentiation and survival. *Development* **130**, 221-232 (2003).

78 Tsuda, H., Jafar-Nejad, H., Patel, A. J., Sun, Y., Chen, H. K., Rose, M. F., Venken, K. J., Botas, J., Orr, H. T., Bellen, H. J. & Zoghbi, H. Y. The AXH domain of Ataxin-1 mediates neurodegeneration through its interaction with Gfi-1/Senseless proteins. *Cell* **122**, 633-644, doi:10.1016/j.cell.2005.06.012 (2005).

79 Kazanjian, A., Wallis, D., Au, N., Nigam, R., Venken, K. J., Cagle, P. T., Dickey, B. F., Bellen, H. J., Gilks, C. B. & Grimes, H. L. Growth factor independence-1 is expressed in primary human neuroendocrine lung carcinomas and mediates the differentiation of murine pulmonary neuroendocrine cells. *Cancer Res* **64**, 6874-6882, doi:10.1158/0008-5472.CAN-04-0633 (2004).

80 Shroyer, N. F., Wallis, D., Venken, K. J., Bellen, H. J. & Zoghbi, H. Y. Gfi1 functions downstream of Math1 to control intestinal secretory cell subtype allocation and differentiation. *Genes Dev* **19**, 2412-2417, doi:10.1101/gad.1353905 (2005).

81 van Lohuizen, M., Verbeek, S., Scheijen, B., Wientjens, E., van der Gulden, H. & Berns, A. Identification of cooperating oncogenes in E mu-myc transgenic mice by provirus tagging. *Cell* **65**, 737-752 (1991).

82 Northcott, P. A., Lee, C., Zichner, T., Stutz, A. M., Erkek, S., Kawauchi, D., Shih, D. J., Hovestadt, V., Zapatka, M., Sturm, D., Jones, D. T., Kool, M., Remke, M., Cavalli, F. M., Zuyderduyn, S., Bader, G. D., VandenBerg, S., Esparza, L. A., Ryzhova, M., Wang, W., Wittmann, A., Stark, S., Sieber, L., Seker-Cin, H., Linke, L., Kratochwil, F., Jager, N., Buchhalter, I., Imbusch, C. D., Zipprich, G., Raeder, B., Schmidt, S., Diessl, N., Wolf, S., Wiemann, S., Brors, B., Lawerenz, C., Eils, J., Warnatz, H. J., Risch, T., Yaspo, M. L., Weber, U. D., Bartholomae, C. C., von Kalle, C., Turanyi, E., Hauser, P., Sanden, E., Darabi, A., Siesjo, P., Sterba, J., Zitterbart, K., Sumerauer, D., van Sluis, P., Versteeg, R., Volckmann, R., Koster, J., Schuhmann, M. U., Ebinger, M., Grimes, H. L., Robinson, G. W., Gajjar, A., Mynarek, M., von Hoff, K., Rutkowski, S., Pietsch, T., Scheurlen, W., Felsberg, J., Reifenberger, G., Kulozik, A. E., von Deimling, A., Witt, O., Eils, R., Gilbertson, R. J., Korshunov, A., Taylor, M. D., Lichter, P., Korbel, J. O., Wechsler-Reya, R. J. & Pfister, S. M. Enhancer hijacking activates

GFI1 family oncogenes in medulloblastoma. *Nature* **511**, 428-434, doi:10.1038/nature13379 (2014).

83 Hock, H., Hamblen, M. J., Rooke, H. M., Traver, D., Bronson, R. T., Cameron, S. & Orkin, S. H. Intrinsic requirement for zinc finger transcription factor Gfi-1 in neutrophil differentiation. *Immunity* **18**, 109-120 (2003).

84 Hock, H., Hamblen, M. J., Rooke, H. M., Schindler, J. W., Saleque, S., Fujiwara, Y. & Orkin, S. H. Gfi-1 restricts proliferation and preserves functional integrity of haematopoietic stem cells. *Nature* **431**, 1002-1007, doi:10.1038/nature02994 (2004).

85 Moroy, T., Zeng, H., Jin, J., Schmid, K. W., Carpinteiro, A. & Gulbins, E. The zinc finger protein and transcriptional repressor Gfi1 as a regulator of the innate immune response. *Immunobiology* **213**, 341-352, doi:10.1016/j.imbio.2007.11.004 (2008).

86 Moroy, T. & Khandanpour, C. Growth factor independence 1 (Gfi1) as a regulator of lymphocyte development and activation. *Semin Immunol* **23**, 368-378, doi:10.1016/j.smim.2011.08.006 (2011).

87 Osawa, M., Yamaguchi, T., Nakamura, Y., Kaneko, S., Onodera, M., Sawada, K., Jegalian, A., Wu, H., Nakauchi, H. & Iwama, A. Erythroid expansion mediated by the Gfi-1B zinc finger protein: role in normal hematopoiesis. *Blood* **100**, 2769-2777, doi:10.1182/blood-2002-01-0182 (2002).

88 Saleque, S., Cameron, S. & Orkin, S. H. The zinc-finger proto-oncogene Gfi-1b is essential for development of the erythroid and megakaryocytic lineages. *Genes Dev* **16**, 301-306, doi:10.1101/gad.959102 (2002).

89 Khandanpour, C., Phelan, J. D., Vassen, L., Schutte, J., Chen, R., Horman, S. R., Gaudreau, M. C., Krongold, J., Zhu, J., Paul, W. E., Duhrsen, U., Gottgens, B., Grimes, H. L. & Moroy, T. Growth factor independence 1 antagonizes a p53-induced DNA damage response pathway in lymphoblastic leukemia. *Cancer Cell* **23**, 200-214, doi:10.1016/j.ccr.2013.01.011 (2013).

90 Grimes, H. L., Chan, T. O., Zweidler-McKay, P. A., Tong, B. & Tsichlis, P. N. The Gfi-1 proto-oncoprotein contains a novel transcriptional repressor domain, SNAG, and inhibits G1 arrest induced by interleukin-2 withdrawal. *Mol Cell Biol* **16**, 6263-6272 (1996).

91 Tong, B., Grimes, H. L., Yang, T. Y., Bear, S. E., Qin, Z., Du, K., El-Deiry, W. S. & Tsichlis, P. N. The Gfi-1B proto-oncoprotein represses p21WAF1 and inhibits myeloid cell differentiation. *Mol Cell Biol* **18**, 2462-2473 (1998).

92 Saleque, S., Kim, J., Rooke, H. M. & Orkin, S. H. Epigenetic regulation of hematopoietic differentiation by Gfi-1 and Gfi-1b is mediated by the cofactors CoREST and LSD1. *Mol Cell* **27**, 562-572, doi:10.1016/j.molcel.2007.06.039 (2007).

93 Chowdhury, A. H., Ramroop, J. R., Upadhyay, G., Sengupta, A., Andrzejczyk, A. & Saleque, S. Differential transcriptional regulation of meis1 by Gfi1b and its co-factors LSD1 and CoREST. *PLoS One* **8**, e53666, doi:10.1371/journal.pone.0053666 (2013).

94 Thambyrajah, R., Mazan, M., Patel, R., Moignard, V., Stefanska, M., Marinopoulou, E., Li, Y., Lancrin, C., Clapes, T., Moroy, T., Robin, C., Miller, C., Cowley, S., Gottgens, B., Kouskoff, V. & Lacaud, G. GFI1 proteins orchestrate the emergence of haematopoietic stem cells through recruitment of LSD1. *Nat Cell Biol* **18**, 21-32, doi:10.1038/ncb3276 (2016).

95 Laurent, B., Randrianarison-Huetz, V., Frisan, E., Andrieu-Soler, C., Soler, E., Fontenay, M., Dusanter-Fourt, I. & Dumenil, D. A short Gfi-1B isoform controls erythroid differentiation by recruiting the LSD1-CoREST complex through the dimethylation of its SNAG domain. *J Cell Sci* **125**, 993-1002, doi:10.1242/jcs.095877 (2012).

96 McGhee, L., Bryan, J., Elliott, L., Grimes, H. L., Kazanjian, A., Davis, J. N. & Meyers, S. Gfi-1 attaches to the nuclear matrix, associates with ETO (MTG8) and histone deacetylase proteins, and represses transcription using a TSA-sensitive mechanism. *J Cell Biochem* **89**, 1005-1018, doi:10.1002/jcb.10548 (2003).

97 Vassen, L., Fiolka, K. & Moroy, T. Gfi1b alters histone methylation at target gene promoters and sites of gamma-satellite containing heterochromatin. *EMBO J* **25**, 2409-2419, doi:10.1038/sj.emboj.7601124 (2006).

98 Montoya-Durango, D. E., Velu, C. S., Kazanjian, A., Rojas, M. E., Jay, C. M., Longmore, G. D. & Grimes, H. L. Ajuba functions as a histone deacetylase-dependent co-repressor for autoregulation of the growth factor-independent-1 transcription factor. *J Biol Chem* **283**, 32056-32065, doi:10.1074/jbc.M802320200 (2008).

99 Chiang, C. & Ayyanathan, K. Snail/Gfi-1 (SNAG) family zinc finger proteins in transcription regulation, chromatin dynamics, cell signaling, development, and disease. *Cytokine Growth Factor Rev* **24**, 123-131, doi:10.1016/j.cytogfr.2012.09.002 (2013).

100 van der Meer, L. T., Jansen, J. H. & van der Reijden, B. A. Gfi1 and Gfi1b: key regulators of hematopoiesis. *Leukemia* **24**, 1834-1843, doi:10.1038/leu.2010.195 (2010).

101 Fiolka, K., Hertzano, R., Vassen, L., Zeng, H., Hermesh, O., Avraham, K. B., Duhrsen, U. & Moroy, T. Gfi1 and Gfi1b act equivalently in haematopoiesis, but have distinct, non-overlapping functions in inner ear development. *EMBO Rep* **7**, 326-333, doi:10.1038/sj.embor.7400618 (2006).

102 Person, R. E., Li, F. Q., Duan, Z., Benson, K. F., Wechsler, J., Papadaki, H. A., Eliopoulos, G., Kaufman, C., Bertolone, S. J., Nakamoto, B., Papayannopoulou, T., Grimes, H. L. & Horwitz, M. Mutations in proto-oncogene GFI1 cause human neutropenia and target ELA2. *Nat Genet* **34**, 308-312, doi:10.1038/ng1170 (2003).

103 Zweidler-Mckay, P. A., Grimes, H. L., Flubacher, M. M. & Tsichlis, P. N. Gfi-1 encodes a nuclear zinc finger protein that binds DNA and functions as a transcriptional repressor. *Mol Cell Biol* **16**, 4024-4034 (1996).

104 Liu, Q., Basu, S., Qiu, Y., Tang, F. & Dong, F. A role of Miz-1 in Gfi-1-mediated transcriptional repression of CDKN1A. *Oncogene* **29**, 2843-2852, doi:10.1038/onc.2010.48 (2010).

105 Duan, Z., Zarebski, A., Montoya-Durango, D., Grimes, H. L. & Horwitz, M. Gfi1 coordinates epigenetic repression of p21Cip/WAF1 by recruitment of histone lysine methyltransferase G9a and histone deacetylase 1. *Mol Cell Biol* **25**, 10338-10351, doi:10.1128/MCB.25.23.10338-10351.2005 (2005).

106 Grimes, H. L., Gilks, C. B., Chan, T. O., Porter, S. & Tsichlis, P. N. The Gfi-1 protooncoprotein represses Bax expression and inhibits T-cell death. *Proc Natl Acad Sci U S A* **93**, 14569-14573 (1996).

107 Moroy, T., Vassen, L., Wilkes, B. & Khandanpour, C. From cytopenia to leukemia: the role of Gfi1 and Gfi1b in blood formation. *Blood* **126**, 2561-2569, doi:10.1182/blood-2015-06-655043 (2015).

108 Velinder, M., Singer, J., Bareyan, D., Meznarich, J., Tracy, C. M., Fulcher, J. M., McClellan, D., Lucente, H., Franklin, S., Sharma, S. & Engel, M. E. GFI1 functions in transcriptional control and cell fate determination require SNAG domain methylation to recruit LSD1. *Biochem J* **473**, 3355-3369, doi:10.1042/BCJ20160558 (2016).

109 Zhu, J., Guo, L., Min, B., Watson, C. J., Hu-Li, J., Young, H. A., Tsichlis, P. N. & Paul, W. E. Growth factor independent-1 induced by IL-4 regulates Th2 cell proliferation. *Immunity* **16**, 733-744 (2002).

110 Huang, D. Y., Kuo, Y. Y. & Chang, Z. F. GATA-1 mediates auto-regulation of Gfi-1B transcription in K562 cells. *Nucleic Acids Res* **33**, 5331-5342, doi:10.1093/nar/gki838 (2005).

111 Duan, Z., Person, R. E., Lee, H. H., Huang, S., Donadieu, J., Badolato, R., Grimes, H. L., Papayannopoulou, T. & Horwitz, M. S. Epigenetic regulation of protein-coding and microRNA genes by the Gfi1-interacting tumor suppressor PRDM5. *Mol Cell Biol* **27**, 6889-6902, doi:10.1128/MCB.00762-07 (2007).

112 Nakazawa, Y., Suzuki, M., Manabe, N., Yamada, T., Kihara-Negishi, F., Sakurai, T., Tenen, D. G., Iwama, A., Mochizuki, M. & Oikawa, T. Cooperative interaction between ETS1 and GFI1 transcription factors in the repression of Bax gene expression. *Oncogene* **26**, 3541-3550, doi:10.1038/sj.onc.1210140 (2007).

113 Basu, S., Liu, Q., Qiu, Y. & Dong, F. Gfi-1 represses CDKN2B encoding p15INK4B through interaction with Miz-1. *Proc Natl Acad Sci U S A* **106**, 1433-1438, doi:10.1073/pnas.0804863106 (2009).

114 Dahl, R., Iyer, S. R., Owens, K. S., Cuylear, D. D. & Simon, M. C. The transcriptional repressor GFI-1 antagonizes PU.1 activity through protein-protein interaction. *J Biol Chem* **282**, 6473-6483, doi:10.1074/jbc.M607613200 (2007).

115 Pajtler, K. W., Weingarten, C., Thor, T., Kunkele, A., Heukamp, L. C., Buttner, R., Suzuki, T., Miyata, N., Grotzer, M., Rieb, A., Sprussel, A., Eggert, A., Schramm, A. & Schulte, J. H. The KDM1A histone demethylase is a promising new target for the epigenetic therapy of medulloblastoma. *Acta Neuropathol Commun* **1**, 19, doi:10.1186/2051-5960-1-19 (2013).

116 Meyer, N., Kim, S. S. & Penn, L. Z. The Oscar-worthy role of Myc in apoptosis. *Semin Cancer Biol* **16**, 275-287, doi:10.1016/j.semcancer.2006.07.011 (2006).

117 Hsu, J. Y., Reimann, J. D., Sorensen, C. S., Lukas, J. & Jackson, P. K. E2F-dependent accumulation of hEmi1 regulates S phase entry by inhibiting APC(Cdh1). *Nat Cell Biol* **4**, 358-366, doi:10.1038/ncb785 (2002).

118 Miller, J. J., Summers, M. K., Hansen, D. V., Nachury, M. V., Lehman, N. L., Loktev, A. & Jackson, P. K. Emi1 stably binds and inhibits the anaphase-promoting complex/cyclosome as a pseudosubstrate inhibitor. *Genes Dev* **20**, 2410-2420, doi:10.1101/gad.1454006 (2006).

119 Pines, J. Cubism and the cell cycle: the many faces of the APC/C. *Nat Rev Mol Cell Biol* **12**, 427-438, doi:10.1038/nrm3132 (2011).

120 Gutgemann, I., Lehman, N. L., Jackson, P. K. & Longacre, T. A. Emi1 protein accumulation implicates misregulation of the anaphase promoting complex/cyclosome pathway in ovarian clear cell carcinoma. *Mod Pathol* **21**, 445-454, doi:10.1038/modpathol.3801022 (2008).

121 Liu, X., Wang, H., Ma, J., Xu, J., Sheng, C., Yang, S., Sun, L. & Ni, Q. The expression and prognosis of Emi1 and Skp2 in breast carcinoma: associated with PI3K/Akt pathway and cell proliferation. *Med Oncol* **30**, 735, doi:10.1007/s12032-013-0735-0 (2013).

122 Vaidyanathan, S., Cato, K., Tang, L., Pavey, S., Haass, N. K., Gabrielli, B. G. & Duijf, P. H. In vivo overexpression of Emi1 promotes chromosome instability and tumorigenesis. *Oncogene* **35**, 5446-5455, doi:10.1038/onc.2016.94 (2016).

123 Zhao, Y., Tang, Q., Ni, R., Huang, X., Wang, Y., Lu, C., Shen, A., Wang, Y., Li, C., Yuan, Q., Chen, H., Cheng, C. & He, S. Early mitotic inhibitor-1, an anaphase-promoting complex/cyclosome inhibitor, can control tumor cell proliferation in hepatocellular carcinoma: correlation with Skp2 stability and degradation of p27(Kip1). *Hum Pathol* **44**, 365-373, doi:10.1016/j.humpath.2012.03.030 (2013).

124 Rhodes, J., Amsterdam, A., Sanda, T., Moreau, L. A., McKenna, K., Heinrichs, S., Ganem, N. J., Ho, K. W., Neuberg, D. S., Johnston, A., Ahn, Y., Kutok, J. L., Hromas, R., Wray, J., Lee, C., Murphy, C., Radtke, I., Downing, J. R., Fleming, M. D., MacConaill, L. E., Amatruda, J. F., Gutierrez, A., Galinsky, I., Stone, R. M., Ross, E. A., Pellman, D. S., Kanki, J. P. & Look, A. T. Emi1 maintains genomic integrity during zebrafish embryogenesis and cooperates with p53 in tumor suppression. *Mol Cell Biol* **29**, 5911-5922, doi:10.1128/MCB.00558-09 (2009).

125 Neelamegam, R., Ricq, E. L., Malvaez, M., Patnaik, D., Norton, S., Carlin, S. M., Hill, I. T., Wood, M. A., Haggarty, S. J. & Hooker, J. M. Brain-penetrant LSD1 inhibitors can block memory consolidation. *ACS Chem Neurosci* **3**, 120-128, doi:10.1021/cn200104y (2012).

126 Hayes, D. N. & Kim, W. Y. The next steps in next-gen sequencing of cancer genomes. *J Clin Invest* **125**, 462-468, doi:10.1172/JCI68339 (2015).

127 Paddison, P. J., Caudy, A. A., Bernstein, E., Hannon, G. J. & Conklin, D. S. Short hairpin RNAs (shRNAs) induce sequence-specific silencing in mammalian cells. *Genes Dev* **16**, 948-958, doi:10.1101/gad.981002 (2002).

128 Brummelkamp, T. R., Bernards, R. & Agami, R. A system for stable expression of short interfering RNAs in mammalian cells. *Science* **296**, 550-553, doi:10.1126/science.1068999 (2002).

129 Sui, G., Soohoo, C., Affar el, B., Gay, F., Shi, Y., Forrester, W. C. & Shi, Y. A DNA vector-based RNAi technology to suppress gene expression in mammalian cells. *Proc Natl Acad Sci U S A* **99**, 5515-5520, doi:10.1073/pnas.082117599 (2002).

130 Westbrook, T. F., Martin, E. S., Schlabach, M. R., Leng, Y., Liang, A. C., Feng, B., Zhao, J. J., Roberts, T. M., Mandel, G., Hannon, G. J., Depinho, R. A., Chin, L. & Elledge, S. J. A genetic screen for candidate tumor suppressors identifies REST. *Cell* **121**, 837-848, doi:10.1016/j.cell.2005.03.033 (2005).

131 Sheng, Z., Li, L., Zhu, L. J., Smith, T. W., Demers, A., Ross, A. H., Moser, R. P. & Green, M. R. A genome-wide RNA interference screen reveals an essential CREB3L2-ATF5-MCL1 survival pathway in malignant glioma with therapeutic implications. *Nat Med* **16**, 671-677, doi:10.1038/nm.2158 (2010).

132 Schramek, D., Sendoel, A., Segal, J. P., Beronja, S., Heller, E., Oristian, D., Reva, B. & Fuchs, E. Direct in vivo RNAi screen unveils myosin IIa as a tumor suppressor of squamous cell carcinomas. *Science* **343**, 309-313, doi:10.1126/science.1248627 (2014).

133 Sa, J. K., Yoon, Y., Kim, M., Kim, Y., Cho, H. J., Lee, J. K., Kim, G. S., Han, S., Kim, W. J., Shin, Y. J., Joo, K. M., Paddison, P. J., Ishitani, T., Lee, J. & Nam, D. H. In vivo RNAi screen identifies NLK as a negative regulator of mesenchymal activity in glioblastoma. *Oncotarget* **6**, 20145-20159, doi:10.18632/oncotarget.3980 (2015).

134 Meacham, C. E., Lawton, L. N., Soto-Feliciano, Y. M., Pritchard, J. R., Joughin, B. A., Ehrenberger, T., Fenouille, N., Zuber, J., Williams, R. T., Young, R. A. & Hemann, M. T. A genome-scale in vivo loss-of-function screen identifies Phf6 as a lineage-specific regulator of leukemia cell growth. *Genes Dev* **29**, 483-488, doi:10.1101/gad.254151.114 (2015).

135 Zender, L., Xue, W., Zuber, J., Semighini, C. P., Krasnitz, A., Ma, B., Zender, P., Kubicka, S., Luk, J. M., Schirmacher, P., McCombie, W. R., Wigler, M., Hicks, J., Hannon, G. J., Powers, S. & Lowe, S. W. An oncogenomics-based in vivo RNAi screen identifies tumor suppressors in liver cancer. *Cell* **135**, 852-864, doi:10.1016/j.cell.2008.09.061 (2008).

136 Jackson, A. L., Bartz, S. R., Schelter, J., Kobayashi, S. V., Burchard, J., Mao, M., Li, B., Cavet, G. & Linsley, P. S. Expression profiling reveals off-target gene regulation by RNAi. *Nat Biotechnol* **21**, 635-637, doi:10.1038/nbt831 (2003).

137 Birmingham, A., Anderson, E. M., Reynolds, A., Ilsley-Tyree, D., Leake, D., Fedorov, Y., Baskerville, S., Maksimova, E., Robinson, K., Karpilow, J., Marshall, W. S. & Khvorova, A. 3' UTR seed matches, but not overall identity, are associated with RNAi off-targets. *Nat Methods* **3**, 199-204, doi:10.1038/nmeth854 (2006).

138 Cong, L., Ran, F. A., Cox, D., Lin, S., Barretto, R., Habib, N., Hsu, P. D., Wu, X., Jiang, W., Marraffini, L. A. & Zhang, F. Multiplex genome engineering using CRISPR/Cas systems. *Science* **339**, 819-823, doi:10.1126/science.1231143 (2013).

139 Yang, H., Wang, H., Shivalila, C. S., Cheng, A. W., Shi, L. & Jaenisch, R. One-step generation of mice carrying reporter and conditional alleles by CRISPR/Cas-mediated genome engineering. *Cell* **154**, 1370-1379, doi:10.1016/j.cell.2013.08.022 (2013).

140 Wang, H., Yang, H., Shivalila, C. S., Dawlaty, M. M., Cheng, A. W., Zhang, F. & Jaenisch, R. One-step generation of mice carrying mutations in multiple genes by CRISPR/Cas-mediated genome engineering. *Cell* **153**, 910-918, doi:10.1016/j.cell.2013.04.025 (2013).

141 Shalem, O., Sanjana, N. E. & Zhang, F. High-throughput functional genomics using CRISPR-Cas9. *Nat Rev Genet* **16**, 299-311, doi:10.1038/nrg3899 (2015).

142 Xue, H. Y., Ji, L. J., Gao, A. M., Liu, P., He, J. D. & Lu, X. J. CRISPR-Cas9 for medical genetic screens: applications and future perspectives. *J Med Genet* **53**, 91-97, doi:10.1136/jmedgenet-2015-103409 (2016).

143 Dupuy, A. J., Akagi, K., Largaespada, D. A., Copeland, N. G. & Jenkins, N. A. Mammalian mutagenesis using a highly mobile somatic Sleeping Beauty transposon system. *Nature* **436**, 221-226, doi:10.1038/nature03691 (2005).

144 Collier, L. S., Carlson, C. M., Ravimohan, S., Dupuy, A. J. & Largaespada, D. A. Cancer gene discovery in solid tumours using transposon-based somatic mutagenesis in the mouse. *Nature* **436**, 272-276, doi:10.1038/nature03681 (2005).

145 Copeland, N. G. & Jenkins, N. A. Harnessing transposons for cancer gene discovery. *Nat Rev Cancer* **10**, 696-706, doi:10.1038/nrc2916 (2010).

146 Mumert, M., Dubuc, A., Wu, X., Northcott, P. A., Chin, S. S., Pedone, C. A., Taylor, M. D. & Fults, D. W. Functional genomics identifies drivers of medulloblastoma dissemination. *Cancer Res* **72**, 4944-4953, doi:10.1158/0008-5472.CAN-12-1629 (2012).

147 Genovesi, L. A., Ng, C. G., Davis, M. J., Remke, M., Taylor, M. D., Adams, D. J., Rust, A. G., Ward, J. M., Ban, K. H., Jenkins, N. A., Copeland, N. G. & Wainwright, B. J. Sleeping Beauty mutagenesis in a mouse medulloblastoma model defines networks that discriminate between human molecular subgroups. *Proc Natl Acad Sci U S A* **110**, E4325-4334, doi:10.1073/pnas.1318639110 (2013).

148 Northcott, P. A., Fernandez, L. A., Hagan, J. P., Ellison, D. W., Grajkowska, W., Gillespie, Y., Grundy, R., Van Meter, T., Rutka, J. T., Croce, C. M., Kenney, A. M. & Taylor, M. D. The miR-17/92 polycistron is up-regulated in sonic hedgehog-driven medulloblastomas and induced by N-myc in sonic hedgehog-treated cerebellar neural precursors. *Cancer Res* **69**, 3249-3255, doi:10.1158/0008-5472.CAN-08-4710 (2009).

149 Parsons, D. W., Li, M., Zhang, X., Jones, S., Leary, R. J., Lin, J. C., Boca, S. M., Carter, H., Samayoa, J., Bettegowda, C., Gallia, G. L., Jallo, G. I., Binder, Z. A., Nikolsky, Y., Hartigan, J., Smith, D. R., Gerhard, D. S., Fults, D. W., VandenBerg, S., Berger, M. S., Marie, S. K., Shinjo, S. M., Clara, C., Phillips, P. C., Minturn, J. E., Biegel, J. A., Judkins, A. R., Resnick, A. C., Storm, P. B., Curran, T., He, Y., Rasheed, B. A., Friedman, H. S., Keir, S. T., McLendon, R., Northcott,

P. A., Taylor, M. D., Burger, P. C., Riggins, G. J., Karchin, R., Parmigiani, G., Bigner, D. D., Yan, H., Papadopoulos, N., Vogelstein, B., Kinzler, K. W. & Velculescu, V. E. The genetic landscape of the childhood cancer medulloblastoma. *Science* **331**, 435-439, doi:10.1126/science.1198056 (2011).

150 Pugh, T. J., Weeraratne, S. D., Archer, T. C., Pomeranz Krummel, D. A., Auclair, D., Bochicchio, J., Carneiro, M. O., Carter, S. L., Cibulskis, K., Erlich, R. L., Greulich, H., Lawrence, M. S., Lennon, N. J., McKenna, A., Meldrim, J., Ramos, A. H., Ross, M. G., Russ, C., Shefler, E., Sivachenko, A., Sogoloff, B., Stojanov, P., Tamayo, P., Mesirov, J. P., Amani, V., Teider, N., Sengupta, S., Francois, J. P., Northcott, P. A., Taylor, M. D., Yu, F., Crabtree, G. R., Kautzman, A. G., Gabriel, S. B., Getz, G., Jager, N., Jones, D. T., Lichter, P., Pfister, S. M., Roberts, T. M., Meyerson, M., Pomeroy, S. L. & Cho, Y. J. Medulloblastoma exome sequencing uncovers subtype-specific somatic mutations. *Nature* **488**, 106-110, doi:10.1038/nature11329 (2012).

151 Dubuc, A. M., Remke, M., Korshunov, A., Northcott, P. A., Zhan, S. H., Mendez-Lago, M., Kool, M., Jones, D. T., Unterberger, A., Morrissy, A. S., Shih, D., Peacock, J., Ramaswamy, V., Rolider, A., Wang, X., Witt, H., Hielscher, T., Hawkins, C., Vibhakar, R., Croul, S., Rutka, J. T., Weiss, W. A., Jones, S. J., Eberhart, C. G., Marra, M. A., Pfister, S. M. & Taylor, M. D. Aberrant patterns of H3K4 and H3K27 histone lysine methylation occur across subgroups in medulloblastoma. *Acta Neuropathol* **125**, 373-384, doi:10.1007/s00401-012-1070-9 (2013).

152 Milde, T., Lodrini, M., Savelyeva, L., Korshunov, A., Kool, M., Brueckner, L. M., Antunes, A. S., Oehme, I., Pekrun, A., Pfister, S. M., Kulozik, A. E., Witt, O. & Deubzer, H. E. HD-MB03 is a novel Group 3 medulloblastoma model demonstrating sensitivity to histone deacetylase inhibitor treatment. *J Neurooncol* **110**, 335-348, doi:10.1007/s11060-012-0978-1 (2012).

153 Tang, Y., Gholamin, S., Schubert, S., Willardson, M. I., Lee, A., Bandopadhayay, P., Bergthold, G., Masoud, S., Nguyen, B., Vue, N., Balansay, B., Yu, F., Oh, S., Woo, P., Chen, S., Ponnuswami, A., Monje, M., Atwood, S. X., Whitson, R. J., Mitra, S., Cheshier, S. H., Qi, J., Beroukhim, R., Tang, J. Y., Wechsler-Reya, R., Oro, A. E., Link, B. A., Bradner, J. E. & Cho, Y. J. Epigenetic targeting of Hedgehog pathway transcriptional output through BET bromodomain inhibition. *Nat Med* **20**, 732-740, doi:10.1038/nm.3613 (2014).

154 Ecker, J., Oehme, I., Mazitschek, R., Korshunov, A., Kool, M., Hielscher, T., Kiss, J., Selt, F., Konrad, C., Lodrini, M., Deubzer, H. E.,

von Deimling, A., Kulozik, A. E., Pfister, S. M., Witt, O. & Milde, T. Targeting class I histone deacetylase 2 in MYC amplified group 3 medulloblastoma. *Acta Neuropathol Commun* **3**, 22, doi:10.1186/s40478-015-0201-7 (2015).

155 Filippakopoulos, P., Qi, J., Picaud, S., Shen, Y., Smith, W. B., Fedorov, O., Morse, E. M., Keates, T., Hickman, T. T., Felletar, I., Philpott, M., Munro, S., McKeown, M. R., Wang, Y., Christie, A. L., West, N., Cameron, M. J., Schwartz, B., Heightman, T. D., La Thangue, N., French, C. A., Wiest, O., Kung, A. L., Knapp, S. & Bradner, J. E. Selective inhibition of BET bromodomains. *Nature* **468**, 1067-1073, doi:10.1038/nature09504 (2010).

156 Delmore, J. E., Issa, G. C., Lemieux, M. E., Rahl, P. B., Shi, J., Jacobs, H. M., Kastritis, E., Gilpatrick, T., Paranal, R. M., Qi, J., Chesi, M., Schinzel, A. C., McKeown, M. R., Heffernan, T. P., Vakoc, C. R., Bergsagel, P. L., Ghobrial, I. M., Richardson, P. G., Young, R. A., Hahn, W. C., Anderson, K. C., Kung, A. L., Bradner, J. E. & Mitsiades, C. S. BET bromodomain inhibition as a therapeutic strategy to target c-Myc. *Cell* **146**, 904-917, doi:10.1016/j.cell.2011.08.017 (2011).

157 Mertz, J. A., Conery, A. R., Bryant, B. M., Sandy, P., Balasubramanian, S., Mele, D. A., Bergeron, L. & Sims, R. J., 3rd. Targeting MYC dependence in cancer by inhibiting BET bromodomains. *Proc Natl Acad Sci U S A* **108**, 16669-16674, doi:10.1073/pnas.1108190108 (2011).

158 Venkataraman, S., Alimova, I., Balakrishnan, I., Harris, P., Birks, D. K., Griesinger, A., Amani, V., Cristiano, B., Remke, M., Taylor, M. D., Handler, M., Foreman, N. K. & Vibhakar, R. Inhibition of BRD4 attenuates tumor cell self-renewal and suppresses stem cell signaling in MYC driven medulloblastoma. *Oncotarget* **5**, 2355-2371, doi:10.18632/oncotarget.1659 (2014).

159 Bandopadhayay, P., Bergthold, G., Nguyen, B., Schubert, S., Gholamin, S., Tang, Y., Bolin, S., Schumacher, S. E., Zeid, R., Masoud, S., Yu, F., Vue, N., Gibson, W. J., Paolella, B. R., Mitra, S. S., Cheshier, S. H., Qi, J., Liu, K. W., Wechsler-Reya, R., Weiss, W. A., Swartling, F. J., Kieran, M. W., Bradner, J. E., Beroukhim, R. & Cho, Y. J. BET bromodomain inhibition of MYC-amplified medulloblastoma. *Clin Cancer Res* **20**, 912-925, doi:10.1158/1078-0432.CCR-13-2281 (2014).

160 Muldoon, L. L., Soussain, C., Jahnke, K., Johanson, C., Siegal, T., Smith, Q. R., Hall, W. A., Hynynen, K., Senter, P. D., Peereboom, D. M. & Neuwelt, E. A. Chemotherapy delivery issues in central nervous

system malignancy: a reality check. *J Clin Oncol* **25**, 2295-2305, doi:10.1200/JCO.2006.09.9861 (2007).

161 Mandula, H., Parepally, J. M., Feng, R. & Smith, Q. R. Role of site-specific binding to plasma albumin in drug availability to brain. *J Pharmacol Exp Ther* **317**, 667-675, doi:10.1124/jpet.105.097402 (2006).

162 Ewing, J. R., Brown, S. L., Lu, M., Panda, S., Ding, G., Knight, R. A., Cao, Y., Jiang, Q., Nagaraja, T. N., Churchman, J. L. & Fenstermacher, J. D. Model selection in magnetic resonance imaging measurements of vascular permeability: Gadomer in a 9L model of rat cerebral tumor. *J Cereb Blood Flow Metab* **26**, 310-320, doi:10.1038/sj.jcbfm.9600189 (2006).

163 Vogelbaum, M. A. Convection enhanced delivery for the treatment of malignant gliomas: symposium review. *J Neurooncol* **73**, 57-69, doi:10.1007/s11060-004-2243-8 (2005).

164 Ali, M. J., Navalitloha, Y., Vavra, M. W., Kang, E. W., Itskovich, A. C., Molnar, P., Levy, R. M. & Groothuis, D. R. Isolation of drug delivery from drug effect: problems of optimizing drug delivery parameters. *Neuro Oncol* **8**, 109-118, doi:10.1215/15228517-2005-007 (2006).

165 van Tellingen, O., Yetkin-Arik, B., de Gooijer, M. C., Wesseling, P., Wurdinger, T. & de Vries, H. E. Overcoming the blood-brain tumor barrier for effective glioblastoma treatment. *Drug Resist Updat* **19**, 1-12, doi:10.1016/j.drup.2015.02.002 (2015).

166 Banks, W. A. From blood-brain barrier to blood-brain interface: new opportunities for CNS drug delivery. *Nat Rev Drug Discov* **15**, 275-292, doi:10.1038/nrd.2015.21 (2016).

167 Siegal, T., Rubinstein, R., Bokstein, F., Schwartz, A., Lossos, A., Shalom, E., Chisin, R. & Gomori, J. M. In vivo assessment of the window of barrier opening after osmotic blood-brain barrier disruption in humans. *J Neurosurg* **92**, 599-605, doi:10.3171/jns.2000.92.4.0599 (2000).

168 Timbie, K. F., Mead, B. P. & Price, R. J. Drug and gene delivery across the blood-brain barrier with focused ultrasound. *J Control Release* **219**, 61-75, doi:10.1016/j.jconrel.2015.08.059 (2015).

169 Choo, E. F., Kurnik, D., Muszkat, M., Ohkubo, T., Shay, S. D., Higginbotham, J. N., Glaeser, H., Kim, R. B., Wood, A. J. & Wilkinson,

G. R. Differential in vivo sensitivity to inhibition of P-glycoprotein located in lymphocytes, testes, and the blood-brain barrier. *J Pharmacol Exp Ther* **317**, 1012-1018, doi:10.1124/jpet.105.099648 (2006).

170 Kemper, E. M., van Zandbergen, A. E., Cleypool, C., Mos, H. A., Boogerd, W., Beijnen, J. H. & van Tellingen, O. Increased penetration of paclitaxel into the brain by inhibition of P-Glycoprotein. *Clin Cancer Res* **9**, 2849-2855 (2003).

171 Kuntner, C., Bankstahl, J. P., Bankstahl, M., Stanek, J., Wanek, T., Stundner, G., Karch, R., Brauner, R., Meier, M., Ding, X., Muller, M., Loscher, W. & Langer, O. Dose-response assessment of tariquidar and elacridar and regional quantification of P-glycoprotein inhibition at the rat blood-brain barrier using (R)-[(11)C]verapamil PET. *Eur J Nucl Med Mol Imaging* **37**, 942-953, doi:10.1007/s00259-009-1332-5 (2010).

172 Elliott, P. J., Hayward, N. J., Huff, M. R., Nagle, T. L., Black, K. L. & Bartus, R. T. Unlocking the blood-brain barrier: a role for RMP-7 in brain tumor therapy. *Exp Neurol* **141**, 214-224, doi:10.1006/exnr.1996.0156 (1996).

173 Inamura, T., Nomura, T., Bartus, R. T. & Black, K. L. Intracarotid infusion of RMP-7, a bradykinin analog: a method for selective drug delivery to brain tumors. *J Neurosurg* **81**, 752-758, doi:10.3171/jns.1994.81.5.0752 (1994).

174 Hamilton, A. M., Aidoudi-Ahmed, S., Sharma, S., Kotamraju, V. R., Foster, P. J., Sugahara, K. N., Ruoslahti, E. & Rutt, B. K. Nanoparticles coated with the tumor-penetrating peptide iRGD reduce experimental breast cancer metastasis in the brain. *J Mol Med (Berl)* **93**, 991-1001, doi:10.1007/s00109-015-1279-x (2015).

175 Gu, G., Gao, X., Hu, Q., Kang, T., Liu, Z., Jiang, M., Miao, D., Song, Q., Yao, L., Tu, Y., Pang, Z., Chen, H., Jiang, X. & Chen, J. The influence of the penetrating peptide iRGD on the effect of paclitaxel-loaded MT1-AF7p-conjugated nanoparticles on glioma cells. *Biomaterials* **34**, 5138-5148, doi:10.1016/j.biomaterials.2013.03.036 (2013).

176 Jiang, Y., Lv, L., Shi, H., Hua, Y., Lv, W., Wang, X., Xin, H. & Xu, Q. PEGylated Polyamidoamine dendrimer conjugated with tumor homing peptide as a potential targeted delivery system for glioma. *Colloids Surf B Biointerfaces* **147**, 242-249, doi:10.1016/j.colsurfb.2016.08.002 (2016).

177 Ying, M., Shen, Q., Zhan, C., Wei, X., Gao, J., Xie, C., Yao, B. & Lu, W. A stabilized peptide ligand for multifunctional glioma targeted drug delivery. *J Control Release* **243**, 86-98, doi:10.1016/j.jconrel.2016.09.035 (2016).

178 Frosina, G. Nanoparticle-mediated drug delivery to high-grade gliomas. *Nanomedicine* **12**, 1083-1093, doi:10.1016/j.nano.2015.12.375 (2016).

179 Tam, V. H., Sosa, C., Liu, R., Yao, N. & Priestley, R. D. Nanomedicine as a non-invasive strategy for drug delivery across the blood brain barrier. *Int J Pharm* **515**, 331-342, doi:10.1016/j.ijpharm.2016.10.031 (2016).

180 Cai, Q., Wang, L., Deng, G., Liu, J., Chen, Q. & Chen, Z. Systemic delivery to central nervous system by engineered PLGA nanoparticles. *Am J Transl Res* **8**, 749-764 (2016).

181 Householder, K. T., DiPerna, D. M., Chung, E. P., Wohlleb, G. M., Dhruv, H. D., Berens, M. E. & Sirianni, R. W. Intravenous delivery of camptothecin-loaded PLGA nanoparticles for the treatment of intracranial glioma. *Int J Pharm* **479**, 374-380, doi:10.1016/j.ijpharm.2015.01.002 (2015).

182 Bidros, D. S., Liu, J. K. & Vogelbaum, M. A. Future of convection-enhanced delivery in the treatment of brain tumors. *Future Oncol* **6**, 117-125, doi:10.2217/fon.09.135 (2010).

183 Barua, N. U., Gill, S. S. & Love, S. Convection-enhanced drug delivery to the brain: therapeutic potential and neuropathological considerations. *Brain Pathol* **24**, 117-127, doi:10.1111/bpa.12082 (2014).

184 Debinski, W. & Tatter, S. B. Convection-enhanced delivery for the treatment of brain tumors. *Expert Rev Neurother* **9**, 1519-1527, doi:10.1586/ern.09.99 (2009).

185 Kunwar, S., Chang, S., Westphal, M., Vogelbaum, M., Sampson, J., Barnett, G., Shaffrey, M., Ram, Z., Piepmeier, J., Prados, M., Croteau, D., Pedain, C., Leland, P., Husain, S. R., Joshi, B. H., Puri, R. K. & Group, P. S. Phase III randomized trial of CED of IL13-PE38QQR vs Gliadel wafers for recurrent glioblastoma. *Neuro Oncol* **12**, 871-881, doi:10.1093/neuonc/nop054 (2010).

186 Sampson, J. H., Archer, G., Pedain, C., Wembacher-Schroder, E., Westphal, M., Kunwar, S., Vogelbaum, M. A., Coan, A., Herndon, J. E., Raghavan, R., Brady, M. L., Reardon, D. A., Friedman, A. H.,

Friedman, H. S., Rodriguez-Ponce, M. I., Chang, S. M., Mittermeyer, S., Croteau, D., Puri, R. K. & Investigators, P. T. Poor drug distribution as a possible explanation for the results of the PRECISE trial. *J Neurosurg* **113**, 301-309, doi:10.3171/2009.11.JNS091052 (2010).